MODEL REDUCTION
FOR
A RESTRAINED DEFORMABLE BODY

by

Yi-shih Lin

A Dissertation Submitted to the Faculty of the

DEPARTMENT OF AEROSPACE AND MECHANICAL ENGINEERING

In Partial Fulfillment of the Requirements
For the Degree of

DOCTOR OF PHILOSOPHY
WITH A MAJOR IN MECHANICAL ENGINEERING

In the Graduate College

THE UNIVERSITY OF ARIZONA

2 0 0 5

THE UNIVERSITY OF ARIZONA
GRADUATE COLLEGE

As members of the Dissertation Committee, we certify that we have read the dissertation prepared by Yi-shih Lin

entitled MODEL REDUCTION OF A RESTRAINED DEFORMABLE BODY

and recommend that it be accepted as fulfilling the dissertation requirement for the Degree of Doctor of Philosophy

_____ Date: April 15, 2005
Dr. Parviz E. Nikravesh

_____ Date: April 15, 2005
Dr. Ara Arabyan

_____ Date: April 15, 2005
Dr. Hussein A. Kamel

_____ Date: April 15, 2005
Dr. Francois E. Cellier

Final approval and acceptance of this dissertation is contingent upon the candidate's submission of the final copies of the dissertation to the Graduate College.

I hereby certify that I have read this dissertation prepared under my direction and recommend that it be accepted as fulfilling the dissertation requirement.

_____ Date: April 15, 2005
Dissertation Director: Dr. Parviz E. Nikravesh

STATEMENT BY AUTHOR

This dissertation has been submitted in partial fulfillment of requirements for an advanced degree at The University of Arizona and is deposited in the University Library to be made available to borrowers under rules of the Library.

Brief quotations from this dissertation are allowable without special permission, provided that accurate acknowledgment of source is made. Requests for permission for extended quotation from or reproduction of this manuscript in whole or in part may be granted by the head of the major department or the Dean of the Graduate College when in his or her judgment the proposed use of the material is in the interests of scholarship. In all other instances, however, permission must be obtained from the author.

SIGNED: _____

Yi-shih Lin

ACKNOWLEDGEMENTS

I am deeply indebted to Dr. Nikravesh. Without his incredible patience and excellent guidance, the completion of this dissertation would not be possible. I would also like express my gratitude to Dr. Arabyan, Dr. Cellier, and Dr. Tharp for I had learned so much while taking courses from them. Finally, I thank all the committee members, including Dr. Chen and Dr. Kamel, for their comments and help along the way.

DEDICATION

In memory of my father, whom I will miss forever.

To my mother, who has always been taking care of the family.

To my siblings, whose support on one another allowed me to be worry-free.

To my guardian angels: Thank you.

To the nature which constantly keeps me curious.

TABLE OF CONTENTS

TABLE OF CONTENTS - *Continued*

TABLE OF CONTENTS - *Continued*

TABLE OF CONTENTS - *Continued*

TABLE OF CONTENTS - *Continued*

LIST OF ILLUSTRATIONS

LIST OF ILLUSTRATIONS - *Continued*

LIST OF TABLES

ABSTRACT

Methods of component mode synthesis, such as Craig and Bampton reduction, are known to generally yield more accurate results in deformable multibody dynamics. The main shortcoming of those methods is that they are intuitively based. Recently Nikravesh developed a reduction method called mode condensation which is derived from the equations of motion and yields the same results as Craig and Bampton reduction. In this dissertation, it is proven that these two methods span the same column space; therefore, they should yield identical results. We propose that mode condensation provides an analytical justification for Craig and Bampton reduction. Test results suggest that Craig and Bampton reduction and mode condensation are appropriate for a broader range of applications because their column space matches up well with the conditions under which the deformable body is restrained. Although Guyan reduction preserves exact solutions for static problems, its applications shall be limited to low frequency excitation because of raised eigen-frequencies. Modal truncation is not recommended for use in multibody dynamic settings because it lacks the ability to receive forces and displacements at the moving boundary. Another issue addressed in this dissertation is the misconception that if mean axes are adopted as the moving reference frame, only free-free modes should be used for model reduction. It was not clear how a restrained deformable body with mean axes can be condensed properly. We have shown that the conventional (nodal-fixed) mode shapes can be used with mean axes as long as the transformation matrix has full rank and contains complete rigid-body mode shapes.

NOMENCLATURE

Abbreviations

abbreviation	full terms
2-D	two-Dimensional
3-D	three-Dimensional
DOF	Degree Of Freedom

Symbols

symbol	description
$\mathbf{d}$	absolute position of a point on a rigid body (a 3-vector) or absolute position of nodes on a deformable body
$\mathbf{r}$	position of a reference frame
$\mathbf{b}$	$\mathbf{b} = \mathbf{s} + \boldsymbol{\delta}$
$\mathbf{s}$	relative location of a point on a rigid body (a 3-vector) or undeformed, relative location of nodes on a deformable body
$\boldsymbol{\delta}$	nodal deformation coordinates
$\mathbf{z}$	modal deformation coordinates
$\mathbf{p}$	Euler parameters
$\mathbf{A}$	orientation matrix
$\boldsymbol{\xi}, \boldsymbol{\eta}, \boldsymbol{\zeta}$	axis unit vectors of a reference frame
$\boldsymbol{\omega}$	angular velocity
$\mathbf{I}$	identity matrix
$\mathbf{J}$	inertia matrix
$\mathbf{M}$	mass matrix, nodal
$\mathbf{K}$	stiffness matrix, nodal
$\bar{\mathbf{M}}$	mass matrix, modal
$\bar{\mathbf{K}}$	stiffness matrix, modal
$\mathbf{f}$	force vector

Operators

operator	name	example	meaning
ˆ	hat	$\hat{\mathbf{I}}$	**I**'s stack vertically; $\hat{\mathbf{I}} = \begin{bmatrix} \mathbf{I} \\ \vdots \\ \mathbf{I} \end{bmatrix}$; $\mathbf{d} = \hat{\mathbf{I}}\mathbf{r} + \mathbf{b}$
~	tilde	$\tilde{\mathbf{b}}$	a vertical stack of skew matrices $\tilde{\mathbf{b}}^j$; $\tilde{\mathbf{b}} = \begin{bmatrix} \vdots \\ \tilde{\mathbf{b}}^j \\ \vdots \end{bmatrix}$, $\tilde{\mathbf{b}}^j = \begin{bmatrix} 0 & -b_3 & b_2 \\ b_3 & 0 & -b_1 \\ -b_2 & b_1 & 0 \end{bmatrix}$ j-th node
–	(over) bar	$\bar{\mathbf{A}}$	**A**'s stack diagonally; $\bar{\mathbf{A}} = \begin{bmatrix} \mathbf{A} & & \\ & \ddots & \\ & & \mathbf{A} \end{bmatrix}$
`	(left) prime	$\grave{\boldsymbol{\delta}}$	in local components; $\boldsymbol{\delta} = \bar{\mathbf{A}}\grave{\boldsymbol{\delta}}$

Notice that the "bar" is used both in the symbols and as an operator. The meaning is determined from the context.

1 INTRODUCTION

A mechanical system typically comprises any number of bodies that are connected to each other by kinematic joints and force elements (springs, dampers, or actuators). Examples are robots and the suspension and steering systems of an automobile. What concern engineers most are the motion (positions, velocities, and accelerations), reaction forces, and required power. In order to meet certain specifications, design changes would be made and the system would be re-analyzed during the design phase. Several prototypes could be constructed and modified many times for field-testing. This process is often costly and time-consuming. Traditional kinematic analyses [1, 2], which are mostly based on graphical interpretation, could be inaccurate and error-prone if performed by hand. Although methods like Lagrangian mechanics and Hamiltonian mechanics [3] can help establish the equations of motion, soon it may become difficult to manage even when there are just a few bodies involved. Besides, dynamic systems are in general highly non-linear and do not have closed form solutions. Therefore, it is usually necessary to solve a problem computationally.

1.1 Computational Multibody Dynamics

Computational multibody dynamics has evolved since the early 1970s [4, 5]. It allows one to model mechanical systems systematically [6, 7, 8, 9]. Some methods such as absolute (or Cartesian) coordinate formulations allow each three-dimensional (3-D) rigid body to have up to six degrees of freedom. Although this method is easy to apply, it is in general computationally inefficient. Other methods such as relative (or joint) coordinate

formulations use a smaller set of variables, which can generally be solved in less time, but are more complicated to set up.

Many computer-aided engineering software tools have been available [10]. ADAMS, the first commercial 3-D mechanical system simulation software, was introduced in 1980 by MDI [11]. (MDI, founded in 1977, was acquired by MSC.Software Corporation in 2002.) The Center for Computer-Aided Design at The University of Iowa initially developed DADS, which was largely sponsored by the US Army Tank-Automotive Command (TACOM) [12]. (Later, LMS International took over and continued to maintain and market DADS.) In these programs, by syntaxes and/or thru graphical user interfaces, one can build complex systems easily. Numerous simulations can be conducted for different designs before a prototype is even constructed or modified, thereby reducing the time and cost to develop products.

1.2 Body Flexibility

Driven by demands and ever-intense competition, the industries are designing new products that are more economic yet still safe to operate at higher speeds. With lighter materials increasingly in use—such as in space structures, chassis designs, and robot systems—flexibility must be taken into account to obtain accurate simulation results [13].

The most popular way to model a deformable body is the finite element method, which was developed in the 1940s for structural analysis [14, 15]. The deformable body is characterized by a stiffness matrix and mass matrix. The stiffness matrix by itself is singular. The mass matrix is either consistent (usually in stripe patterns) or lumped (on

the diagonal only); in any case, it must be positive definite. A damping matrix, if needed, is often constructed by modal damping or Rayleigh damping.

Structures are usually bound to the ground, permitting no rigid-body motion. Other systems may exhibit some rigid-body motion. One particular problem is beam-like deformable bodies attached to a moving support [16]. Such examples are aircraft propellers, helicopter rotor blades, etc. The forces of rotary inertia due to fast angular rotation can be significant. Yet the so-called dynamic stiffening effects (centrifugal stiffening and Coriolis forces) were sometimes missing [16, 17, 18] because these terms were included incompletely in ad hoc manners or because the governing equations were prematurely linearized.

Comprehensive formulations in the context of multibody dynamics have emerged since the mid 1980s [19, 20]. A floating reference frame is assigned to trace the large rigid-body motion of a deformable body [21]. Six axis conditions are required to anchor the axes to the deformable body. One widely used frame is the nodal-fixed axes [20], which sets a total of six nodal deflections to zero. Another less known frame is the mean axes [22, 23, 20], which minimizes the deformation kinetic energy to the frame motion. Principal axes can also be used as a reference frame [24, 25]; the origin is at the mass center, and the products of inertia in the principal axes are zeros [26].

1.3 Reduction Methods

The stiffness and mass matrices generated by the finite element method can be large (more than tens of thousand degrees of freedom). The computation time to solve full

eigen-problems or equations of motion in these cases may be unacceptable. In order to perform more effectively, many researchers have proposed various reduction methods [41].

Suppose that the nodal coordinates of a finite element model are split into two sets. One set has no applied and inertia forces associated with it. By *static condensation* [41], the model is reduced to the size of the other set by a transformation matrix. No approximation is introduced; the reduced model faithfully represents the original model. Guyan [27] suggested that the same technique can still be used even though some inertia forces are not totally negligible. This is called *mass condensation* technique or sometimes *eigenvalue economizer* [41]. Eitelberg proposed a reduction method for linear time invariant systems [28, 29]. It offers zero steady state errors and minimizes dynamic errors. When applied to structures, this method effectively becomes Guyan reduction.

Although static condensation (or mass condensation) can preserve exact solutions for static problems, large errors may occur at higher frequencies if applied to dynamic problems. The reason is that a statically condensed model usually does not have the same eigen-properties as the original model. Many modifications were since proposed but they were generally aimed to improve the eigen-vectors, not the eigen-values [33, 30, 31].

Paz reported an approach, *dynamic condensation* [32, 33], that can yield a reduced model whose eigen-properties are a subset of the original model. Effectively, it solves a generalized eigen-problem partially. The reduced model remains in nodal space. Nikravesh and Pereira [34] developed another version of dynamic condensation. It is fundamentally the same as Paz's but it is derived quite differently. Their derivation

better reveals the connection between nodal and modal spaces of deformation for the reduced model. *Modal truncation* is a conventional approach for model reduction. We often truncate higher eigen-modes or just solve for lower eigen-modes. The condensed matrices usually are served in modal space. In fact, dynamic condensation can be regarded as a special case of modal truncation converted back to nodal space.

Despite having preserved the eigen-properties, dynamic condensation and modal truncation do not always have better responses than static condensation especially when the deformable body is restrained. Yoo and Haug [35, 36] improved the response by combining vibration normal and residual attachment modes. MacNeal [37] used residual flexibility to correct for the static effects when some normal modes are missing. Based on MacMeal's method, Rubin [38] included the inertial effects of the missing normal modes. With different assumptions, the method of Herting [39] can become that of Guyan, Hurty [42], Craig and Bampton [43], or Rubin. Herting's method has been implemented in MSC/NASTRAN since the late 1970s [40]. (NASA contracted with McNeal-Schwendler Corp. to develop NASTRAN in the 1960s.)

Component mode synthesis [41] is a family of methods that combine different types of modes to improve the quality of model reduction. Hurty [42] composed nodal displacements from three categories: rigid-body modes (from determinate constraints), constraint modes (from redundant constraints if any), and normal modes. But it is not always clear which constraints should be considered determinate and which others should be considered redundant. Craig and Bampton [43] instead treated all boundary nodes in the same manner, producing only the constraint modes. The rigid-body modes are hereby

included in the constraint modes implicitly. The normal modes are still obtained as before. According to Craig and Bampton, their approach may be considered as a generalization of branch mode analysis [48] for substructures with redundant constraints at the boundaries. Friburg [44] rejected the rigid-body modes that hide within the constraint modes; an explicit reference frame is then attached when needed. The modal flexibility method in ADAMS/Flex is based on Craig and Bampton's method with only subtle changes [45]. In place of using the regular constraint modes (as commonly employed in component mode synthesis), quasi-static mode (QSM) compensation [46] tunes by using a "centering frequency" that controls the dynamic range of interest. Multiple sets of QSMs are also feasible [47].

Gladwell [48] described a method called *branch mode analysis*. A large system is divided into branches of components. For each branch, a set of branch modes is obtained. All sets of branch modes are then combined. This method is claimed to achieve greater accuracy, provided that those branch modes are chosen appropriately. Yet, according to Craig and Bampton [43], "it may be seen that the boundary between two substructures is assumed to be rigid, a restriction that can not be accepted for cases of highly redundant boundaries between substructures." Benfield and Hruda's *component mode substitution* [49] is similar to both Hurty's and Gladwell's methods.

1.4 Objectives

Although methods of component mode synthesis, which intuitively combine different types of modes, seem to improve the quality of model reduction in many cases, no

physical explanations have been provided to justify the various constructions. Recently Nikravesh developed a different reduction method called *mode condensation* [50], which is derived from the equations of motion rather than based on pure intuition. Initial tests indicate that this new method yields practically the same results as Craig and Bampton reduction does. Nikravesh's method may be equivalent to Craig and Bampton reduction. If true, it helps understand why a method such as Craig and Bampton reduction works.

Selected reduction methods are to be assessed from two aspects: (1) deformed profiles and (2) time simulations. First, we compare the deformed profiles when a set of modal coordinates is used and when a set of nodal coordinates is given for the reduction methods to fit. Second, time simulations of three scenarios are carried out. Those scenarios represent typical applications where a deformable body is under various boundary conditions: no rigid-body motion, limited rigid-body motion, and general rigid-body motion. We want to know which reduction method or methods are suitable for a broader range of applications.

Finally we consider a misconception that exists in the community of multibody dynamics that if mean axes are adopted as the moving reference frame for a deformable body, only free-free modes should be used (or not at all) for model reduction. It was not clear how a restrained deformable body can be condensed properly if mean axes are the choice. We show that mean axes can be indeed used under this circumstance. In the end, model reduction with mean axes is as easy as model reduction with nodal-fixed axes.

1.5 Organization

Chapter 2 reviews the basics of rigid multibody dynamics, which includes general kinematics, unconstrained and constrained equations of motion, and time integration. Chapter 3 prepares the equations of motion for a structure bound to the ground and an unconstrained moving deformable body. For the moving deformable body, the unconstrained equations of motion (without axis conditions and kinematic constraints) are derived using the Lagrange's equations. Chapter 4 mostly describes nodal-fixed and mean axis conditions. Chapter 5 formulates the complete equations of motion for a typical rigid-deformable multibody system in which one rigid body and one deformable body are connected by a spherical joint. Nodal and modal formulations with nodal-fixed and mean axis frames are presented. The advantages of mean axes over nodal-fixed axes are also pointed out. Chapter 6 highlights reduction methods such as static condensation, modal truncation, Craig and Bampton reduction, mode condensation (developed by Nikravesh), and Eitelberg’s method. Special interest is paid in the last two methods. Chapter 7 compares different reduction methods. Base on the results, comments and recommendations are made. Chapter 8 proposes an implementation that allows reduction methods in conventional (nodal-fixed) mode shapes to work with mean axes even if the moving deformable body is restrained by joints and/or forces at the boundary. This defies the common misconception that only free-free modes are compatible with mean axes. Chapter 9 states the conclusion and future work.

2 BASICS OF RIGID MULTIBODY DYNAMICS

This chapter provides the basic knowledge on rigid multibody dynamics. Only a few topics are discussed before we start to deal with deformable bodies, which begins in Chapter 3. The reader is advised to consult general textbooks such as [1, 3] for comprehensive principles on dynamics. Treatments on computational multibody dynamics can be found, for example, in [4, 6, 7, 8].

2.1 Kinematics

A rigid body generally moves and rotates in space. To define the kinematics of any point on the body, a reference frame is first attached to the body. The position, velocity, and acceleration of the point can then be derived. Attention is paid to the use of Euler parameters in describing the angular orientation of a body because of their advantages—no computation of trigonometric functions and being free of singularity—over conventional parameters such as Euler angles. Kinematic joints connect bodies. Commonly seen joints are spherical (or ball), universal, revolute, translational (or prismatic), cylindrical, and screw joints. Here, we only show the derivation of spherical joint constraints. For the details on other types of joints, please consult [6, 7].

2.1.1 General motion

A rigid body is moving and rotating freely in the inertial coordinate system, the **xyz** frame, as show in Figure 2-1. A reference frame, $\xi\eta\zeta$, is attached to the body. Vector **r** positions the origin of the $\xi\eta\zeta$ frame from the origin of the **xyz** frame. Matrix **A**

describes the orientation of the $\xi\eta\zeta$ frame in the **xyz** frame by direction cosines. A fixed point, *P*, on the body is located by vector **s** from the origin of the $\xi\eta\zeta$ frame. Vector **s** contains coordinates with respect to the **xyz** frame. For an observer who is stationary on the body, the same vector is seen differently as vector **`s**. Vector **`s** contains coordinates, which are constant, with respect to the $\xi\eta\zeta$ frame. The relation between the two vectors is $\mathbf{s} = \mathbf{A}\mathbf{`s}$. The absolute position of point *P* is

$$\mathbf{d} = \mathbf{r} + \mathbf{s} \tag{2.1}$$

The velocity and acceleration of point *P* are

$$\dot{\mathbf{d}} = \dot{\mathbf{r}} + \dot{\mathbf{s}} = \dot{\mathbf{r}} + \tilde{\boldsymbol{\omega}}\mathbf{s} = \dot{\mathbf{r}} - \tilde{\mathbf{s}}\boldsymbol{\omega} = \begin{bmatrix}\mathbf{I} & -\tilde{\mathbf{s}}\end{bmatrix}\begin{Bmatrix}\dot{\mathbf{r}} \\ \boldsymbol{\omega}\end{Bmatrix} \tag{2.2}$$

and

$$\ddot{\mathbf{d}} = \ddot{\mathbf{r}} + \ddot{\mathbf{s}} = \ddot{\mathbf{r}} + \dot{\tilde{\boldsymbol{\omega}}}\mathbf{s} + \tilde{\boldsymbol{\omega}}\dot{\mathbf{s}} = \ddot{\mathbf{r}} - \tilde{\mathbf{s}}\dot{\boldsymbol{\omega}} + \tilde{\boldsymbol{\omega}}\tilde{\boldsymbol{\omega}}\mathbf{s} = \begin{bmatrix}\mathbf{I} & -\tilde{\mathbf{s}}\end{bmatrix}\begin{Bmatrix}\ddot{\mathbf{r}} \\ \dot{\boldsymbol{\omega}}\end{Bmatrix} + \tilde{\boldsymbol{\omega}}\tilde{\boldsymbol{\omega}}\mathbf{s} \tag{2.3}$$

respectively where $\boldsymbol{\omega}$ and $\dot{\boldsymbol{\omega}}$ are the angular velocity and acceleration of the body.

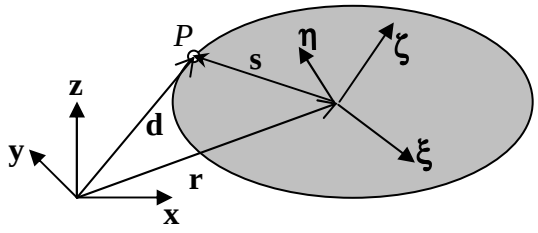

Figure 2-1: kinematics of a rigid body

2.1.2 Euler parameters

There are different ways to describe the angular orientation of a body (or a reference frame). Our choice is Euler parameters because the use of them can significantly simplify mathematical expressions. The Euler parameters consist of four parameters: e_0, e_1, e_2, and e_3. According to Euler's theorem [6], "the general displacement of a body with one point fixed is a rotation about some axis." Let the angle of rotation be ϕ and the axis of rotation be about a unit vector **u**. Furthermore,

$$e_0 = \cos(\tfrac{\phi}{2}) \tag{2.4}$$

$$\mathbf{e} = \sin(\tfrac{\phi}{2})\mathbf{u} \tag{2.5}$$

where

$$\mathbf{e} = \begin{Bmatrix} e_1 \\ e_2 \\ e_3 \end{Bmatrix} \tag{2.6}$$

The orientation matrix is computed by

$$\mathbf{A} = \left(2e_0^2 - 1\right)\mathbf{I} + 2\left(\mathbf{e}\mathbf{e}^{\mathbf{T}} + e_0\tilde{\mathbf{e}}\right) \tag{2.7}$$

Conversely, the Euler parameters can be determined from the direction cosines in **A**.* Note that the Euler parameters are not independent:†

$$\mathbf{p}^{\mathrm{T}}\mathbf{p} = e_0^2 + \mathbf{e}^{\mathrm{T}}\mathbf{e} = e_0^2 + e_1^2 + e_2^2 + e_3^2 = 1 \tag{2.8}$$

where

---

* For the details, see [6].

† There are only three rotational degrees of freedom for a floating reference frame.

$$\mathbf{p} = \begin{Bmatrix} e_0 \\ \mathbf{e} \end{Bmatrix} \tag{2.9}$$

The time derivative of **p** is convertible to and from the global angular velocity by

$$\boldsymbol{\omega} = 2\mathbf{G}\dot{\mathbf{p}} \tag{2.10}$$

and

$$\dot{\mathbf{p}} = \frac{1}{2}\mathbf{G}^{\mathrm{T}}\boldsymbol{\omega} \tag{2.11}$$

in which

$$\mathbf{G} = [-\mathbf{e}, \tilde{\mathbf{e}} + e_0\mathbf{I}] \tag{2.12}$$

Similarly, $\dot{\mathbf{p}}$ can be converted to and from the local angular velocity by

$$\grave{\boldsymbol{\omega}} = 2\mathbf{L}\dot{\mathbf{p}} \tag{2.13}$$

and

$$\dot{\mathbf{p}} = \frac{1}{2}\mathbf{L}^{\mathrm{T}}\grave{\boldsymbol{\omega}} \tag{2.14}$$

in which

$$\mathbf{L} = [-\mathbf{e}, -\tilde{\mathbf{e}} + e_0\mathbf{I}] \tag{2.15}$$

The angular velocities of $\boldsymbol{\omega}$ and $\grave{\boldsymbol{\omega}}$ are related by

$$\boldsymbol{\omega} = \mathbf{A}\grave{\boldsymbol{\omega}} \tag{2.16}$$

The relations between $\dot{\boldsymbol{\omega}}$, $\dot{\grave{\boldsymbol{\omega}}}$, and $\ddot{\mathbf{p}}$ are as follows:

$$\dot{\boldsymbol{\omega}} = \mathbf{A}\dot{\grave{\boldsymbol{\omega}}} \tag{2.17}$$

$$\dot{\boldsymbol{\omega}} = 2\mathbf{G}\ddot{\mathbf{p}} \tag{2.18}$$

$$\dot{\grave{\boldsymbol{\omega}}} = 2\mathbf{L}\ddot{\mathbf{p}} \tag{2.19}$$

$$\ddot{\mathbf{p}} = \frac{1}{2}\mathbf{G}^{\mathrm{T}}\dot{\boldsymbol{\omega}} - \frac{1}{4}\|\boldsymbol{\omega}\|\mathbf{p} \tag{2.20}$$

$$\ddot{\mathbf{p}} = \frac{1}{2}\mathbf{L}^{\mathrm{T}}\grave{\dot{\boldsymbol{\omega}}} - \frac{1}{4}\|\grave{\boldsymbol{\omega}}\|\mathbf{p} \tag{2.21}$$

where $\|\boldsymbol{\omega}\| = \|\grave{\boldsymbol{\omega}}\|$ (the norm or magnitude of the angular velocities). For more details on Euler parameters, please refer to [6].

2.1.3 Spherical joint

In Figure 2-2, body *i* and body *j* are connected at point *P* by a spherical joint. There are three relative rotational DOFs between the two bodies. Since the two bodies can not separate at point *P*, the position constraints are $\mathbf{d}_i = \mathbf{d}_j$ or

$$\mathbf{r}_i + \mathbf{s}_i = \mathbf{r}_j + \mathbf{s}_j \tag{2.22}$$

The velocity constraints are $\dot{\mathbf{d}}_i = \dot{\mathbf{d}}_j$ or

$$\begin{bmatrix}\mathbf{I} & -\tilde{\mathbf{s}}_i\end{bmatrix}\begin{Bmatrix}\dot{\mathbf{r}}_i \\ \boldsymbol{\omega}_i\end{Bmatrix} = \begin{bmatrix}\mathbf{I} & -\tilde{\mathbf{s}}_j\end{bmatrix}\begin{Bmatrix}\dot{\mathbf{r}}_j \\ \boldsymbol{\omega}_j\end{Bmatrix} \tag{2.23}$$

The acceleration constraints are $\ddot{\mathbf{d}}_i = \ddot{\mathbf{d}}_j$ or

$$\begin{bmatrix}\mathbf{I} & -\tilde{\mathbf{s}}_i\end{bmatrix}\begin{Bmatrix}\ddot{\mathbf{r}}_i \\ \dot{\boldsymbol{\omega}}_i\end{Bmatrix} - \begin{bmatrix}\mathbf{I} & -\tilde{\mathbf{s}}_j\end{bmatrix}\begin{Bmatrix}\ddot{\mathbf{r}}_j \\ \dot{\boldsymbol{\omega}}_j\end{Bmatrix} = -\tilde{\boldsymbol{\omega}}_i\tilde{\boldsymbol{\omega}}_i\mathbf{s}_i + \tilde{\boldsymbol{\omega}}_j\tilde{\boldsymbol{\omega}}_j\mathbf{s}_j \tag{2.24}$$

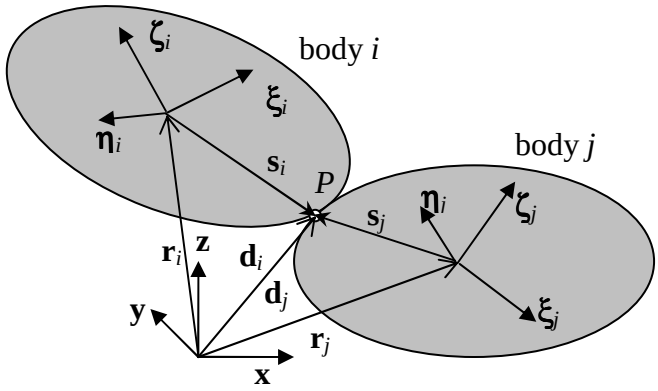

Figure 2-2: a spherical joint between two rigid bodies

2.2 Equations of Motion

Assume that a body-attached reference frame, $\xi\eta\zeta$, is located at the mass center of a rigid body. The mass of the body is *m*. Inertia matrix **J**, whose entries are expressed with respect to the inertial frame (**xyz**), contains the mass moments of inertia about the mass center. The vector of resultant forces is **f**. The vector of resultant moments is **n**. The unconstrained equations of motion are

$$\begin{bmatrix} m\mathbf{I} & \mathbf{0} \\ \mathbf{0} & \mathbf{J} \end{bmatrix} \begin{Bmatrix} \ddot{\mathbf{r}} \\ \dot{\boldsymbol{\omega}} \end{Bmatrix} = \begin{Bmatrix} \mathbf{f} \\ -\tilde{\boldsymbol{\omega}}\mathbf{J}\boldsymbol{\omega} + \mathbf{n} \end{Bmatrix} \tag{2.25}$$

The second row (Euler's equations) of Eq. (2.25) is often written in local components as

$$\grave{\mathbf{J}}\dot{\grave{\boldsymbol{\omega}}} = -\tilde{\grave{\boldsymbol{\omega}}}\grave{\mathbf{J}}\grave{\boldsymbol{\omega}} + \grave{\mathbf{n}} \tag{2.26}$$

The inertia matrix $\grave{\mathbf{J}}$, whose entries are expressed with respect to the $\xi\eta\zeta$ frame, is constant. The relation between the two inertia matrices is $\mathbf{J} = \mathbf{A}\grave{\mathbf{J}}\mathbf{A}^{\mathrm{T}}$. Note that Eqs. (2.25) and (2.26) are invalid if the $\xi\eta\zeta$ frame is not at the mass center. For non-centroidal equations of motion, see [6].

When a rigid body is constrained, the reaction forces and moments can be incorporated by the method of Lagrange multipliers. We demonstrate this concept by the two-body shown system in Figure 2-3. Both of their body-attached reference frames are located at the mass centers. There is a spherical joint that connects body 1 and body 2 at point *P*. A second spherical joint connects body 1 to the ground at point *Q*. The locations of points *P* and *Q* from the origins of the reference frames are also marked. The constrained equations of motion are

$$\begin{bmatrix} m_1\mathbf{I} & \mathbf{0} & \mathbf{0} & \mathbf{0} & \mathbf{I} & -\mathbf{I} \\ \mathbf{0} & \mathbf{J}_1 & \mathbf{0} & \mathbf{0} & -\tilde{\mathbf{s}}_1^{P^{\mathrm{T}}} & \tilde{\mathbf{s}}_1^{Q^{\mathrm{T}}} \\ \mathbf{0} & \mathbf{0} & m_2\mathbf{I} & \mathbf{0} & -\mathbf{I} & \mathbf{0} \\ \mathbf{0} & \mathbf{0} & \mathbf{0} & \mathbf{J}_2 & \tilde{\mathbf{s}}_2^{P^{\mathrm{T}}} & \mathbf{0} \\ \mathbf{I} & -\tilde{\mathbf{s}}_1^{P} & -\mathbf{I} & \tilde{\mathbf{s}}_2^{P} & \mathbf{0} & \mathbf{0} \\ -\mathbf{I} & \tilde{\mathbf{s}}_1^{Q} & \mathbf{0} & \mathbf{0} & \mathbf{0} & \mathbf{0} \end{bmatrix} \begin{Bmatrix} \ddot{\mathbf{r}}_1 \\ \dot{\boldsymbol{\omega}}_1 \\ \ddot{\mathbf{r}}_2 \\ \dot{\boldsymbol{\omega}}_2 \\ \boldsymbol{\lambda}_P \\ \boldsymbol{\lambda}_Q \end{Bmatrix} = \begin{Bmatrix} \mathbf{f}_1 \\ -\tilde{\boldsymbol{\omega}}_1\mathbf{J}_1\boldsymbol{\omega}_1 + \mathbf{n}_1 \\ \mathbf{f}_2 \\ -\tilde{\boldsymbol{\omega}}_2\mathbf{J}_2\boldsymbol{\omega}_2 + \mathbf{n}_2 \\ -\tilde{\boldsymbol{\omega}}_1\tilde{\boldsymbol{\omega}}_1\mathbf{s}_1^P + \tilde{\boldsymbol{\omega}}_2\tilde{\boldsymbol{\omega}}_2\mathbf{s}_2^P \\ \tilde{\boldsymbol{\omega}}_1\tilde{\boldsymbol{\omega}}_1\mathbf{s}_1^Q \end{Bmatrix} \tag{2.27}$$

where $\boldsymbol{\lambda}_P$ and $\boldsymbol{\lambda}_Q$ are the Lagrange multipliers associated with the two spherical joints.*

* The formulation of Eq. (2.27) is in absolute coordinates. They can be transformed into a smaller set of coordinates (such as joint coordinates), thereby eliminating some or all of the Lagrange multipliers [6].

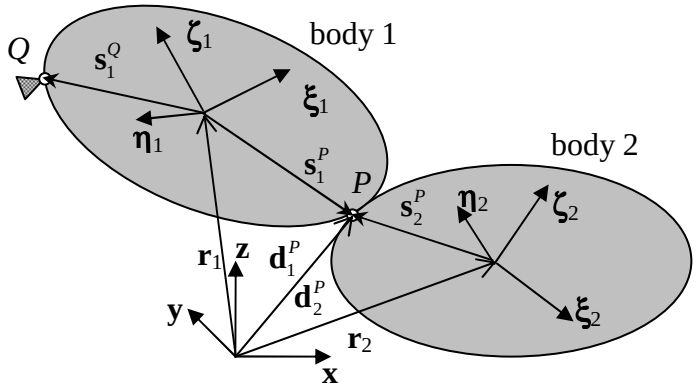

Figure 2-3: a simple two-body system

2.3 Time Integration

For each rigid body, once the accelerations ($\ddot{\mathbf{r}}$ and $\dot{\boldsymbol{\omega}}$) are obtained, they can be integrated over time to obtain the velocities ($\dot{\mathbf{r}}$ and $\boldsymbol{\omega}$). At the same time, the velocities ($\dot{\mathbf{r}}$ and $\dot{\mathbf{p}}$) are integrated for the positional coordinates ($\mathbf{r}$ and $\mathbf{p}$). That is,

$$\begin{Bmatrix} \mathbf{r} \\ \mathbf{p} \\ \dot{\mathbf{r}} \\ \boldsymbol{\omega} \end{Bmatrix} = \int_{t_0} \begin{Bmatrix} \dot{\mathbf{r}} \\ \dot{\mathbf{p}} \\ \ddot{\mathbf{r}} \\ \dot{\boldsymbol{\omega}} \end{Bmatrix} dt \tag{2.28}$$

Because there are no direct position variables for $\boldsymbol{\omega}$, it is converted to $\dot{\mathbf{p}}$ using Eq. (2.11) before integration.

3 DYNAMICS OF A DEFORMABLE BODY

In structural analysis, a structure is often constrained to the ground. Either all the boundary nodes are fixed or some of them may move in a prescribed manner of time. In these cases, since there is no (large) rigid-body motion, the equations of motion have a simpler form. But when a deformable body is allowed to translate and rotate in space, the dynamics becomes more complex. We first introduce the general kinematics. The equations of motion (without axis conditions and kinematic constraints) are then derived.

3.1 Structural Dynamic Analysis

A deformable body may drift away if not adequately constrained. In structural analysis, a 3-D structure often exhibits no rigid-body motion because at least six DOFs are properly constrained by so-called boundary conditions or simply called constraints.

3.1.1 Without constraints

In structural analysis, the equations of motion without constraints are posed as

$$\mathbf{M}\ddot{\boldsymbol{\delta}} + \mathbf{C}\dot{\boldsymbol{\delta}} + \mathbf{K}\boldsymbol{\delta} = \mathbf{f} \tag{3.1}$$

or

$$\mathbf{M}\ddot{\boldsymbol{\delta}} = -\mathbf{C}\dot{\boldsymbol{\delta}} - \mathbf{K}\boldsymbol{\delta} + \mathbf{f} \tag{3.2}$$

where $\mathbf{M}$ is the mass matrix, $\mathbf{C}$ is the damping matrix, $\mathbf{K}$ is the stiffness matrix, $\boldsymbol{\delta}$ is the vector of nodal deflections, and $\mathbf{f}$ is the vector of applied forces. Without at least six DOFs of rigid-body motion being properly removed, the body may drift under forces.

Since no moving reference frame is in place to follow the body, its dynamics can not be adequately determined.

3.1.2 Simple constraints

Suppose that at least six coordinates of a finite element model are grounded with zero displacements; label them as set *o*. The remaining coordinates are labeled as set *u*. Equation (3.2) is partitioned accordingly as

$$\begin{bmatrix} \mathbf{M}_{oo} & \mathbf{M}_{ou} \\ \mathbf{M}_{uo} & \mathbf{M}_{uu} \end{bmatrix} \begin{Bmatrix} \ddot{\boldsymbol{\delta}}_o \\ \ddot{\boldsymbol{\delta}}_u \end{Bmatrix} = -\begin{bmatrix} \mathbf{C}_{oo} & \mathbf{C}_{ou} \\ \mathbf{C}_{uo} & \mathbf{C}_{uu} \end{bmatrix} \begin{Bmatrix} \dot{\boldsymbol{\delta}}_o \\ \dot{\boldsymbol{\delta}}_u \end{Bmatrix} - \begin{bmatrix} \mathbf{K}_{oo} & \mathbf{K}_{ou} \\ \mathbf{K}_{uo} & \mathbf{K}_{uu} \end{bmatrix} \begin{Bmatrix} \boldsymbol{\delta}_o \\ \boldsymbol{\delta}_u \end{Bmatrix} + \begin{Bmatrix} \mathbf{f}_o \\ \mathbf{f}_u \end{Bmatrix} \tag{3.3}$$

Because $\boldsymbol{\delta}_o = \dot{\boldsymbol{\delta}}_o = \ddot{\boldsymbol{\delta}}_o = \mathbf{0}$ (simple constraints), the corresponding rows and columns in Eq. (3.3) may be removed, leading to the grounded equations of motion:

$$\mathbf{M}_{uu}\ddot{\boldsymbol{\delta}}_u = -\mathbf{C}_{uu}\dot{\boldsymbol{\delta}}_u - \mathbf{K}_{uu}\boldsymbol{\delta}_u + \mathbf{f}_u \tag{3.4}$$

Alternatively, these simple constraints can be introduced by the method of Lagrange multipliers:

$$\begin{bmatrix} \mathbf{M} & \mathbf{D}^{\mathrm{T}} \\ \mathbf{D} & \mathbf{0} \end{bmatrix} \begin{Bmatrix} \ddot{\boldsymbol{\delta}} \\ -\boldsymbol{\lambda} \end{Bmatrix} = \begin{Bmatrix} -\mathbf{C}\dot{\boldsymbol{\delta}} - \mathbf{K}\boldsymbol{\delta} + \mathbf{f} \\ \mathbf{0} \end{Bmatrix} \tag{3.5}$$

where $\mathbf{D} = \begin{bmatrix} \mathbf{I}_{oo} & \mathbf{0}_{ou} \end{bmatrix}$ is the Jacobian matrix and $\boldsymbol{\lambda}$ contains the Lagrange multipliers. The product of $\mathbf{D}^{\mathrm{T}}\boldsymbol{\lambda}$ accounts for the reaction forces due to the constraints. The second row, $\mathbf{D}\ddot{\boldsymbol{\delta}} = \begin{bmatrix} \mathbf{I}_{oo} & \mathbf{0}_{ou} \end{bmatrix} \begin{Bmatrix} \ddot{\boldsymbol{\delta}}_o \\ \ddot{\boldsymbol{\delta}}_u \end{Bmatrix} = \ddot{\boldsymbol{\delta}}_o = \mathbf{0}$, reflects the constraints at the acceleration level.

3.1.3 General constraints

General constraint equations can be explicitly a function of time as

$$\boldsymbol{\phi}(\boldsymbol{\delta}) = \mathbf{h}(t) \tag{3.6}$$

The first time derivatives are

$$\mathbf{D}\dot{\boldsymbol{\delta}} = \dot{\mathbf{h}} \tag{3.7}$$

where $\mathbf{D} = \dfrac{\partial \boldsymbol{\phi}}{\partial \boldsymbol{\delta}}$. The second time derivatives become

$$\mathbf{D}\ddot{\boldsymbol{\delta}} + \dot{\mathbf{D}}\dot{\boldsymbol{\delta}} = \ddot{\mathbf{h}} \quad \text{or} \quad \mathbf{D}\ddot{\boldsymbol{\delta}} = -\dot{\mathbf{D}}\dot{\boldsymbol{\delta}} + \ddot{\mathbf{h}} \tag{3.8}$$

The general equations of motion for a grounded structure are

$$\begin{bmatrix} \mathbf{M} & \mathbf{D}^{\mathrm{T}} \\ \mathbf{D} & \mathbf{0} \end{bmatrix} \begin{Bmatrix} \ddot{\boldsymbol{\delta}} \\ -\boldsymbol{\lambda} \end{Bmatrix} = \begin{Bmatrix} -\mathbf{C}\dot{\boldsymbol{\delta}} - \mathbf{K}\boldsymbol{\delta} + \mathbf{f} \\ -\dot{\mathbf{D}}\dot{\boldsymbol{\delta}} + \ddot{\mathbf{h}} \end{Bmatrix} \tag{3.9}$$

Note that Eq. (3.9) may only apply for cases where at least six coordinates have been fixed—zero or displaced (small). It is not valid for a structure that possesses (large) rigid-body motion.

3.2 Dynamics of a Moving Deformable Body

If a deformable body is allowed to translate and rotate in space, it makes sense to assign the body a floating reference frame. Doing so allows us to track large overall motion and still measure small deformation of the body.

3.2.1 Kinematics

In Figure 3-1, the **xyz** frame is the inertial coordinate system. A reference frame, $\xi\eta\zeta$, is assigned to the body. Vector **r** positions the origin of the $\xi\eta\zeta$ frame from the origin of

the **xyz** frame. Matrix **A** describes the orientation of the $\xi\eta\zeta$ frame in the **xyz** frame by direction cosines. Note that $\mathbf{A}^{-1} = \mathbf{A}^{\mathrm{T}}$ because **A** is orthogonal. When undeformed, a typical node, *j*, is located by $\mathbf{s}^j$ relative to the $\xi\eta\zeta$ frame. When deformed, the node displaces by $\boldsymbol{\delta}^j$; it is now located by $\mathbf{b}^j$, which is equal to $\mathbf{s}^j + \boldsymbol{\delta}^j$. Vectors $\mathbf{s}^j$, $\boldsymbol{\delta}^j$, and $\mathbf{b}^j$ contain coordinates with respect to the **xyz** frame. Vectors $\grave{\mathbf{s}}^j = \mathbf{A}^{\mathrm{T}}\mathbf{s}^j$, $\grave{\boldsymbol{\delta}}^j = \mathbf{A}^{\mathrm{T}}\boldsymbol{\delta}^j$, and $\grave{\mathbf{b}}^j = \mathbf{A}^{\mathrm{T}}\mathbf{b}^j$ contain coordinates with respect to the $\xi\eta\zeta$ frame; $\grave{\mathbf{b}}^j = \grave{\mathbf{s}}^j + \grave{\boldsymbol{\delta}}^j$. Vector $\mathbf{d}^j = \mathbf{r} + \mathbf{b}^j$ points to the absolute position of node *j* in the **xyz** frame.

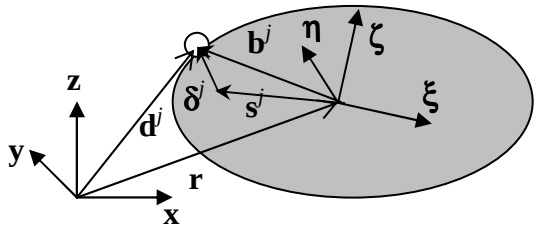

Figure 3-1: node kinematics

To vectorize the notation, all 3-vectors are stacked up:

$$\mathbf{s} = \bar{\mathbf{A}}\grave{\mathbf{s}} \tag{3.10}$$

$$\boldsymbol{\delta} = \bar{\mathbf{A}}\grave{\boldsymbol{\delta}} \tag{3.11}$$

$$\grave{\mathbf{b}} = \grave{\mathbf{s}} + \grave{\boldsymbol{\delta}} \tag{3.12}$$

$$\mathbf{b} = \mathbf{s} + \boldsymbol{\delta} = \bar{\mathbf{A}}\grave{\mathbf{b}} \tag{3.13}$$

$$\mathbf{d} = \hat{\mathbf{I}}\mathbf{r} + \mathbf{b} = \hat{\mathbf{I}}\mathbf{r} + \mathbf{s} + \boldsymbol{\delta} \tag{3.14}$$

Taking time derivative of Eq. (3.14) yields

$$\dot{\mathbf{d}} = \hat{\mathbf{I}}\dot{\mathbf{r}} + \dot{\mathbf{s}} + \tfrac{d}{dt}\left(\bar{\mathbf{A}}\grave{}\boldsymbol{\delta}\right) = \hat{\mathbf{I}}\dot{\mathbf{r}} + \bar{\tilde{\boldsymbol{\omega}}}\mathbf{s} + \left(\bar{\dot{\mathbf{A}}}\grave{}\boldsymbol{\delta} + \bar{\mathbf{A}}\grave{}\dot{\boldsymbol{\delta}}\right)$$
$$= \hat{\mathbf{I}}\dot{\mathbf{r}} + \bar{\tilde{\boldsymbol{\omega}}}\mathbf{s} + \left(\bar{\tilde{\boldsymbol{\omega}}}\bar{\mathbf{A}}\grave{}\boldsymbol{\delta} + \bar{\mathbf{A}}\grave{}\dot{\boldsymbol{\delta}}\right) = \hat{\mathbf{I}}\dot{\mathbf{r}} + \bar{\tilde{\boldsymbol{\omega}}}\left(\mathbf{s}+\boldsymbol{\delta}\right) + \dot{\boldsymbol{\delta}}$$

$$= \hat{\mathbf{I}}\dot{\mathbf{r}} - \tilde{\mathbf{b}}\boldsymbol{\omega} + \dot{\boldsymbol{\delta}} = \begin{bmatrix}\hat{\mathbf{I}} & -\tilde{\mathbf{b}} & \bar{\mathbf{I}}\end{bmatrix}\begin{Bmatrix}\dot{\mathbf{r}}\\ \boldsymbol{\omega}\\ \dot{\boldsymbol{\delta}}\end{Bmatrix} \tag{3.15}$$

where $\dot{\mathbf{A}} = \tilde{\boldsymbol{\omega}}\mathbf{A}$, and

$$\dot{\boldsymbol{\delta}} \triangleq \bar{\mathbf{A}}\grave{}\dot{\boldsymbol{\delta}} \tag{3.16}$$

since $\bar{\mathbf{A}}$ and $\grave{}\dot{\boldsymbol{\delta}}$ show up together so often; notice that $\dot{\boldsymbol{\delta}} \neq \tfrac{d}{dt}\left(\bar{\mathbf{A}}\grave{}\boldsymbol{\delta}\right)$. The time derivative of Eq. (3.15) is

$$\ddot{\mathbf{d}} = \hat{\mathbf{I}}\ddot{\mathbf{r}} - \dot{\tilde{\mathbf{b}}}\boldsymbol{\omega} - \tilde{\mathbf{b}}\dot{\boldsymbol{\omega}} + \frac{d\dot{\boldsymbol{\delta}}}{dt} = \hat{\mathbf{I}}\ddot{\mathbf{r}} + \bar{\tilde{\boldsymbol{\omega}}}\left(\bar{\tilde{\boldsymbol{\omega}}}\mathbf{b} + \dot{\boldsymbol{\delta}}\right) - \tilde{\mathbf{b}}\dot{\boldsymbol{\omega}} + \left(\bar{\tilde{\boldsymbol{\omega}}}\dot{\boldsymbol{\delta}} + \ddot{\boldsymbol{\delta}}\right)$$
$$= \hat{\mathbf{I}}\ddot{\mathbf{r}} - \tilde{\mathbf{b}}\dot{\boldsymbol{\omega}} + \ddot{\boldsymbol{\delta}} + \mathbf{w} = \begin{bmatrix}\hat{\mathbf{I}} & -\tilde{\mathbf{b}} & \bar{\mathbf{I}}\end{bmatrix}\begin{Bmatrix}\ddot{\mathbf{r}}\\ \dot{\boldsymbol{\omega}}\\ \ddot{\boldsymbol{\delta}}\end{Bmatrix} + \mathbf{w} \tag{3.17}$$

where

$$\ddot{\boldsymbol{\delta}} \triangleq \bar{\mathbf{A}}\grave{}\ddot{\boldsymbol{\delta}} \tag{3.18}$$

$$\mathbf{w} = \bar{\tilde{\boldsymbol{\omega}}}\bar{\tilde{\boldsymbol{\omega}}}\mathbf{b} + 2\bar{\tilde{\boldsymbol{\omega}}}\dot{\boldsymbol{\delta}} \tag{3.19}$$

in which $\bar{\tilde{\boldsymbol{\omega}}}\bar{\tilde{\boldsymbol{\omega}}}\mathbf{b}$ is the centrifugal acceleration and $2\bar{\tilde{\boldsymbol{\omega}}}\dot{\boldsymbol{\delta}}$ is the Coriolis acceleration.

The stiffness, mass, and damping matrices in the **xyz** frame are

$$\mathbf{K} = \bar{\mathbf{A}}\grave{}\mathbf{K}\bar{\mathbf{A}}^{\mathrm{T}} \tag{3.20}$$

$$\mathbf{M} = \bar{\mathbf{A}}\grave{}\mathbf{M}\bar{\mathbf{A}}^{\mathrm{T}} \tag{3.21}$$

$$\mathbf{C} = \bar{\mathbf{A}}\grave{}\mathbf{C}\bar{\mathbf{A}}^{\mathrm{T}} \tag{3.22}$$

while $\mathbf{`K}$, $\mathbf{`M}$, and $\mathbf{`C}$ are the corresponding matrices in the $\xi\eta\zeta$ frame. The inverse versions of Eqs. (3.20), (3.21), and (3.22) are

$$\mathbf{`K} = \bar{\mathbf{A}}^{-1}\mathbf{K}\bar{\mathbf{A}}^{-\mathrm{T}} = \bar{\mathbf{A}}^{\mathrm{T}}\mathbf{K}\bar{\mathbf{A}} \tag{3.23}$$

$$\mathbf{`M} = \bar{\mathbf{A}}^{-1}\mathbf{M}\bar{\mathbf{A}}^{-\mathrm{T}} = \bar{\mathbf{A}}^{\mathrm{T}}\mathbf{M}\bar{\mathbf{A}} \tag{3.24}$$

$$\mathbf{`C} = \bar{\mathbf{A}}^{-1}\mathbf{C}\bar{\mathbf{A}}^{-\mathrm{T}} = \bar{\mathbf{A}}^{\mathrm{T}}\mathbf{C}\bar{\mathbf{A}} \tag{3.25}$$

Note that $\mathbf{M} = \mathbf{`M}$ (constant) and

$$\dot{\mathbf{M}} = \dot{\bar{\mathbf{A}}}\mathbf{`M}\bar{\mathbf{A}}^{\mathrm{T}} + \cancel{\bar{\mathbf{A}}\mathbf{`M}\dot{\bar{\mathbf{A}}}^{\mathrm{T}}} + \bar{\mathbf{A}}\mathbf{`M}\dot{\bar{\mathbf{A}}}^{\mathrm{T}} = \bar{\tilde{\boldsymbol{\omega}}}\mathbf{M} - \mathbf{M}\bar{\tilde{\boldsymbol{\omega}}} \tag{3.26}$$

which vanishes ($\dot{\mathbf{M}} = \mathbf{0}$) if the mass matrix ($\mathbf{`M}$) is consistent or lumped. If the mass matrix is ever condensed (such as by Guyan reduction or other methods), quite likely $\mathbf{M} \neq \mathbf{`M}$ and $\dot{\mathbf{M}} \neq \mathbf{0}$.

3.2.2 Kinetics

Assume that a deformable body is unconstrained. Initially, no springs or other force elements that store potential energy are attached. Neither is it in any force fields such as gravity. If present, they can be introduced later in this section at appropriate points.

The kinetic energy is

$$T = \frac{1}{2}\dot{\mathbf{d}}^{\mathrm{T}}\mathbf{M}\dot{\mathbf{d}} \tag{3.27}$$

The potential (strain) energy is

$$V = \frac{1}{2}\boldsymbol{\delta}^{\mathrm{T}}\mathbf{K}\boldsymbol{\delta} \tag{3.28}$$

The Lagrangian function is

$$L = T - V \tag{3.29}$$

The Lagrange's equations are

$$\frac{d}{dt}\left(\frac{\partial L}{\partial \dot{\mathbf{d}}}\right)^{\mathrm{T}} - \left(\frac{\partial L}{\partial \mathbf{d}}\right)^{\mathrm{T}} = \mathbf{f}^{<\mathrm{L}>} \tag{3.30}$$

where

$$\frac{d}{dt}\left(\frac{\partial L}{\partial \dot{\mathbf{d}}}\right)^{\mathrm{T}} = \frac{d}{dt}\left(\frac{\partial T}{\partial \dot{\mathbf{d}}}\right)^{\mathrm{T}} = \frac{d}{dt}\left(\mathbf{M}\dot{\mathbf{d}}\right) = \mathbf{M}\ddot{\mathbf{d}} + \dot{\mathbf{M}}\dot{\mathbf{d}} \tag{3.31}$$

$$\left(\frac{\partial L}{\partial \mathbf{d}}\right)^{\mathrm{T}} = -\left(\frac{\partial V}{\partial \mathbf{d}}\right)^{\mathrm{T}} = -\mathbf{K}\boldsymbol{\delta} \tag{3.32}$$

The right-hand-side of Eq. (3.30), $\mathbf{f}^{<\mathrm{L}>}$, consists of forces from various sources:

- conservative forces that are not included in V such as spring forces and gravitational force $\mathbf{M}\hat{\mathbf{g}}$ *
- non-conservative forces such as damper forces, structural damping $-\mathbf{C}\dot{\boldsymbol{\delta}}$, and directly applied forces

Expanding Eq. (3.30) and using Eqs. (3.31) and (3.32) produces the equations of motion in $\ddot{\mathbf{d}}$:

$$\mathbf{M}\ddot{\mathbf{d}} = -\dot{\mathbf{M}}\dot{\mathbf{d}} - \mathbf{K}\boldsymbol{\delta} + \mathbf{f}^{<\mathrm{L}>} = \mathbf{f}^{<\mathrm{d}>} \tag{3.33}$$

The accelerations $\ddot{\mathbf{d}}$ can be solved from Eq. (3.33) if its right-hand-side is known.

Substituting Eq. (3.17) into Eq. (3.33) gives

---

* On the Earth surface, the vector of gravity constants, **g**, is $\{0,0,-9.80665\}^{\mathrm{T}}$ pointing "downwards."

$$\mathbf{MQ}\begin{Bmatrix}\ddot{\mathbf{r}}\\ \dot{\boldsymbol{\omega}}\\ \ddot{\boldsymbol{\delta}}\end{Bmatrix} = -\mathbf{Mw} + \mathbf{f}^{<d>} = \mathbf{f} \tag{3.34}$$

in which

$$\mathbf{Q} = \begin{bmatrix}\hat{\mathbf{I}} & -\tilde{\mathbf{b}} & \bar{\mathbf{I}}\end{bmatrix} \tag{3.35}$$

Pre-multiplying Eq. (3.34) by $\mathbf{Q}^{\mathrm{T}}$ yields the equations of motion in $\ddot{\boldsymbol{\delta}}$:

$$\mathbf{Q}^{\mathrm{T}}\mathbf{MQ}\begin{Bmatrix}\ddot{\mathbf{r}}\\ \dot{\boldsymbol{\omega}}\\ \ddot{\boldsymbol{\delta}}\end{Bmatrix} = \mathbf{Q}^{\mathrm{T}}\mathbf{f} \tag{3.36}$$

or

$$\begin{bmatrix} \hat{\mathbf{I}}^{\mathrm{T}}\mathbf{M}\hat{\mathbf{I}} & -\hat{\mathbf{I}}^{\mathrm{T}}\mathbf{M}\tilde{\mathbf{b}} & \hat{\mathbf{I}}^{\mathrm{T}}\mathbf{M} \\ -\tilde{\mathbf{b}}^{\mathrm{T}}\mathbf{M}\hat{\mathbf{I}} & \tilde{\mathbf{b}}^{\mathrm{T}}\mathbf{M}\tilde{\mathbf{b}} & -\tilde{\mathbf{b}}^{\mathrm{T}}\mathbf{M} \\ \mathbf{M}\hat{\mathbf{I}} & -\mathbf{M}\tilde{\mathbf{b}} & \mathbf{M} \end{bmatrix}\begin{Bmatrix}\ddot{\mathbf{r}}\\ \dot{\boldsymbol{\omega}}\\ \ddot{\boldsymbol{\delta}}\end{Bmatrix} = \begin{Bmatrix} \hat{\mathbf{I}}^{\mathrm{T}}\mathbf{f} \\ -\tilde{\mathbf{b}}^{\mathrm{T}}\mathbf{f} \\ \mathbf{f} \end{Bmatrix} \tag{3.37}$$

Substituting $\ddot{\boldsymbol{\delta}} \triangleq \bar{\mathbf{A}}\grave{\ddot{\boldsymbol{\delta}}}$ into Eq. (3.37) and pre-multiplying the third row by $\bar{\mathbf{A}}^{\mathrm{T}}$ yields the equations of motion in $\grave{\ddot{\boldsymbol{\delta}}}$:

$$\begin{bmatrix} \hat{\mathbf{I}}^{\mathrm{T}}\mathbf{M}\hat{\mathbf{I}} & -\hat{\mathbf{I}}^{\mathrm{T}}\mathbf{M}\tilde{\mathbf{b}} & \hat{\mathbf{I}}^{\mathrm{T}}\mathbf{M}\bar{\mathbf{A}} \\ -\tilde{\mathbf{b}}^{\mathrm{T}}\mathbf{M}\hat{\mathbf{I}} & \tilde{\mathbf{b}}^{\mathrm{T}}\mathbf{M}\tilde{\mathbf{b}} & -\tilde{\mathbf{b}}^{\mathrm{T}}\mathbf{M}\bar{\mathbf{A}} \\ \bar{\mathbf{A}}^{\mathrm{T}}\mathbf{M}\hat{\mathbf{I}} & -\bar{\mathbf{A}}^{\mathrm{T}}\mathbf{M}\tilde{\mathbf{b}} & \bar{\mathbf{A}}^{\mathrm{T}}\mathbf{M}\bar{\mathbf{A}} \end{bmatrix}\begin{Bmatrix}\ddot{\mathbf{r}}\\ \dot{\boldsymbol{\omega}}\\ \grave{\ddot{\boldsymbol{\delta}}}\end{Bmatrix} = \begin{Bmatrix} \hat{\mathbf{I}}^{\mathrm{T}}\mathbf{f} \\ -\tilde{\mathbf{b}}^{\mathrm{T}}\mathbf{f} \\ \bar{\mathbf{A}}^{\mathrm{T}}\mathbf{f} \end{Bmatrix} \tag{3.38}$$

On the left-hand-side of Eq. (3.37) or Eq. (3.38),

$$\hat{\mathbf{I}}^{\mathrm{T}}\mathbf{M}\hat{\mathbf{I}} = m\mathbf{I} \tag{3.39}$$

where the total mass, *m*, shows. The inertia matrix is revealed by

$$\tilde{\mathbf{b}}^{\mathrm{T}}\mathbf{M}\tilde{\mathbf{b}} = \mathbf{J} = \mathbf{A}\grave{\mathbf{J}}\mathbf{A}^{\mathrm{T}} = \mathbf{A}\left(\grave{\tilde{\mathbf{b}}}^{\mathrm{T}}\grave{\mathbf{M}}\grave{\tilde{\mathbf{b}}}\right)\mathbf{A}^{\mathrm{T}} \tag{3.40}$$

On the right-hand-side, all the forces are summed up to the resultant forces by

$$\hat{\mathbf{I}}^{\mathrm{T}}\mathbf{f} = \sum \mathbf{f}^{j} \tag{3.41}$$

Also, all the moments are summed up to the resultant moments by

$$-\tilde{\mathbf{b}}^{\mathrm{T}}\mathbf{f} = \sum \tilde{\mathbf{b}}^{j}\mathbf{f}^{j} = \mathbf{A}\sum \grave{\tilde{\mathbf{b}}}^{j}\grave{\mathbf{f}}^{j} = \mathbf{A}\left(-\grave{\tilde{\mathbf{b}}}^{\mathrm{T}}\grave{\mathbf{f}}\right) \tag{3.42}$$

Although $\mathbf{M}$ is non-singular, $\mathbf{Q}^{\mathrm{T}}\mathbf{M}\mathbf{Q}$ has six rank deficiencies owing to the introduction of the floating reference frame. Consequently, Eqs. (3.37) and (3.38) can not be solved until the so-called axis conditions are defined. Chapter 4 AXIS CONDITIONS will resolve this issue. Once the axis conditions are defined, $\ddot{\mathbf{r}}$, $\dot{\boldsymbol{\omega}}$, and $\grave{\ddot{\boldsymbol{\delta}}}$ can be solved and then integrated to advance in time.

In this section, we have discussed the case where a deformable body is unconstrained (that is, free of kinematic joints); springs and other forces, conservative or not, may exist. For the equations of motion for a deformable body that is connected to another body or bodies (such as thru spherical joints), please refer to Chapter 5 RIGID-DEFORMABLE MULTIBODY SYSTEM.

4 AXIS CONDITIONS

A floating reference frame is introduced to follow the deformable body and to measure its nodal deformation. Since the reference frame itself brings in six additional DOFs in 3-D space, six mathematical constraints or axis conditions must be established. Although there are different types of axis conditions [21], in this chapter we only discuss a few of them.

4.1 Nodal-Fixed Axes

A simple and common way for attaching a reference frame to a deformable body in motion is by nodal-fixed axes. Basically six nodal deformation coordinates are set to zero, thereby anchoring the axes to the body (or vice versa, depending on how one sees it). In the cases where each node has three translational and three rotational DOFs, setting all six nodal deflections of one node to zero is good enough although other options are available. But when each node has only three translational DOFs, the six anchoring coordinates must come from more than one node. As shown in Figure 4-1, a usual setup calls for three nodes, for instance, *i*, *j*, and *k*. The origin, *O*, of the reference frame is always at node *i*; this requires $\grave{\delta}^i_\xi = \grave{\delta}^i_\eta = \grave{\delta}^i_\zeta = 0$. The ξ axis goes through node *j*, which demands $\grave{\delta}^j_\eta = \grave{\delta}^j_\zeta = 0$. For node *k* to stay on the $\xi\eta$ plane, $\grave{\delta}^k_\zeta = 0$ is needed. That is just one possible configuration, listed as the first entry in Table 4-1. Altogether there are six configurations, depending on which axis goes through node *j* and which plane node *k* is on.

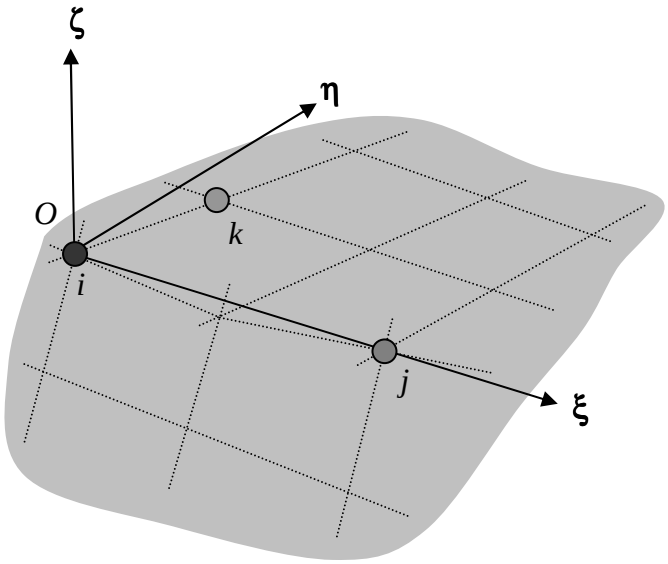

Figure 4-1: nodal-fixed axes

Table 4-1: nodal-fixed axis conditions

i		*j*		*k*	
at	three zeros	through	two zeros	on	one zero
O	$\grave{\delta}_{\xi}^{i} = \grave{\delta}_{\eta}^{i} = \grave{\delta}_{\zeta}^{i} = 0$	ξ	$\grave{\delta}_{\eta}^{j} = \grave{\delta}_{\zeta}^{j} = 0$	ξη	$\grave{\delta}_{\zeta}^{k} = 0$
				ξζ	$\grave{\delta}_{\eta}^{k} = 0$
		η	$\grave{\delta}_{\zeta}^{j} = \grave{\delta}_{\xi}^{j} = 0$	ηζ	$\grave{\delta}_{\xi}^{k} = 0$
				ηξ	$\grave{\delta}_{\zeta}^{k} = 0$
		ζ	$\grave{\delta}_{\xi}^{j} = \grave{\delta}_{\eta}^{j} = 0$	ζξ	$\grave{\delta}_{\eta}^{k} = 0$
				ζη	$\grave{\delta}_{\xi}^{k} = 0$

The nodal-fixed axis conditions set six coordinates to zero; label them as set *o*. The remaining coordinates are labeled as set *u*. The nodal deformation in local coordinates may be split and rewritten as

$$\grave{\boldsymbol{\delta}} = \begin{Bmatrix} \grave{\boldsymbol{\delta}}_o \\ \grave{\boldsymbol{\delta}}_u \end{Bmatrix} = \grave{\boldsymbol{\Psi}} \grave{\boldsymbol{\delta}}_u \tag{4.1}$$

where

$$\grave{\boldsymbol{\Psi}} = \begin{bmatrix} \mathbf{0}_{ou} \\ \mathbf{I}_{uu} \end{bmatrix} \tag{4.2}$$

Matrix $\grave{\boldsymbol{\Psi}}$ ensures that $\grave{\boldsymbol{\delta}}_o$ is zero and $\grave{\boldsymbol{\delta}}_u$ is unchanged. Similarly,

$$\dot{\grave{\boldsymbol{\delta}}} = \grave{\boldsymbol{\Psi}}\dot{\grave{\boldsymbol{\delta}}}_u \tag{4.3}$$

$$\ddot{\grave{\boldsymbol{\delta}}} = \grave{\boldsymbol{\Psi}}\ddot{\grave{\boldsymbol{\delta}}}_u \tag{4.4}$$

Substituting Eq. (4.4) into Eq. (3.38) and pre-multiplying its third row by $\grave{\boldsymbol{\Psi}}^{\mathrm{T}}$ yields the equations of motion that are now equipped with the nodal-fixed axis conditions*

$$\begin{bmatrix} \hat{\mathbf{I}}^{\mathrm{T}}\mathbf{M}\hat{\mathbf{I}} & -\hat{\mathbf{I}}^{\mathrm{T}}\mathbf{M}\tilde{\mathbf{b}} & \hat{\mathbf{I}}^{\mathrm{T}}\mathbf{M}\boldsymbol{\Psi} \\ -\tilde{\mathbf{b}}^{\mathrm{T}}\mathbf{M}\hat{\mathbf{I}} & \tilde{\mathbf{b}}^{\mathrm{T}}\mathbf{M}\tilde{\mathbf{b}} & -\tilde{\mathbf{b}}^{\mathrm{T}}\mathbf{M}\boldsymbol{\Psi} \\ \boldsymbol{\Psi}^{\mathrm{T}}\mathbf{M}\hat{\mathbf{I}} & -\boldsymbol{\Psi}^{\mathrm{T}}\mathbf{M}\tilde{\mathbf{b}} & \boldsymbol{\Psi}^{\mathrm{T}}\mathbf{M}\boldsymbol{\Psi} \end{bmatrix} \begin{Bmatrix} \ddot{\mathbf{r}} \\ \dot{\boldsymbol{\omega}} \\ \ddot{\grave{\boldsymbol{\delta}}}_u \end{Bmatrix} = \begin{Bmatrix} \hat{\mathbf{I}}^{\mathrm{T}}\mathbf{f} \\ -\tilde{\mathbf{b}}^{\mathrm{T}}\mathbf{f} \\ \boldsymbol{\Psi}^{\mathrm{T}}\mathbf{f} \end{Bmatrix} \tag{4.5}$$

in which

$$\boldsymbol{\Psi} \triangleq \bar{\mathbf{A}}\grave{\boldsymbol{\Psi}} \tag{4.6}$$

$$\boldsymbol{\Psi}^{\mathrm{T}}\mathbf{M}\boldsymbol{\Psi} = \grave{\boldsymbol{\Psi}}^{\mathrm{T}}\grave{\mathbf{M}}\grave{\boldsymbol{\Psi}} = \grave{\mathbf{M}}_{uu} \tag{4.7}$$

$$\boldsymbol{\Psi}^{\mathrm{T}}\mathbf{f} = \grave{\boldsymbol{\Psi}}^{\mathrm{T}}\grave{\mathbf{f}} = \grave{\mathbf{f}}_u \tag{4.8}$$

Equation (4.7) shows that $\boldsymbol{\Psi}^{\mathrm{T}}\mathbf{M}\boldsymbol{\Psi}$ evaluates to $\grave{\mathbf{M}}_{uu}$, which is constant.

---

* Alternatively, we can introduce the nodal-fixed axis conditions by the method of Lagrange multipliers.

4.2 Mean Axes

To establish a reference frame, mean axes require six mathematical constraints obtained by minimizing the deformation kinetic energy to the frame motion [22, 23, 20]. The kinetic energy associated with deformation is

$$KE = \frac{1}{2}\dot{\boldsymbol{\delta}}^{\mathrm{T}}\mathbf{M}\dot{\boldsymbol{\delta}} \tag{4.9}$$

By setting to zero the partial derivatives of KE with respect to $\dot{\mathbf{r}}$ and $\boldsymbol{\omega}$, we obtain

$$-\left(\frac{\partial KE}{\partial \dot{\mathbf{r}}}\right)^{\mathrm{T}} = \hat{\mathbf{I}}^{\mathrm{T}}\mathbf{M}\dot{\boldsymbol{\delta}} = \mathbf{0} \tag{4.10}$$

$$\left(\frac{\partial KE}{\partial \boldsymbol{\omega}}\right)^{\mathrm{T}} = \tilde{\mathbf{b}}^{\mathrm{T}}\mathbf{M}\dot{\boldsymbol{\delta}} = \mathbf{0} \tag{4.11}$$

Indeed this is happening at the minimum, not the maximum, because its second partial derivatives are positive definite; i.e.,

$$\frac{\partial}{\partial \dot{\mathbf{r}}}\left(\frac{\partial KE}{\partial \dot{\mathbf{r}}}\right)^{\mathrm{T}} = \hat{\mathbf{I}}^{\mathrm{T}}\mathbf{M}\hat{\mathbf{I}} = m\mathbf{I} \tag{4.12}$$

$$\frac{\partial}{\partial \boldsymbol{\omega}}\left(\frac{\partial KE}{\partial \boldsymbol{\omega}}\right)^{\mathrm{T}} = \tilde{\mathbf{b}}^{\mathrm{T}}\mathbf{M}\tilde{\mathbf{b}} = \mathbf{J} \tag{4.13}$$

Equations (4.10) and (4.11) are transformed into local form as

$$\mathbf{A}^{\mathrm{T}}\left[\hat{\mathbf{I}}^{\mathrm{T}}\mathbf{M}\dot{\boldsymbol{\delta}}\right] = \hat{\mathbf{I}}^{\mathrm{T}}\grave{\mathbf{M}}\grave{\boldsymbol{\delta}} = \mathbf{0} \tag{4.14}$$

$$\mathbf{A}^{\mathrm{T}}\left[\tilde{\mathbf{b}}^{\mathrm{T}}\mathbf{M}\dot{\boldsymbol{\delta}}\right] = \grave{\tilde{\mathbf{b}}}^{\mathrm{T}}\grave{\mathbf{M}}\grave{\boldsymbol{\delta}} = \mathbf{0} \tag{4.15}$$

The time derivatives of Eqs. (4.14) and (4.15) are

$$\hat{\mathbf{I}}^{\mathrm{T}}\grave{\mathbf{M}}\ddot{\boldsymbol{\delta}} = \mathbf{0} \tag{4.16}$$

$$\grave{\tilde{\mathbf{b}}}^T \grave{\mathbf{M}} \ddot{\grave{\boldsymbol{\delta}}} = -\dot{\tilde{\grave{\boldsymbol{\delta}}}}^T \grave{\mathbf{M}} \dot{\grave{\boldsymbol{\delta}}} \tag{4.17}$$

Equations (4.16) and (4.17) in global form are

$$\hat{\mathbf{I}}^T \mathbf{M} \ddot{\boldsymbol{\delta}} = \mathbf{0} \tag{4.18}$$

$$\tilde{\mathbf{b}}^T \mathbf{M} \ddot{\boldsymbol{\delta}} = -\dot{\tilde{\boldsymbol{\delta}}}^T \mathbf{M} \dot{\boldsymbol{\delta}} \tag{4.19}$$

Note that $\dot{\tilde{\grave{\boldsymbol{\delta}}}}^T \grave{\mathbf{M}} \dot{\grave{\boldsymbol{\delta}}}$, as well as $\dot{\tilde{\boldsymbol{\delta}}}^T \mathbf{M} \dot{\boldsymbol{\delta}}$, is all zeros if $\grave{\mathbf{M}}$ is constructed properly—consistent or lumped. The statement is not true, for example, if $\grave{\mathbf{M}}$ is Guyan-reduced. The time integration of Eq. (4.14) is

$$\hat{\mathbf{I}}^T \grave{\mathbf{M}} \dot{\grave{\boldsymbol{\delta}}} = \mathbf{0} \tag{4.20}$$

The global form of Eq. (4.20) is

$$\hat{\mathbf{I}}^T \mathbf{M} \dot{\boldsymbol{\delta}} = \mathbf{0} \tag{4.21}$$

There is no corresponding integral for Eq. (4.15) because it is non-holonomic. Table 4-2 summarizes the mean axis conditions (MACs) at all three levels in both global and local forms.

Table 4-2: mean axis conditions

MAC		global	local
positional	translational	$\hat{\mathbf{I}}^T \mathbf{M} \boldsymbol{\delta} = \mathbf{0}$	$\hat{\mathbf{I}}^T \grave{\mathbf{M}} \grave{\boldsymbol{\delta}} = \mathbf{0}$
	rotational		
velocity	translational	$\hat{\mathbf{I}}^T \mathbf{M} \dot{\boldsymbol{\delta}} = \mathbf{0}$	$\hat{\mathbf{I}}^T \grave{\mathbf{M}} \dot{\grave{\boldsymbol{\delta}}} = \mathbf{0}$
	rotational	$\tilde{\mathbf{b}}^T \mathbf{M} \dot{\boldsymbol{\delta}} = \mathbf{0}$	$\grave{\tilde{\mathbf{b}}}^T \grave{\mathbf{M}} \dot{\grave{\boldsymbol{\delta}}} = \mathbf{0}$
acceleration	translational	$\hat{\mathbf{I}}^T \mathbf{M} \ddot{\boldsymbol{\delta}} = \mathbf{0}$	$\hat{\mathbf{I}}^T \grave{\mathbf{M}} \ddot{\grave{\boldsymbol{\delta}}} = \mathbf{0}$
	rotational	$\tilde{\mathbf{b}}^T \mathbf{M} \ddot{\boldsymbol{\delta}} = -\dot{\tilde{\boldsymbol{\delta}}}^T \mathbf{M} \dot{\boldsymbol{\delta}}$	$\grave{\tilde{\mathbf{b}}}^T \grave{\mathbf{M}} \ddot{\grave{\boldsymbol{\delta}}} = -\dot{\tilde{\grave{\boldsymbol{\delta}}}}^T \grave{\mathbf{M}} \dot{\grave{\boldsymbol{\delta}}}$

If the origin of a reference frame is positioned at the mass center when the body is undeformed ($\hat{\mathbf{I}}^T \grave{\mathbf{M}} \grave{\mathbf{s}} = \mathbf{0}$), the positional translational mean axis conditions ($\hat{\mathbf{I}}^T \grave{\mathbf{M}} \grave{\boldsymbol{\delta}} = \mathbf{0}$)

guarantee that the origin will always stay at the mass center when the body moves and deforms (because $\hat{\mathbf{I}}^{\mathrm{T}}\grave{\mathbf{M}}\grave{\mathbf{b}} = \mathbf{0}$ where $\grave{\mathbf{b}} = \grave{\mathbf{s}} + \grave{\boldsymbol{\delta}}$), as illustrated in Figure 4-2. If the origin is not initially at the mass center, i.e., $\hat{\mathbf{I}}^{\mathrm{T}}\grave{\mathbf{M}}\grave{\mathbf{s}} \neq \mathbf{0}$, then the origin will certainly remain so and not at the mass center because $\hat{\mathbf{I}}^{\mathrm{T}}\grave{\mathbf{M}}\grave{\mathbf{b}} = \hat{\mathbf{I}}^{\mathrm{T}}\grave{\mathbf{M}}\left(\grave{\mathbf{s}} + \grave{\boldsymbol{\delta}}\right) \neq \mathbf{0}$, but the mean axis conditions stated in Table 4-2 are still true. Since there are no positional rotational constraints, there are no requirements on how to align the axes initially. Note that mean axes are not physically fixed but mathematically tied to all the nodes.

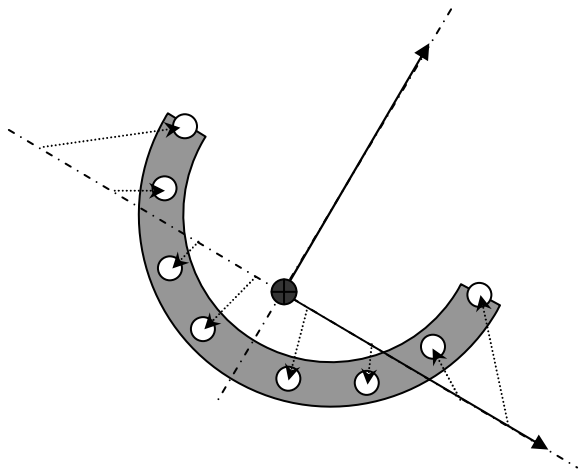

Figure 4-2: mean axes

The mean axis conditions can be introduced implicitly as stated in [20]. Or, one may explicitly introduce the mean axis conditions, Eqs. (4.18) and (4.19), into the equations of motion, Eq. (3.37), by the method of Lagrange multipliers:

$$\left[\begin{array}{ccc|cc} \hat{\mathbf{I}}^{\mathrm{T}}\mathbf{M}\hat{\mathbf{I}} & -\hat{\mathbf{I}}^{\mathrm{T}}\mathbf{M}\tilde{\mathbf{b}} & \hat{\mathbf{I}}^{\mathrm{T}}\mathbf{M} & \mathbf{0} & \mathbf{0} \\ -\tilde{\mathbf{b}}^{\mathrm{T}}\mathbf{M}\hat{\mathbf{I}} & \tilde{\mathbf{b}}^{\mathrm{T}}\mathbf{M}\tilde{\mathbf{b}} & -\tilde{\mathbf{b}}^{\mathrm{T}}\mathbf{M} & \mathbf{0} & \mathbf{0} \\ \mathbf{M}\hat{\mathbf{I}} & -\mathbf{M}\tilde{\mathbf{b}} & \mathbf{M} & \mathbf{M}\hat{\mathbf{I}} & \mathbf{M}\tilde{\mathbf{b}} \\ \hline \mathbf{0} & \mathbf{0} & \hat{\mathbf{I}}^{\mathrm{T}}\mathbf{M} & \mathbf{0} & \mathbf{0} \\ \mathbf{0} & \mathbf{0} & \tilde{\mathbf{b}}^{\mathrm{T}}\mathbf{M} & \mathbf{0} & \mathbf{0} \end{array}\right] \left\{\begin{array}{c} \ddot{\mathbf{r}} \\ \dot{\boldsymbol{\omega}} \\ \ddot{\boldsymbol{\delta}} \\ \hline \boldsymbol{\lambda}_1 \\ \boldsymbol{\lambda}_2 \end{array}\right\} = \left\{\begin{array}{c} \hat{\mathbf{I}}^{\mathrm{T}}\mathbf{f} \\ -\tilde{\mathbf{b}}^{\mathrm{T}}\mathbf{f} \\ \mathbf{f} \\ \hline \mathbf{0} \\ -\tilde{\dot{\boldsymbol{\delta}}}^{\mathrm{T}}\mathbf{M}\dot{\boldsymbol{\delta}} \end{array}\right\} \tag{4.22}$$

Note that $\tilde{\mathbf{b}}^{\mathrm{T}}\mathbf{M}\hat{\mathbf{I}}$, which is equal to the transpose of $\hat{\mathbf{I}}^{\mathrm{T}}\mathbf{M}\tilde{\mathbf{b}}$, should be zero if the origin is at the mass center and the mass matrix is consistent or lumped.

4.3 Principal Axes

For a deformable body described by a finite element model, the inertia matrix in local components is computed as

$$\grave{\tilde{\mathbf{b}}}^{\mathrm{T}}\grave{\mathbf{M}}\grave{\tilde{\mathbf{b}}} = \grave{\mathbf{J}} = \begin{bmatrix} \grave{J}_{\xi\xi} & \grave{J}_{\xi\eta} & \grave{J}_{\xi\zeta} \\ \grave{J}_{\eta\xi} & \grave{J}_{\eta\eta} & \grave{J}_{\eta\zeta} \\ \grave{J}_{\zeta\xi} & \grave{J}_{\zeta\eta} & \grave{J}_{\zeta\zeta} \end{bmatrix} \tag{4.23}$$

where $\grave{\mathbf{J}}$ is symmetric; i.e., $\grave{J}_{\xi\eta} = \grave{J}_{\eta\xi}$, $\grave{J}_{\eta\zeta} = \grave{J}_{\zeta\eta}$, and $\grave{J}_{\zeta\xi} = \grave{J}_{\xi\zeta}$. For the coordinate axes to coincide with the principal axes, the products of inertia—$\grave{J}_{\xi\eta}$, $\grave{J}_{\eta\zeta}$, and $\grave{J}_{\zeta\xi}$—must vanish [26], which provides three constraint equations. The other three constraint equations are borrowed from the translational mean axis conditions that place the origin at the mass center. For details, please refer to [24, 25].

4.4 Comments

For a deformable body in 3-D space, six axis conditions are required to define its floating reference frame with which its overall body motion is tracked and from which its small nodal deformation is measured. What is interesting about the axis conditions is that,

when incorporated by the method of Lagrange multipliers, their Lagrange multipliers are found zero. This is no surprise since the axes are set up deliberately not to incur any reaction forces. Whereas nodal-fixed axes are physically attached to some nodes, mean axes and principal axes are not but mathematically tied to all the nodes. A nodal-fixed frame may be easier to understand and deploy, yet there are disadvantages. When simulation results are expected to be symmetrical, nodal-fixed frames might be unable to offer so. For details, see Section 5.3.3 Nodal-fixed axes versus mean axes.

5 RIGID-DEFORMABLE MULTIBODY SYSTEM

In this chapter, we discuss the complete equations of motion for a typical rigid-deformable multibody system in which one rigid body and one deformable body are connected by a spherical joint. Nodal and modal formulations with nodal-fixed and mean axis frames are presented. The advantages of mean axes over nodal-fixed axes are also pointed out. The purposes of this chapter are to finally put together what have been discussed in previous chapters (amounting to the nodal formulations) and to simply announce what will be further discussed in later chapters (mainly for the modal formulations). Because of this nature, some of the materials are brief.

5.1 A Typical System

In Figure 5-1, a spherical joint connects a rigid body (left subscript *R*) and a deformable body. Point *j* on the rigid body meets node *j* on the deformable body. There are springs, dampers, and/or actuators between the two bodies. These two bodies may be connected to other bodies in a similar manner. Other forces (not shown) may also act on individual bodies. For simplicity, yet without any lose of generality, this system is shown to consist of only one rigid body, one deformable body, and one spherical joint. Applications can be easily extended to mixed rigid/deformable bodies and multiple joints (even joints of different types).

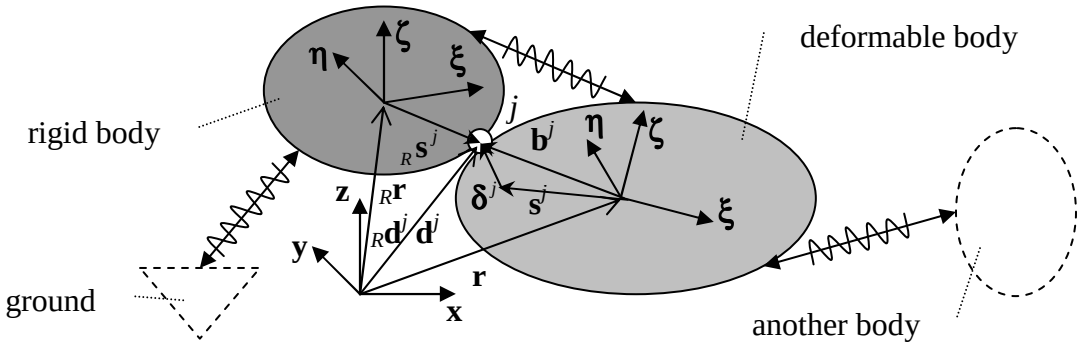

Figure 5-1: a rigid-deformable multibody system

5.2 Spherical Joint

As shown in Figure 5-1, point *j* on the rigid body meets node *j* on the deformable body. Point *j* is located by ${}_R\mathbf{d}^j = {}_R\mathbf{r} + {}_R\mathbf{s}^j$; node *j* is located by $\mathbf{d}^j = \mathbf{r} + \mathbf{s}^j + \boldsymbol{\delta}^j$. The two bodies can pivot freely relative to each other but may not separate, thus forming a spherical joint. The constraint equations at the position level are ${}_R\mathbf{d}^j = \mathbf{d}^j$ or

$$ {}_R\mathbf{r} + {}_R\mathbf{s}^j = \mathbf{r} + \mathbf{s}^j + \boldsymbol{\delta}^j \tag{5.1} $$

The constraint equations at the velocity and acceleration levels are

$$ {}_R\dot{\mathbf{r}} + {}_R\tilde{\boldsymbol{\omega}}_R\mathbf{s}^j = \dot{\mathbf{r}} - \tilde{\mathbf{b}}^j\boldsymbol{\omega} + \dot{\boldsymbol{\delta}}^j \tag{5.2} $$

$$ {}_R\ddot{\mathbf{r}} + {}_R\dot{\tilde{\boldsymbol{\omega}}}_R\mathbf{s}^j + {}_R\tilde{\boldsymbol{\omega}}_R\dot{\mathbf{s}}^j = \ddot{\mathbf{r}} - \tilde{\mathbf{b}}^j\dot{\boldsymbol{\omega}} + \ddot{\boldsymbol{\delta}}^j + \mathbf{w}^j \tag{5.3} $$

where

$$ {}_R\dot{\mathbf{s}}^j = {}_R\tilde{\boldsymbol{\omega}}_R\mathbf{s}^j \tag{5.4} $$

$$ \mathbf{w}^j = \tilde{\boldsymbol{\omega}}\tilde{\boldsymbol{\omega}}\mathbf{b}^j + 2\tilde{\boldsymbol{\omega}}\dot{\boldsymbol{\delta}}^j \tag{5.5} $$

The term $\ddot{\boldsymbol{\delta}}^j$ can be rewritten as

$$\ddot{\boldsymbol{\delta}}^j = \begin{bmatrix} \mathbf{0} & \mathbf{I} & \mathbf{0} \end{bmatrix} \begin{Bmatrix} \vdots \\ \ddot{\boldsymbol{\delta}}^j \\ \vdots \end{Bmatrix} \triangleq \bar{\mathbf{I}}^j \ddot{\boldsymbol{\delta}} \tag{5.6}$$

Substituting Eq. (5.6) into Eq. (5.3) and rearranging it yields

$$\left[\mathbf{I} \quad -{}_R\tilde{\mathbf{s}}^j \;\middle|\; -\mathbf{I} \quad +\tilde{\mathbf{b}}^j \quad -\bar{\mathbf{I}}^j \right] \begin{Bmatrix} {}_R\ddot{\mathbf{r}} \\ {}_R\dot{\boldsymbol{\omega}} \\ \hline \ddot{\mathbf{r}} \\ \dot{\boldsymbol{\omega}} \\ \ddot{\boldsymbol{\delta}} \end{Bmatrix} = -{}_R\tilde{\boldsymbol{\omega}}_R \dot{\mathbf{s}}^j + \mathbf{w}^j \tag{5.7}$$

The coefficient matrix in Eq. (5.7) is the Jacobian matrix or simply the Jacobian.

5.3 Nodal Formulations

In nodal formulations, the accelerations to be solved for the deformable body are $\ddot{\mathbf{r}}$, $\dot{\boldsymbol{\omega}}$, and $\ddot{\boldsymbol{\delta}}$ or $\ddot{\boldsymbol{\delta}}$. The following equations are needed:

- unconstrained equations of motion for the rigid body, Eq. (2.25)
- unconstrained equations of motion for the deformable body, Eq. (3.37)
- constraint equations for the spherical joint, Eq. (5.7)

Thru the method of Lagrange multipliers, the connected equations of motion are

$$\left[\begin{array}{cc|ccc|c} {}_Rm\mathbf{I} & \mathbf{0} & \mathbf{0} & \mathbf{0} & \mathbf{0} & \mathbf{I}^{\mathrm{T}} \\ \mathbf{0} & {}_R\mathbf{J} & \mathbf{0} & \mathbf{0} & \mathbf{0} & -{}_R\tilde{\mathbf{s}}^{j\mathrm{T}} \\ \hline \mathbf{0} & \mathbf{0} & \hat{\mathbf{I}}^{\mathrm{T}}\mathbf{M}\hat{\mathbf{I}} & -\hat{\mathbf{I}}^{\mathrm{T}}\mathbf{M}\tilde{\mathbf{b}} & \hat{\mathbf{I}}^{\mathrm{T}}\mathbf{M} & -\mathbf{I}^{\mathrm{T}} \\ \mathbf{0} & \mathbf{0} & -\tilde{\mathbf{b}}^{\mathrm{T}}\mathbf{M}\hat{\mathbf{I}} & \tilde{\mathbf{b}}^{\mathrm{T}}\mathbf{M}\tilde{\mathbf{b}} & -\tilde{\mathbf{b}}^{\mathrm{T}}\mathbf{M} & \tilde{\mathbf{b}}^{j\mathrm{T}} \\ \mathbf{0} & \mathbf{0} & \mathbf{M}\hat{\mathbf{I}} & -\mathbf{M}\tilde{\mathbf{b}} & \mathbf{M} & -\bar{\mathbf{I}}^{j\mathrm{T}} \\ \hline \mathbf{I} & -{}_R\tilde{\mathbf{s}}^j & -\mathbf{I} & \tilde{\mathbf{b}}^j & -\bar{\mathbf{I}}^j & \mathbf{0} \end{array}\right] \begin{Bmatrix} {}_R\ddot{\mathbf{r}} \\ {}_R\dot{\boldsymbol{\omega}} \\ \hline \ddot{\mathbf{r}} \\ \dot{\boldsymbol{\omega}} \\ \ddot{\boldsymbol{\delta}} \\ \hline \boldsymbol{\lambda} \end{Bmatrix} = \begin{Bmatrix} {}_R\mathbf{f} \\ \hline -{}_R\tilde{\boldsymbol{\omega}}_R\mathbf{J}_R\boldsymbol{\omega} + {}_R\mathbf{n} \\ \hline \hat{\mathbf{I}}^{\mathrm{T}}\mathbf{f} \\ -\tilde{\mathbf{b}}^{\mathrm{T}}\mathbf{f} \\ \mathbf{f} \\ \hline -{}_R\tilde{\boldsymbol{\omega}}_R\dot{\mathbf{s}}^j + \mathbf{w}^j \end{Bmatrix} \tag{5.8}$$

For still lack of axis conditions, the left-hand-side matrix is singular. To complete Eq. (5.8), we must decide what type of axes to use.

5.3.1 Nodal formulation with nodal-fixed axes

Nodal-fixed axes set six nodal deflections, $\grave{\boldsymbol{\delta}}_o$, to zero. This can be accomplished by having six properly selected rows of zeros in $\grave{\boldsymbol{\Psi}}$ from Eq. (4.2). Substituting Eq. (4.4) into Eq. (3.18) yields

$$\ddot{\boldsymbol{\delta}} \triangleq \bar{\mathbf{A}}\grave{\ddot{\boldsymbol{\delta}}} = \bar{\mathbf{A}}\grave{\boldsymbol{\Psi}}\grave{\ddot{\boldsymbol{\delta}}}_u \triangleq \boldsymbol{\Psi}\grave{\ddot{\boldsymbol{\delta}}}_u \tag{5.9}$$

where $\boldsymbol{\Psi} = \bar{\mathbf{A}}\grave{\boldsymbol{\Psi}}$. Substituting Eq. (5.9) into Eq. (5.8) and pre-multiplying its fifth row by $\boldsymbol{\Psi}^{\mathrm{T}}$ yields

$$\left[\begin{array}{cc|ccc|c}
{}_R m\mathbf{I} & \mathbf{0} & \mathbf{0} & \mathbf{0} & \mathbf{0} & \mathbf{I}^{\mathrm{T}} \\
\mathbf{0} & {}_R\mathbf{J} & \mathbf{0} & \mathbf{0} & \mathbf{0} & -{}_R\tilde{\mathbf{s}}^{j\mathrm{T}} \\
\hline
\mathbf{0} & \mathbf{0} & \hat{\mathbf{I}}^{\mathrm{T}}\mathbf{M}\hat{\mathbf{I}} & -\hat{\mathbf{I}}^{\mathrm{T}}\mathbf{M}\tilde{\mathbf{b}} & \hat{\mathbf{I}}^{\mathrm{T}}\mathbf{M}\boldsymbol{\Psi} & -\mathbf{I}^{\mathrm{T}} \\
\mathbf{0} & \mathbf{0} & -\tilde{\mathbf{b}}^{\mathrm{T}}\mathbf{M}\hat{\mathbf{I}} & \tilde{\mathbf{b}}^{\mathrm{T}}\mathbf{M}\tilde{\mathbf{b}} & -\tilde{\mathbf{b}}^{\mathrm{T}}\mathbf{M}\boldsymbol{\Psi} & \tilde{\mathbf{b}}^{j\mathrm{T}} \\
\mathbf{0} & \mathbf{0} & \boldsymbol{\Psi}^{\mathrm{T}}\mathbf{M}\hat{\mathbf{I}} & -\boldsymbol{\Psi}^{\mathrm{T}}\mathbf{M}\tilde{\mathbf{b}} & \boldsymbol{\Psi}^{\mathrm{T}}\mathbf{M}\boldsymbol{\Psi} & -\boldsymbol{\Psi}^{\mathrm{T}}\bar{\mathbf{I}}^{j\mathrm{T}} \\
\hline
\mathbf{I} & -{}_R\tilde{\mathbf{s}}^{j} & -\mathbf{I} & \tilde{\mathbf{b}}^{j} & -\bar{\mathbf{I}}^{j}\boldsymbol{\Psi} & \mathbf{0}
\end{array}\right]
\left\{\begin{array}{c}
{}_R\ddot{\mathbf{r}} \\
{}_R\dot{\boldsymbol{\omega}} \\
\hline
\ddot{\mathbf{r}} \\
\dot{\boldsymbol{\omega}} \\
\grave{\ddot{\boldsymbol{\delta}}}_u \\
\hline
\boldsymbol{\lambda}
\end{array}\right\}
=
\left\{\begin{array}{c}
{}_R\mathbf{f} \\
\hline
-{}_R\tilde{\boldsymbol{\omega}}_R\mathbf{J}_R\boldsymbol{\omega} + {}_R\mathbf{n} \\
\hline
\hat{\mathbf{I}}^{\mathrm{T}}\mathbf{f} \\
-\tilde{\mathbf{b}}^{\mathrm{T}}\mathbf{f} \\
\boldsymbol{\Psi}^{\mathrm{T}}\mathbf{f} \\
\hline
-{}_R\tilde{\boldsymbol{\omega}}_R\dot{\mathbf{s}}^{j} + \mathbf{w}^{j}
\end{array}\right\} \tag{5.10}$$

Equation (5.10) is the complete equations of motion for the rigid-deformable multibody system, in which nodal-fixed axes are adopted. Since $\grave{\ddot{\boldsymbol{\delta}}}_o$ and $\grave{\dot{\boldsymbol{\delta}}}_o$ are always zeros, one may integrate over time on $\grave{\ddot{\boldsymbol{\delta}}}_u$ and $\grave{\dot{\boldsymbol{\delta}}}_u$ only.

5.3.2 Nodal formulation with mean axes

Mean axis conditions set up six algebraic equations. Equations (4.18) and (4.19) are the mean axis conditions at the acceleration level. Introducing them into Eq. (5.8) by the method of Lagrange multipliers yields

$$\left[\begin{array}{cc|ccc|ccc} {}_R m\mathbf{I} & \mathbf{0} & \mathbf{0} & \mathbf{0} & \mathbf{0} & \mathbf{0} & \mathbf{0} & \mathbf{I}^{\mathrm{T}} \\ \mathbf{0} & {}_R\mathbf{J} & \mathbf{0} & \mathbf{0} & \mathbf{0} & \mathbf{0} & \mathbf{0} & -{}_R\tilde{\mathbf{s}}^{j\mathrm{T}} \\ \hline \mathbf{0} & \mathbf{0} & \hat{\mathbf{I}}^{\mathrm{T}}\mathbf{M}\hat{\mathbf{I}} & -\hat{\mathbf{I}}^{\mathrm{T}}\mathbf{M}\tilde{\mathbf{b}} & \hat{\mathbf{I}}^{\mathrm{T}}\mathbf{M} & \mathbf{0} & \mathbf{0} & -\mathbf{I}^{\mathrm{T}} \\ \mathbf{0} & \mathbf{0} & -\tilde{\mathbf{b}}^{\mathrm{T}}\mathbf{M}\hat{\mathbf{I}} & \tilde{\mathbf{b}}^{\mathrm{T}}\mathbf{M}\tilde{\mathbf{b}} & -\tilde{\mathbf{b}}^{\mathrm{T}}\mathbf{M} & \mathbf{0} & \mathbf{0} & \tilde{\mathbf{b}}^{j\mathrm{T}} \\ \mathbf{0} & \mathbf{0} & \mathbf{M}\hat{\mathbf{I}} & -\mathbf{M}\tilde{\mathbf{b}} & \mathbf{M} & \mathbf{M}\hat{\mathbf{I}} & \mathbf{M}\tilde{\mathbf{b}} & -\bar{\mathbf{I}}^{j\mathrm{T}} \\ \hline \mathbf{0} & \mathbf{0} & \mathbf{0} & \mathbf{0} & \hat{\mathbf{I}}^{\mathrm{T}}\mathbf{M} & \mathbf{0} & \mathbf{0} & \mathbf{0} \\ \mathbf{0} & \mathbf{0} & \mathbf{0} & \mathbf{0} & \tilde{\mathbf{b}}^{\mathrm{T}}\mathbf{M} & \mathbf{0} & \mathbf{0} & \mathbf{0} \\ \mathbf{I} & -{}_R\tilde{\mathbf{s}}^{j} & -\mathbf{I} & \tilde{\mathbf{b}}^{j} & -\bar{\mathbf{I}}^{j} & \mathbf{0} & \mathbf{0} & \mathbf{0} \end{array}\right] \left\{\begin{array}{c} {}_R\ddot{\mathbf{r}} \\ {}_R\dot{\boldsymbol{\omega}} \\ \hline \ddot{\mathbf{r}} \\ \dot{\boldsymbol{\omega}} \\ \ddot{\boldsymbol{\delta}} \\ \hline \boldsymbol{\lambda}_1 \\ \boldsymbol{\lambda}_2 \\ \boldsymbol{\lambda}_3 \end{array}\right\} = \left\{\begin{array}{c} {}_R\mathbf{f} \\ -{}_R\tilde{\boldsymbol{\omega}}_R\mathbf{J}_R\boldsymbol{\omega} + {}_R\mathbf{n} \\ \hline \hat{\mathbf{I}}^{\mathrm{T}}\mathbf{f} \\ -\tilde{\mathbf{b}}^{\mathrm{T}}\mathbf{f} \\ \mathbf{f} \\ \hline \mathbf{0} \\ -\tilde{\dot{\boldsymbol{\delta}}}^{\mathrm{T}}\mathbf{M}\dot{\boldsymbol{\delta}} \\ -{}_R\tilde{\boldsymbol{\omega}}_R\dot{\mathbf{s}}^{j} + \mathbf{w}^{j} \end{array}\right\} \quad (5.11)$$

Equation (5.11) is the complete equations of motion for the rigid-deformable multibody system, in which mean axes are adopted. Before integration, $\ddot{\boldsymbol{\delta}}$ is transformed to $\ddot{\boldsymbol{\delta}}_{\backprime}$ by $\ddot{\boldsymbol{\delta}}_{\backprime} = \bar{\mathbf{A}}^{\mathrm{T}}\ddot{\boldsymbol{\delta}}$. Then, $\dot{\boldsymbol{\delta}}_{\backprime} = \int \ddot{\boldsymbol{\delta}}_{\backprime}\, dt$ and $\boldsymbol{\delta}_{\backprime} = \int \dot{\boldsymbol{\delta}}_{\backprime}\, dt$.

5.3.3 Nodal-fixed axes versus mean axes

Though a nodal-fixed frame is easy to use, there is one serious fault. Because nodal-fixed axes are installed over a selected node or nodes, some nodes are treated differently than the others. Errors are hence introduced. Though the errors may not be apparent in most simulations, they could be noticeable in some cases. For example, the computed response could become non-symmetric but a symmetric response is expected. On the contrary, since mean axes are impartial to all the nodes, retaining symmetricity is not a

problem if anticipated. This phenomenon can be observed by an example from [24], which is briefed next.

Shown in Figure 5-2 is a deformable plank hung under four rigid links (slender rods). The four links are all two meters long with a mass of 1 kg. Link *AB* is connected to the ground at point *A*; link *BC* is connected to link *AB* at point *B*. Link *DE* is connected to the ground at point *D*; link *EF* is connected to link *DE* at point *E*. The plank is modeled by solid (or brick) elements that contains thirty nodes—fifteen on the front and fifteen on the back (see APPENDIX B). It is connected to links *BC* and *EF* through nodes 3 and 15, respectively. All six connections (at points *A*, *B*, *C*, *D*, *E*, and *F*) are spherical joints. In addition, there is an external force of 250 N (not shown) pulling downwards at node 22 (behind node 7). Gravity (9.80665 m/s^2) is also present.

To set up a nodal-fixed frame, the origin is located at node 8; the ξ axis is chosen going through node 14; the η axis lies on the plane defined by the ξ axis and node 23 (behind node 8). For the mean axes frame, at the undeformed state, the origin is at the mass center, which is at the mid point between nodes 8 and 23; the ξ axis points to the right, the η axis goes towards the back, and the ζ axis is directed upwards.

The system is released from the shown configuration without any initial velocities. The simulation is repeated for both nodal-fixed and mean axes.[*] With the nodal-fixed axes, the responses of two symmetrically positioned nodes such as nodes 3

---

[*] The reaction forces are supposed to be symmetric if the system itself is symmetric and all external forces are applied symmetrically. Under this setting, we compare the outcomes of using nodal-fixed and mean axes.

and 15 are non-symmetric as revealed by Figure 5-3(a). The x coordinates of nodes 3 and 15 ($-\mathbf{d}_x^3$ and $+\mathbf{d}_x^{15}$) versus time begin to separate after the plank hits the bottom at around 0.5 seconds. The reaction forces generated on nodes 3 and 15 are not the same, which steers the system off symmetry. With the mean axes, in contrast, the plank does bounce upward symmetrically, as it should, after it hits the bottom because the reaction forces are always equal. The x coordinates of nodes 3 and 15 are seen as one curve in Figure 5-3(b).

The results suggest that nodal-fixed axes are not suitable for systems from which we expect symmetric responses, especially when flexible bodies are not totally restrained. Slightly imbalanced reaction forces at joints on the flexible bodies due to an improper installation of the nodal-fixed axes can throw the systems off symmetry as it has been demonstrated in the example.* Mean axes do not suffer from this problem and, therefore, are recommended for these cases.

---

* It is possible to install a nodal-fixed frame such that the responses come out symmetric but this requires one's attention to set up the nodal-fixed axes carefully, which is not practical.

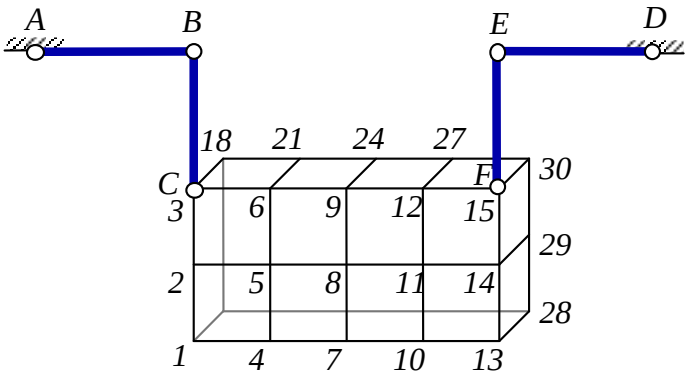

Figure 5-2: a deformable plank hung under four rigid links

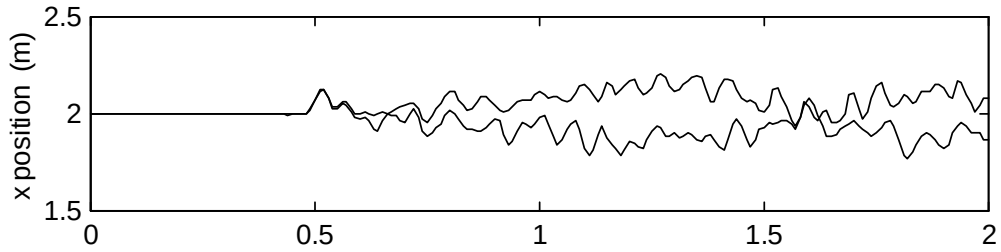

(a) **using nodal-fixed axes**

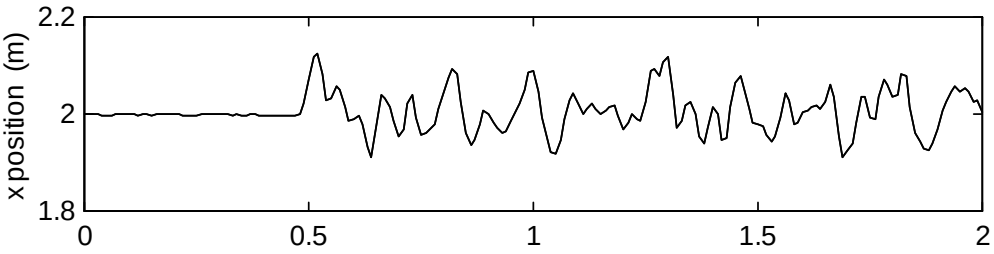

(b) **using mean axes**

Figure 5-3: x coordinates of nodes 3 and 15

5.4 Modal Formulations

Although the nodal formulations in the previous section have defined the equations of motion for the rigid-deformable body system, the computation time can be costly due to large degrees of freedom. Since often not all frequencies are excited, it is desirable to

perform model reduction on the deformable body by transforming the original nodal coordinates into a much smaller set of modal coordinates using

$$\grave{\boldsymbol{\delta}} = \grave{\boldsymbol{\Psi}}\mathbf{z} \tag{5.12}$$

$$\dot{\grave{\boldsymbol{\delta}}} = \grave{\boldsymbol{\Psi}}\dot{\mathbf{z}} \tag{5.13}$$

$$\ddot{\grave{\boldsymbol{\delta}}} = \grave{\boldsymbol{\Psi}}\ddot{\mathbf{z}} \tag{5.14}$$

where $\grave{\boldsymbol{\Psi}}$ is the transformation matrix of reduction. Only significant modes are kept in $\grave{\boldsymbol{\Psi}}$ to reduce the problem size; the other modes are truncated. Substituting Eqs. (5.12), (5.13), and (5.14) into Eqs. (3.11), (3.16), and (3.18) yields

$$\boldsymbol{\delta} = \bar{\mathbf{A}}\grave{\boldsymbol{\delta}} = \bar{\mathbf{A}}\grave{\boldsymbol{\Psi}}\mathbf{z} = \boldsymbol{\Psi}\mathbf{z} \tag{5.15}$$

$$\dot{\boldsymbol{\delta}} \triangleq \bar{\mathbf{A}}\dot{\grave{\boldsymbol{\delta}}} = \bar{\mathbf{A}}\grave{\boldsymbol{\Psi}}\dot{\mathbf{z}} = \boldsymbol{\Psi}\dot{\mathbf{z}} \tag{5.16}$$

$$\ddot{\boldsymbol{\delta}} \triangleq \bar{\mathbf{A}}\ddot{\grave{\boldsymbol{\delta}}} = \bar{\mathbf{A}}\grave{\boldsymbol{\Psi}}\ddot{\mathbf{z}} = \boldsymbol{\Psi}\ddot{\mathbf{z}} \tag{5.17}$$

where $\boldsymbol{\Psi} = \bar{\mathbf{A}}\grave{\boldsymbol{\Psi}}$. Note that the mode shapes in $\grave{\boldsymbol{\Psi}}$ should not be arbitrary [51]. They depend on how a deformable body is restrained. Different reduction methods are characterized by their construction of the $\grave{\boldsymbol{\Psi}}$ matrix, which will be discussed in Chapter 6. Here we assume that a $\grave{\boldsymbol{\Psi}}$ matrix is already made available.

5.4.1 Modal formulation with nodal-fixed axes

To introduce a nodal-fixed frame, six columns (for a 3-D deformable body) of $\grave{\boldsymbol{\Psi}}$ are removed. These columns correspond to the coordinates that the nodal-fixed frame is anchored to. Effectively, six nodal deflections are set to zero. Substituting Eq. (5.17) into Eq. (5.8) and pre-multiplying its fifth row by $\boldsymbol{\Psi}^{\mathrm{T}}$ yields

$$\left[\begin{array}{cc|ccc|c} {}_R m\mathbf{I} & \mathbf{0} & \mathbf{0} & \mathbf{0} & \mathbf{0} & \mathbf{I}^{\mathrm{T}} \\ \mathbf{0} & {}_R\mathbf{J} & \mathbf{0} & \mathbf{0} & \mathbf{0} & -{}_R\tilde{\mathbf{s}}^{j\,\mathrm{T}} \\ \hline \mathbf{0} & \mathbf{0} & \hat{\mathbf{I}}^{\mathrm{T}}\mathbf{M}\hat{\mathbf{I}} & -\hat{\mathbf{I}}^{\mathrm{T}}\mathbf{M}\tilde{\mathbf{b}} & \hat{\mathbf{I}}^{\mathrm{T}}\mathbf{M}\boldsymbol{\Psi} & -\mathbf{I}^{\mathrm{T}} \\ \mathbf{0} & \mathbf{0} & -\tilde{\mathbf{b}}^{\mathrm{T}}\mathbf{M}\hat{\mathbf{I}} & \tilde{\mathbf{b}}^{\mathrm{T}}\mathbf{M}\tilde{\mathbf{b}} & -\tilde{\mathbf{b}}^{\mathrm{T}}\mathbf{M}\boldsymbol{\Psi} & \tilde{\mathbf{b}}^{j\,\mathrm{T}} \\ \mathbf{0} & \mathbf{0} & \boldsymbol{\Psi}^{\mathrm{T}}\mathbf{M}\hat{\mathbf{I}} & -\boldsymbol{\Psi}^{\mathrm{T}}\mathbf{M}\tilde{\mathbf{b}} & \boldsymbol{\Psi}^{\mathrm{T}}\mathbf{M}\boldsymbol{\Psi} & -\boldsymbol{\Psi}^{\mathrm{T}}\bar{\mathbf{I}}^{j\,\mathrm{T}} \\ \hline \mathbf{I} & -{}_R\tilde{\mathbf{s}}^{j} & -\mathbf{I} & \tilde{\mathbf{b}}^{j} & -\bar{\mathbf{I}}^{j}\boldsymbol{\Psi} & \mathbf{0} \end{array}\right] \left\{\begin{array}{c} {}_R\ddot{\mathbf{r}} \\ {}_R\dot{\boldsymbol{\omega}} \\ \hline \ddot{\mathbf{r}} \\ \dot{\boldsymbol{\omega}} \\ \ddot{\mathbf{z}} \\ \hline \boldsymbol{\lambda} \end{array}\right\} = \left\{\begin{array}{c} {}_R\mathbf{f} \\ \hline -{}_R\tilde{\boldsymbol{\omega}}_R\mathbf{J}_R\boldsymbol{\omega} + {}_R\mathbf{n} \\ \hline \hat{\mathbf{I}}^{\mathrm{T}}\mathbf{f} \\ -\tilde{\mathbf{b}}^{\mathrm{T}}\mathbf{f} \\ \boldsymbol{\Psi}^{\mathrm{T}}\mathbf{f} \\ \hline -{}_R\tilde{\boldsymbol{\omega}}_R\dot{\mathbf{s}}^{j} + \mathbf{w}^{j} \end{array}\right\} \tag{5.18}$$

Equation (5.18) is the complete equations of motion in $\ddot{\mathbf{z}}$ with nodal-fixed axes for the rigid-deformable multibody system.

5.4.2 Modal formulation with mean axes

Section 5.3.2 established the nodal formulation with mean axes. What we need to do here is to transform the deformation coordinates from nodal to modal space. Substituting Eq. (5.17) into Eq. (5.11) and pre-multiplying its fifth row by $\boldsymbol{\Psi}^{\mathrm{T}}$ yields

$$\left[\begin{array}{cc|ccc|ccc} {}_R m\mathbf{I} & \mathbf{0} & \mathbf{0} & \mathbf{0} & \mathbf{0} & \mathbf{0} & \mathbf{0} & \mathbf{I}^{\mathrm{T}} \\ \mathbf{0} & {}_R\mathbf{J} & \mathbf{0} & \mathbf{0} & \mathbf{0} & \mathbf{0} & \mathbf{0} & -{}_R\tilde{\mathbf{s}}^{j\,\mathrm{T}} \\ \hline \mathbf{0} & \mathbf{0} & \hat{\mathbf{I}}^{\mathrm{T}}\mathbf{M}\hat{\mathbf{I}} & -\hat{\mathbf{I}}^{\mathrm{T}}\mathbf{M}\tilde{\mathbf{b}} & \hat{\mathbf{I}}^{\mathrm{T}}\mathbf{M}\boldsymbol{\Psi} & \mathbf{0} & \mathbf{0} & -\mathbf{I}^{\mathrm{T}} \\ \mathbf{0} & \mathbf{0} & -\tilde{\mathbf{b}}^{\mathrm{T}}\mathbf{M}\hat{\mathbf{I}} & \tilde{\mathbf{b}}^{\mathrm{T}}\mathbf{M}\tilde{\mathbf{b}} & -\tilde{\mathbf{b}}^{\mathrm{T}}\mathbf{M}\boldsymbol{\Psi} & \mathbf{0} & \mathbf{0} & \tilde{\mathbf{b}}^{j\,\mathrm{T}} \\ \mathbf{0} & \mathbf{0} & \boldsymbol{\Psi}^{\mathrm{T}}\mathbf{M}\hat{\mathbf{I}} & -\boldsymbol{\Psi}^{\mathrm{T}}\mathbf{M}\tilde{\mathbf{b}} & \boldsymbol{\Psi}^{\mathrm{T}}\mathbf{M}\boldsymbol{\Psi} & \boldsymbol{\Psi}^{\mathrm{T}}\mathbf{M}\hat{\mathbf{I}} & \boldsymbol{\Psi}^{\mathrm{T}}\mathbf{M}\tilde{\mathbf{b}} & -\boldsymbol{\Psi}^{\mathrm{T}}\bar{\mathbf{I}}^{j\,\mathrm{T}} \\ \hline \mathbf{0} & \mathbf{0} & \mathbf{0} & \mathbf{0} & \hat{\mathbf{I}}^{\mathrm{T}}\mathbf{M}\boldsymbol{\Psi} & \mathbf{0} & \mathbf{0} & \mathbf{0} \\ \mathbf{0} & \mathbf{0} & \mathbf{0} & \mathbf{0} & \tilde{\mathbf{b}}^{\mathrm{T}}\mathbf{M}\boldsymbol{\Psi} & \mathbf{0} & \mathbf{0} & \mathbf{0} \\ \mathbf{I} & -{}_R\tilde{\mathbf{s}}^{j} & -\mathbf{I} & \tilde{\mathbf{b}}^{j} & -\bar{\mathbf{I}}^{j}\boldsymbol{\Psi} & \mathbf{0} & \mathbf{0} & \mathbf{0} \end{array}\right] \left\{\begin{array}{c} {}_R\ddot{\mathbf{r}} \\ {}_R\dot{\boldsymbol{\omega}} \\ \hline \ddot{\mathbf{r}} \\ \dot{\boldsymbol{\omega}} \\ \ddot{\mathbf{z}} \\ \hline \boldsymbol{\lambda}_1 \\ \boldsymbol{\lambda}_2 \\ \boldsymbol{\lambda}_3 \end{array}\right\} = \left\{\begin{array}{c} {}_R\mathbf{f} \\ \hline -{}_R\tilde{\boldsymbol{\omega}}_R\mathbf{J}_R\boldsymbol{\omega} + {}_R\mathbf{n} \\ \hline \hat{\mathbf{I}}^{\mathrm{T}}\mathbf{f} \\ -\tilde{\mathbf{b}}^{\mathrm{T}}\mathbf{f} \\ \boldsymbol{\Psi}^{\mathrm{T}}\mathbf{f} \\ \hline \mathbf{0} \\ -\tilde{\tilde{\boldsymbol{\delta}}}^{\mathrm{T}}\mathbf{M}\dot{\boldsymbol{\delta}} \\ -{}_R\tilde{\boldsymbol{\omega}}_R\dot{\mathbf{s}}^{j} + \mathbf{w}^{j} \end{array}\right\} \tag{5.19}$$

Equation (5.19) is the complete equations of motion in $\ddot{\mathbf{z}}$ with mean axes for the rigid-deformable multibody system. Although the above process of transformation seems trivial, there is one important question to answer: Are the mode shapes in $\boldsymbol{\Psi}$ compatible with mean axes? The answer is positive and will be explained in Chapter 8 MODEL REDUCTION WITH MEAN AXES.

6 REDUCTION METHODS

For a complex structure, the finite element method (FEM) could result in matrices that are too large to handle effectively. Condensation is thus desired in order to perform more efficient computation. Well-known methods such as static condensation and modal truncation are simple to use but have some shortcomings when applied to moving deformable bodies. To improve the quality of model reduction, component mode synthesis combines different types of modes. One method in this family to be reviewed is Craig and Bampton reduction. A newly developed method by Nikravesh is further investigated, which is proven equivalent to Craig and Bampton reduction. Eitelberg's method for linear time invariant systems is also examined, which is found identical to Guyan reduction for structures.

6.1 Equations of Motion for a Deformable Body

By the finite element method, a deformable body is characterized by a mass matrix and a stiffness matrix. The deformable body is divided into a finite number of elements that are interconnected at nodes. In a multibody environment, some of the nodes may be firmly connected to other bodies (including the ground) by joints. Some other nodes may (or will) be under strong influence of applied forces or attached springs. Collectively they are referred to as boundary nodes or DOFs, which are labeled as set *b*. The other nodes are referred to as interior nodes or DOFs, which are labeled as set *i*. Without considering the details about how the deformable body is connected to its surrounding, the (undamped) equations of motion are

$$\begin{bmatrix} \mathbf{M}_{bb} & \mathbf{M}_{bi} \\ \mathbf{M}_{ib} & \mathbf{M}_{ii} \end{bmatrix} \begin{Bmatrix} \ddot{\boldsymbol{\delta}}_b \\ \ddot{\boldsymbol{\delta}}_i \end{Bmatrix} + \begin{bmatrix} \mathbf{K}_{bb} & \mathbf{K}_{bi} \\ \mathbf{K}_{ib} & \mathbf{K}_{ii} \end{bmatrix} \begin{Bmatrix} \boldsymbol{\delta}_b \\ \boldsymbol{\delta}_i \end{Bmatrix} = \begin{Bmatrix} \mathbf{f}_b \\ \mathbf{f}_i \end{Bmatrix} \tag{6.1}$$

where the mass and stiffness matrices, the force vector, and the deformation coordinates (including the accelerations) have been partitioned into sets *b* and *i* accordingly. Since the total number of coordinates for a full model can be large, it is desirable to reduce the problem size by transforming the coordinates into a much smaller set of coordinates. Different reduction methods differ in the transformation matrix, which will be reviewed in the sections that follow. To accompany the discussions, a simple 2-D beam model will serve as the example throughout this chapter. The beam is composed of four beam elements with five nodes which are evenly spaced; in total there are ten DOFs. For details of the model, see APPENDIX A.

6.2 Static Condensation

Among a large number of nodes, often not all are of equal interest. For example, rotational (deformation) DOFs sometimes have insignificant dynamic effects compared to translational (deformation) DOFs. In these cases, we may wish to pay attention only to the translational degrees of freedom. Another instance is that a much refined FEM mesh might not be necessary for certain applications (e.g., maybe it is acceptable for static analysis but is too expensive for eigen-analysis). In these cases, we may wish to observe only selected nodes. In the so-called static condensation or Guyan reduction [27], one decides what DOFs or nodes to keep, which are called “masters” (set *b*), and what DOFs or nodes to delete, which are called “slaves” (set *i*). It is assumed that all the inertia and

external forces on the slaves will be redistributed to the masters. Hence, Eq. (6.1) is rewritten as

$$\begin{bmatrix} \grave{\mathbf{M}}_{\mathrm{G}} & \mathbf{0} \\ \mathbf{0} & \mathbf{0} \end{bmatrix} \begin{Bmatrix} \ddot{\grave{\boldsymbol{\delta}}}_b \\ \ddot{\grave{\boldsymbol{\delta}}}_i \end{Bmatrix} + \begin{bmatrix} \grave{\mathbf{K}}_{bb} & \grave{\mathbf{K}}_{bi} \\ \grave{\mathbf{K}}_{ib} & \grave{\mathbf{K}}_{ii} \end{bmatrix} \begin{Bmatrix} \grave{\boldsymbol{\delta}}_b \\ \grave{\boldsymbol{\delta}}_i \end{Bmatrix} = \begin{Bmatrix} \grave{\mathbf{f}}_{\mathrm{G}} \\ \mathbf{0} \end{Bmatrix} \tag{6.2}$$

in which $\grave{\mathbf{M}}_{\mathrm{G}}$ is the would-be reduced (or condensed) mass matrix and $\grave{\mathbf{f}}_{\mathrm{G}}$ is the would-be reduced force vector. From the second row of Eq. (6.2), we obtain

$$\grave{\boldsymbol{\delta}}_i = -\grave{\mathbf{K}}_{ii}^{-1} \grave{\mathbf{K}}_{ib} \grave{\boldsymbol{\delta}}_b = \grave{\boldsymbol{\Psi}}_s \grave{\boldsymbol{\delta}}_b \tag{6.3}$$

where $\grave{\boldsymbol{\Psi}}_s = -\grave{\mathbf{K}}_{ii}^{-1} \grave{\mathbf{K}}_{ib}$; i.e., $\grave{\boldsymbol{\delta}}_i$ is related to $\grave{\boldsymbol{\delta}}_b$ thru $\grave{\boldsymbol{\Psi}}_s$. Therefore, the transformation for reduction is

$$\grave{\boldsymbol{\delta}} = \begin{Bmatrix} \grave{\boldsymbol{\delta}}_b \\ \grave{\boldsymbol{\delta}}_i \end{Bmatrix} = \begin{bmatrix} \mathbf{I} \\ \grave{\boldsymbol{\Psi}}_s \end{bmatrix} \grave{\boldsymbol{\delta}}_b = \grave{\boldsymbol{\Psi}} \grave{\boldsymbol{\delta}}_b \tag{6.4}$$

where

$$\grave{\boldsymbol{\Psi}} = \begin{bmatrix} \mathbf{I} \\ \grave{\boldsymbol{\Psi}}_s \end{bmatrix} \tag{6.5}$$

The columns of $\grave{\boldsymbol{\Psi}}$ are called constraint modes. Substituting Eq. (6.4) into Eq. (6.1) and pre-multiplying it by $\grave{\boldsymbol{\Psi}}^{\mathrm{T}}$ yields

$$\grave{\mathbf{M}}_{\mathrm{G}} \ddot{\grave{\boldsymbol{\delta}}}_b + \grave{\mathbf{K}}_{\mathrm{G}} \grave{\boldsymbol{\delta}}_b = \grave{\mathbf{f}}_{\mathrm{G}} \tag{6.6}$$

in which

$$\grave{\mathbf{M}}_{\mathrm{G}} = \grave{\boldsymbol{\Psi}}^{\mathrm{T}} \grave{\mathbf{M}} \grave{\boldsymbol{\Psi}} = \grave{\mathbf{M}}_{bb} + \grave{\mathbf{M}}_{bi} \grave{\boldsymbol{\Psi}}_s + \grave{\boldsymbol{\Psi}}_s^{\mathrm{T}} \grave{\mathbf{M}}_{ib} + \grave{\boldsymbol{\Psi}}_s^{\mathrm{T}} \grave{\mathbf{M}}_{ii} \grave{\boldsymbol{\Psi}}_s \tag{6.7}$$

$$\grave{\mathbf{K}}_{\mathrm{G}} = \grave{\boldsymbol{\Psi}}^{\mathrm{T}} \grave{\mathbf{K}} \grave{\boldsymbol{\Psi}} = \grave{\mathbf{K}}_{bb} + \grave{\mathbf{K}}_{bi} \grave{\boldsymbol{\Psi}}_s \tag{6.8}$$

$$\grave{\mathbf{f}}_{\mathrm{G}} = \grave{\boldsymbol{\Psi}}^{\mathrm{T}} \grave{\mathbf{f}} = \grave{\mathbf{f}}_b + \grave{\boldsymbol{\Psi}}_s^{\mathrm{T}} \grave{\mathbf{f}}_i \tag{6.9}$$

where $\grave{\mathbf{K}}_G$ is the reduced stiffness matrix. Equation (6.6) is the reduced equations of motion. Once $\grave{\boldsymbol{\delta}}_b$ is solved, $\grave{\boldsymbol{\delta}}_i$ can be restored by Eq. (6.3). Although static condensation can preserve exact solutions for static problems, large errors may occur at higher frequencies if applied to dynamic problems. The reason is that a statically condensed model usually does not have the same corresponding eigen-properties of the original model.

6.2.1 Free-free modes

When a deformable body is totally unconstrained (like floating in space), its eigen-properties are called "free-free" modes. Take the beam model from APPENDIX A for example. Its free-free modes can be computed by $[\grave{\mathbf{V}}, \boldsymbol{\Lambda}] = \text{eig}(\grave{\mathbf{K}}, \grave{\mathbf{M}})$. Among the ten mode shapes in $\grave{\mathbf{V}}$, three of them are rigid-body modes (corresponding to the zero eigen-values in $\boldsymbol{\Lambda}$) and seven of them are deformation modes (corresponding to the non-zero eigen-values in $\boldsymbol{\Lambda}$). The deformation modes are plotted in Figure 6-1, which shows three bending modes on the left and four axial modes on the right.

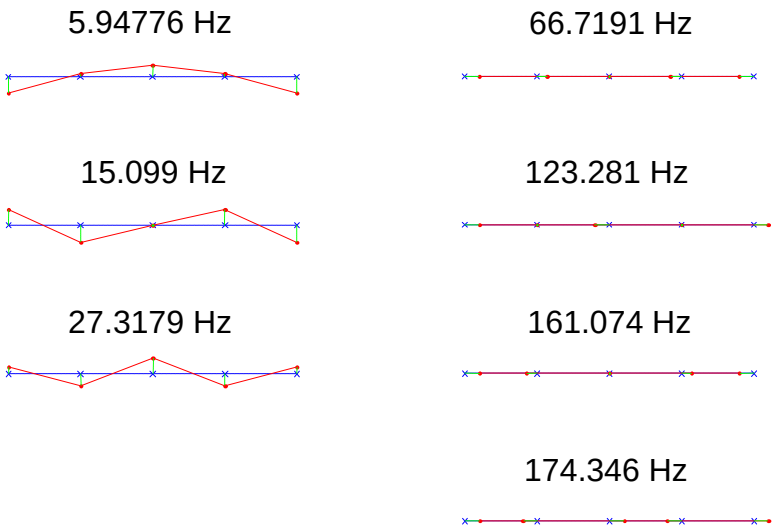

Figure 6-1: free-free deformation modes of the full beam model

To reduce the model to a smaller size, nodes 1, 3, and 5 are chosen as the master nodes of the reduced beam model (a) in Figure 6-2. The transformation matrix and reduced stiffness and mass matrices are referred to as $\grave{\mathbf{\Psi}}^{(a)}$, $\grave{\mathbf{K}}_G^{(a)}$, and $\grave{\mathbf{M}}_G^{(a)}$, respectively. The free-free modes can be computed by $[\grave{\mathbf{V}}^{(a)}, \mathbf{\Lambda}^{(a)}] = \text{eig}(\grave{\mathbf{K}}_G^{(a)}, \grave{\mathbf{M}}_G^{(a)})$. Besides three rigid-body modes, there are three deformation modes which are plotted in Figure 6-3(a). The first mode is a bending mode, which has a slightly higher natural frequency (5.95823 Hz) than the first bending mode (5.94776 Hz) in Figure 6-1. The second mode is an axial mode, which has a noticeable higher natural frequency (71.1763 Hz) than the first axial mode (66.7191 Hz) in Figure 6-1. The third mode is also an axial mode, which happens to have the same natural frequency (123.281 Hz) and mode shape as the second axial mode in Figure 6-1. These observations reveal that, in general, a reduced model has higher (corresponding) natural frequencies than the original model.

This is the cause of large errors when higher modes are excited if the reduced model is subjected to dynamic forces.

The reduced beam model (b) in Figure 6-2 is another possible choice. Nodes 1, 2, and 5 are chosen as the master nodes. The transformation matrix and reduced stiffness and mass matrices are referred to as $\grave{\mathbf{\Psi}}^{(b)}$, $\grave{\mathbf{K}}_G^{(b)}$, and $\grave{\mathbf{M}}_G^{(b)}$, respectively. The free-free modes can be computed by $[\grave{\mathbf{V}}^{(b)}, \mathbf{\Lambda}^{(b)}] = \text{eig}(\grave{\mathbf{K}}_G^{(b)}, \grave{\mathbf{M}}_G^{(b)})$. Besides three rigid-body modes, there are three deformation modes which are plotted in Figure 6-3(b). The first mode is a bending mode but it has an even higher natural frequency (6.33897 Hz) than its counterpart (5.95823 Hz) in Figure 6-3(a). Though the second mode has a lower frequency (69.5245 Hz) than the second one (71.1763 Hz) in Figure 6-3(a) and is close to the similar one (66.7191 Hz) in Figure 6-1, this axial mode is actually not symmetric. The third mode is an axial mode that is unlike any axial modes in Figure 6-3(a) and Figure 6-1. These observations suggest that it is better to spread out the selection of master nodes as uniformly as possible to avoid this phenomenon.

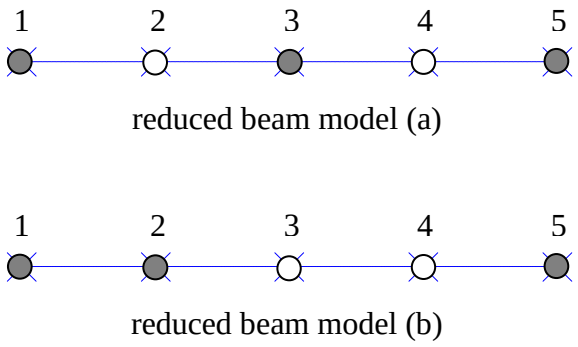

Figure 6-2: reduced beam models (a) and (b)

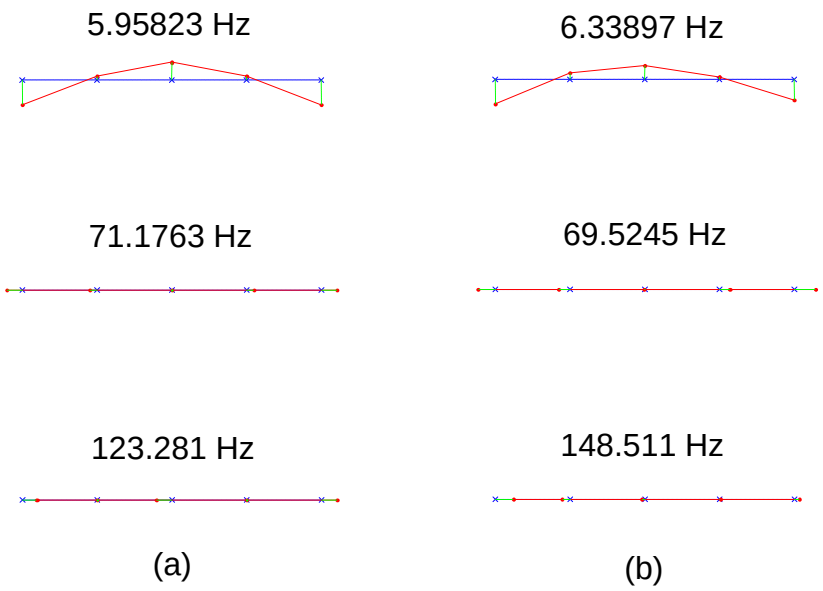

Figure 6-3: free-free deformation modes of the reduced beam models (a) and (b)

6.2.2 Constraint modes

There are occasions when we are interested in having only few master nodes. Imagine that the beam represents a rod which connects a crank and piston in an engine. The rod experiences strong joint forces at its two ends. We may choose nodes 1 and 5 as the master nodes of the reduced beam model (c) in Figure 6-4. The transformation matrix of reduction is here referred to as $\grave{\Psi}^{(c)}$, which is a 10 (ten nodal DOFs) by 4 (four constraint modes) matrix. The four constraint modes, according to Eq. (6.5), are in fact the static solutions when the master nodal DOFs are displaced one at a time as shown in Figure 6-5. Though they seem to appear as different deformation modes, there is only one real deformation mode because they all deform in the same manner along the beam.

Three rigid-body modes hide among the constraint modes in $\grave{\Psi}^{(c)}$.* To improve the accuracy of dynamic responses, often we would combine the few constraint modes with another type of modes. For example, the Craig-Bampton method combines constraint and normal modes, which will be discussed in Section 6.4.

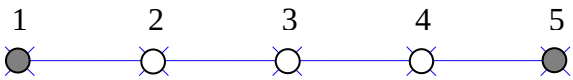

Figure 6-4: reduced beam model (c)

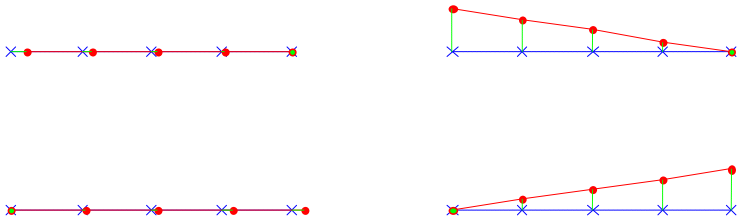

Figure 6-5: constraint modes of the reduced beam model (c)

6.3 Modal Truncation

A model reduced by static condensation has higher natural frequencies, which may cause large errors when the body is subjected to dynamic forces especially if it is constrained (e.g., a fixed-free cantilever beam). To eliminate this effect, the boundary DOFs (deformation) are kept in nodal space whereas the interior DOFs are transformed into modal space:

---

* This is also true for $\grave{\Psi}^{(a)}$ and $\grave{\Psi}^{(b)}$.

$$\begin{Bmatrix} \grave{\boldsymbol{\delta}}_b \\ \grave{\boldsymbol{\delta}}_i \end{Bmatrix} = \begin{bmatrix} \mathbf{I} & \mathbf{0} \\ \mathbf{0} & \grave{\boldsymbol{\Psi}}_n \end{bmatrix} \begin{Bmatrix} \grave{\boldsymbol{\delta}}_b \\ \mathbf{z}_n \end{Bmatrix} \tag{6.10}$$

Matrix $\grave{\boldsymbol{\Psi}}_n$ contains the mode shapes obtained while the boundary DOFs are fixed. They are thus called fixed-constraint normal modes. The eigen-properties for the interior DOFs can be computed by

$$\left[\grave{\boldsymbol{\Psi}}_n, \boldsymbol{\Lambda}_n\right] = \mathrm{eig}\left(\grave{\mathbf{K}}_{ii}, \grave{\mathbf{M}}_{ii}\right) \tag{6.11}$$

in which $\boldsymbol{\Lambda}_n$ is a diagonal matrix with the corresponding eigen-values on its diagonal. Substituting Eq. (6.10) into Eq. (6.1) yields

$$\begin{bmatrix} \grave{\mathbf{M}}_{bb} & \grave{\mathbf{M}}_{bi}\grave{\boldsymbol{\Psi}}_n \\ \grave{\boldsymbol{\Psi}}_n^{\mathrm{T}}\grave{\mathbf{M}}_{ib} & \grave{\boldsymbol{\Psi}}_n^{\mathrm{T}}\grave{\mathbf{M}}_{ii}\grave{\boldsymbol{\Psi}}_n \end{bmatrix} \begin{Bmatrix} \ddot{\grave{\boldsymbol{\delta}}}_b \\ \ddot{\mathbf{z}}_n \end{Bmatrix} + \begin{bmatrix} \grave{\mathbf{K}}_{bb} & \grave{\mathbf{K}}_{bi}\grave{\boldsymbol{\Psi}}_n \\ \grave{\boldsymbol{\Psi}}_n^{\mathrm{T}}\grave{\mathbf{K}}_{ib} & \grave{\boldsymbol{\Psi}}_n^{\mathrm{T}}\grave{\mathbf{K}}_{ii}\grave{\boldsymbol{\Psi}}_n \end{bmatrix} \begin{Bmatrix} \grave{\boldsymbol{\delta}}_b \\ \mathbf{z}_n \end{Bmatrix} = \begin{Bmatrix} \grave{\mathbf{f}}_b \\ \grave{\boldsymbol{\Psi}}_n^{\mathrm{T}}\grave{\mathbf{f}}_i \end{Bmatrix} \tag{6.12}$$

Note that

$$\grave{\boldsymbol{\Psi}}_n^{\mathrm{T}}\grave{\mathbf{M}}_{ii}\grave{\boldsymbol{\Psi}}_n = \grave{\bar{\mathbf{M}}}_n \tag{6.13}$$

and

$$\grave{\boldsymbol{\Psi}}_n^{\mathrm{T}}\grave{\mathbf{K}}_{ii}\grave{\boldsymbol{\Psi}}_n = \grave{\bar{\mathbf{K}}}_n \tag{6.14}$$

are both diagonal. If the normal modes are split into the *k*ept and *d*eleted sets, Eq. (6.12) is rewritten as

$$\begin{bmatrix} \grave{\mathbf{M}}_{bb} & \grave{\mathbf{M}}_{bi}\grave{\boldsymbol{\Psi}}_n^k & \grave{\mathbf{M}}_{bi}\grave{\boldsymbol{\Psi}}_n^d \\ \grave{\boldsymbol{\Psi}}_n^{k\,\mathrm{T}}\grave{\mathbf{M}}_{ib} & \grave{\bar{\mathbf{M}}}_n^k & \mathbf{0} \\ \grave{\boldsymbol{\Psi}}_n^{d\,\mathrm{T}}\grave{\mathbf{M}}_{ib} & \mathbf{0} & \grave{\bar{\mathbf{M}}}_n^d \end{bmatrix} \begin{Bmatrix} \ddot{\grave{\boldsymbol{\delta}}}_b \\ \ddot{\mathbf{z}}_n^k \\ \ddot{\mathbf{z}}_n^d \end{Bmatrix} + \begin{bmatrix} \grave{\mathbf{K}}_{bb} & \grave{\mathbf{K}}_{bi}\grave{\boldsymbol{\Psi}}_n^k & \grave{\mathbf{K}}_{bi}\grave{\boldsymbol{\Psi}}_n^d \\ \grave{\boldsymbol{\Psi}}_n^{k\,\mathrm{T}}\grave{\mathbf{K}}_{ib} & \grave{\bar{\mathbf{K}}}_n^k & \mathbf{0} \\ \grave{\boldsymbol{\Psi}}_n^{d\,\mathrm{T}}\grave{\mathbf{K}}_{ib} & \mathbf{0} & \grave{\bar{\mathbf{K}}}_n^d \end{bmatrix} \begin{Bmatrix} \grave{\boldsymbol{\delta}}_b \\ \mathbf{z}_n^k \\ \mathbf{z}_n^d \end{Bmatrix} = \begin{Bmatrix} \grave{\mathbf{f}}_b \\ \grave{\boldsymbol{\Psi}}_n^{k\,\mathrm{T}}\grave{\mathbf{f}}_i \\ \grave{\boldsymbol{\Psi}}_n^{d\,\mathrm{T}}\grave{\mathbf{f}}_i \end{Bmatrix} \tag{6.15}$$

To reduce the problem size, the rows and columns associated with the deleted modes are removed:

$$\begin{bmatrix} \grave{\mathbf{M}}_{bb} & \grave{\mathbf{M}}_{bi}\grave{\boldsymbol{\Psi}}_n^k \\ \grave{\boldsymbol{\Psi}}_n^{k\,\mathrm{T}}\grave{\mathbf{M}}_{ib} & \grave{\bar{\mathbf{M}}}_n^k \end{bmatrix} \begin{Bmatrix} \ddot{\grave{\boldsymbol{\delta}}}_b \\ \ddot{\mathbf{z}}_n^k \end{Bmatrix} + \begin{bmatrix} \grave{\mathbf{K}}_{bb} & \grave{\mathbf{K}}_{bi}\grave{\boldsymbol{\Psi}}_n^k \\ \grave{\boldsymbol{\Psi}}_n^{k\,\mathrm{T}}\grave{\mathbf{K}}_{ib} & \grave{\bar{\mathbf{K}}}_n^k \end{bmatrix} \begin{Bmatrix} \grave{\boldsymbol{\delta}}_b \\ \mathbf{z}_n^k \end{Bmatrix} = \begin{Bmatrix} \grave{\mathbf{f}}_b \\ \grave{\boldsymbol{\Psi}}_n^{k\,\mathrm{T}}\grave{\mathbf{f}}_i \end{Bmatrix} \tag{6.16}$$

Equation (6.16) could also be obtained directly by transforming Eq. (6.1) using the following transformation:

$$\begin{Bmatrix} \grave{\boldsymbol{\delta}}_b \\ \grave{\boldsymbol{\delta}}_i \end{Bmatrix} = \begin{bmatrix} \mathbf{I} & \mathbf{0} \\ \mathbf{0} & \grave{\boldsymbol{\Psi}}_n^k \end{bmatrix} \begin{Bmatrix} \grave{\boldsymbol{\delta}}_b \\ \mathbf{z}_n^k \end{Bmatrix} \tag{6.17}$$

where only selected modes are kept. In structural analysis, the boundary DOFs are often fixed.* Therefore, Eq. (6.16) simply becomes

$$\grave{\bar{\mathbf{M}}}_n^k \ddot{\mathbf{z}}_n^k + \grave{\bar{\mathbf{K}}}_n^k \mathbf{z}_n^k = \grave{\boldsymbol{\Psi}}_n^{k\,\mathrm{T}}\grave{\mathbf{f}}_i \tag{6.18}$$

In the settings of multibody dynamics, however, generally $\grave{\boldsymbol{\delta}}_b$ is allowed to deform.† Failing to include the motion from boundary DOFs may lead to large errors.

6.3.1 Mode shapes

To see a sample of mode shapes in the transformation matrix of Eq. (6.10), we continue to use the reduced beam model (c) from Section 6.2.2. Four boundary DOFs (of nodes 1 and 5) are displaced one at a time as shown in Figure 6-6, which are the first four columns (**I**) of the transformation matrix. Six (fixed-constraint) normal modes are shown in Figure 6-7, which are the last six columns ($\grave{\boldsymbol{\Psi}}_n$) of the transformation matrix. For the

---

* In structural analysis, usually at least six DOFs are fixed to the ground ($\grave{\boldsymbol{\delta}}_b = \mathbf{0}$) so that there is not rigid-body motion.

† If a nodal-fixed frame is used, there would be three (2-D) or six (3-D) zeros in $\grave{\boldsymbol{\delta}}_b$.

purpose of model reduction, only selected normal modes will be kept ($\tilde{\Psi}_n^k$). In the extreme case when no normal mode is selected, there are no deformations for the interior DOFs (nodes 2, 3, and 4). The "modes" in Figure 6-6 alone do not contribute any deformation to the interior nodes. This contradicts the fact that all the nodes are connected. Large errors are certainly expected. However, this is not a problem as long as the transformation matrix is square (i.e., no truncation ever happens).*

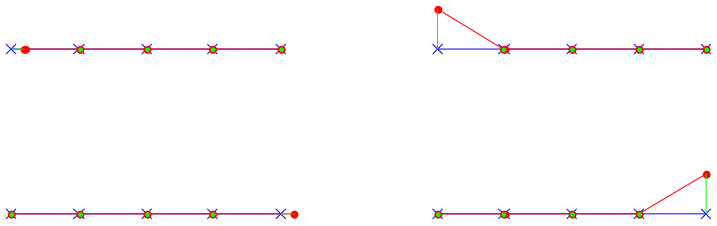

Figure 6-6: boundary movements

* Even filling up the transformation matrix with random numbers will do, provided that it has the full rank.

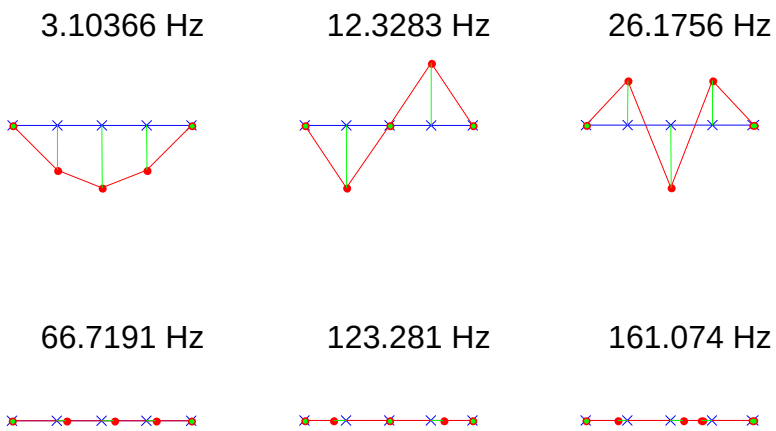

Figure 6-7: normal modes

6.4 Craig and Bampton Reduction

Neither static condensation nor modal truncation alone can give satisfactory results for a greater range of applications. It was found that, when only a limited number of DOFs are allowed, combining different types of modes can improve accuracy. Hurty [42] composed nodal displacements from three categories: rigid-body modes, constraint modes, and normal modes. The rigid-body modes, which result from displacing determinate constraints*, cause no stresses to the body. The constraint modes exist only if there are redundant constraints†; these modes are obtained by statically giving each

---

* Determinate constraints can uniquely define the configuration of a body, rigid or deformable, in space. For a 2-D body, it requires three constraints; for a 3-D body, it requires six constraints.

† If there are more constraints than required in defining the configuration of a (deformable) body, the extra constraints (at one's discretion) are considered as redundant constraints.

redundant constraint an arbitrary displacement successively with all other constraints fixed and all interior nodes free. The normal modes are eigen-modes that define how the interior nodes may vibrate when all the constraints are fixed.* To reduce the total number of DOFs, only a small number of normal modes are kept.

Unlike Hurty who separated the determinate and redundant constraints—for a highly constrained component, it is often not clear which ones should be considered determinate and which others should be considered redundant—Craig and Bampton [43] instead treated all boundary nodes in the same manner, producing only the constraint modes. The rigid-body modes are hereby included in the constraint modes implicitly. The normal modes are still obtained as before. The remaining of this section constructs the transformation matrix of reduction and expands the reduced stiffness and mass matrices.

The nodal coordinates are divided into two sets: Set *b* is for the boundary coordinates and set *i* is for the interior coordinates. The stiffness and mass matrices are partitioned according to sets *b* and *i* as in Eq. (6.1). The modal coordinates are also divided into two sets: constraint modes and normal modes. The constraint modes (the portion for the interior coordinates) are prepared by $\grave{\mathbf{\Psi}}_s = -\grave{\mathbf{K}}_{ii}^{-1}\grave{\mathbf{K}}_{ib}$.† The normal

---

* Thus they are also called fixed-constraint or fixed-interface normal modes.

† Matrix $\grave{\mathbf{K}}_{ii}$ is invertible only if at least six DOFs (for a 3-D deformable body) have been designated properly as the boundary coordinates.

modes are prepared by $\left[\grave{\boldsymbol{\Psi}}_n, \boldsymbol{\Lambda}_n\right] = \mathrm{eig}\left(\grave{\mathbf{K}}_{ii}, \grave{\mathbf{M}}_{ii}\right)$. All of the constraint modes and some of the normal modes are combined to form the transformation matrix of reduction

$$\grave{\boldsymbol{\Psi}} = \begin{bmatrix} \mathbf{I} & \mathbf{0} \\ \grave{\boldsymbol{\Psi}}_s & \grave{\boldsymbol{\Psi}}_n^k \end{bmatrix} \tag{6.19}$$

Matrix $\grave{\boldsymbol{\Psi}}_n^k$ contains the normal modes that are kept; the rest of them ($\grave{\boldsymbol{\Psi}}_n^d$) are deleted. Therefore, the reduced stiffness matrix becomes

$$\grave{\boldsymbol{\Psi}}^{\mathrm{T}} \grave{\mathbf{K}} \grave{\boldsymbol{\Psi}} = \begin{bmatrix} \grave{\mathbf{K}}_{\mathrm{G}} & \mathbf{0} \\ \mathbf{0} & \grave{\bar{\mathbf{K}}}_n^k \end{bmatrix} \tag{6.20}$$

where

$$\grave{\mathbf{K}}_{\mathrm{G}} = \grave{\mathbf{K}}_{bb} - \grave{\mathbf{K}}_{bi} \grave{\mathbf{K}}_{ii}^{-1} \grave{\mathbf{K}}_{ib} \tag{6.21}$$

$$\grave{\bar{\mathbf{K}}}_n^k = \grave{\boldsymbol{\Psi}}_n^{k\,\mathrm{T}} \grave{\mathbf{K}}_{ii} \grave{\boldsymbol{\Psi}}_n^k \tag{6.22}$$

The reduced mass matrix becomes

$$\grave{\boldsymbol{\Psi}}^{\mathrm{T}} \grave{\mathbf{M}} \grave{\boldsymbol{\Psi}} = \begin{bmatrix} \grave{\mathbf{M}}_{\mathrm{G}} & \grave{\mathbf{M}}_{bi} \grave{\boldsymbol{\Psi}}_n + \grave{\boldsymbol{\Psi}}_s^{\mathrm{T}} \grave{\mathbf{M}}_{ii} \grave{\boldsymbol{\Psi}}_n \\ \grave{\boldsymbol{\Psi}}_n^{\mathrm{T}} \grave{\mathbf{M}}_{ib} + \grave{\boldsymbol{\Psi}}_n^{\mathrm{T}} \grave{\mathbf{M}}_{ii} \grave{\boldsymbol{\Psi}}_s & \grave{\bar{\mathbf{M}}}_n^k \end{bmatrix} \tag{6.23}$$

in which

$$\grave{\mathbf{M}}_{\mathrm{G}} = \grave{\mathbf{M}}_{bb} + \grave{\mathbf{M}}_{bi} \grave{\boldsymbol{\Psi}}_s + \grave{\boldsymbol{\Psi}}_s^{\mathrm{T}} \grave{\mathbf{M}}_{ib} + \grave{\boldsymbol{\Psi}}_s^{\mathrm{T}} \grave{\mathbf{M}}_{ii} \grave{\boldsymbol{\Psi}}_s \tag{6.24}$$

$$\grave{\bar{\mathbf{M}}}_n^k = \grave{\boldsymbol{\Psi}}_n^{k\,\mathrm{T}} \grave{\mathbf{M}}_{ii} \grave{\boldsymbol{\Psi}}_n^k \tag{6.25}$$

Note that $\grave{\mathbf{K}}_{\mathrm{G}}$ and $\grave{\mathbf{M}}_{\mathrm{G}}$ are the Guyan reduced stiffness and mass matrices. Also, $\grave{\bar{\mathbf{K}}}_n^k$ and $\grave{\bar{\mathbf{M}}}_n^k$ are both diagonal because $\grave{\mathbf{K}}_{ii}$ and $\grave{\mathbf{M}}_{ii}$ are simultaneously diagonalized by $\grave{\boldsymbol{\Psi}}_n$.

6.4.1 Mode shapes

To visualize the mode shapes in Eq. (6.19), we are back on the reduced beam model (c) from Section 6.2.2. Nodes 1 and 5 are the boundary nodes. Hence, there are four constraint modes, which are exactly those of Figure 6-5. They are repeated in the left column of Figure 6-8. Nodes 2, 3, and 4 are the interior nodes. Hence, there are six (fixed-constraint) normal modes, which are exactly those of Figure 6-7. If we could only afford to keep two normal modes, likely we would pick the first and second bending modes from Figure 6-7.* They are repeated in the right column of Figure 6-8. This reduction method comprises the ingredients from both static condensation and modal truncation, resulting in exact static solutions and less dynamic errors.

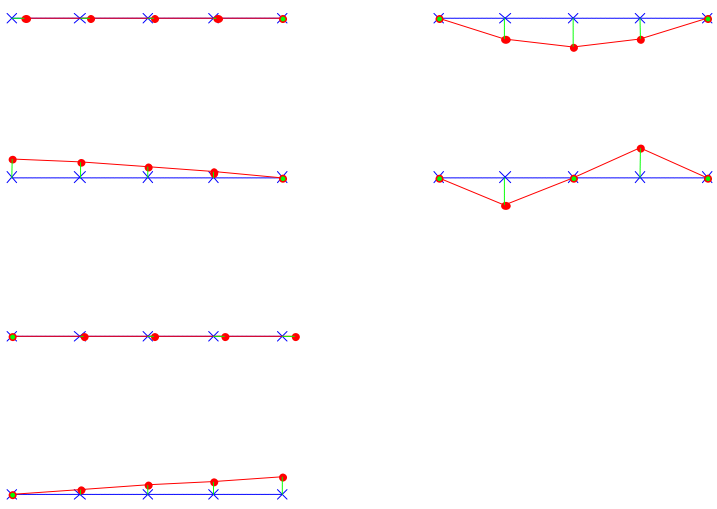

Figure 6-8: constraint and normal modes

* Two reasons for choosing them: First, they have the lowest natural frequencies among the normal modes. Secondly, there lack bending modes in the constraint modes.

6.5 Mode Condensation

Although methods of component mode synthesis, which intuitively combine different types of modes, seem to improve the quality of model reduction in many cases, no physical explanations have been provided to justify the various constructions. This leads to the following questions: Why are, for example, constraint modes and normal modes simply pieced together to form the transformation matrix of reduction? What is the reasoning behind it? In a separate attempt to better understand how to properly condense a deformable body restrained by joints or forces in a multibody system, Nikravesh found a different reduction method called mode condensation [50]. An alternative approach to derive the new method is provided in this section. This new method is also proven equivalent to Craig and Bampton reduction [43].

6.5.1 Nikravesh's method

Nikravesh developed a condensation method that begins with the one in Section 6.3. Similar to a statement for (nodal) static condensation [52][*], he assumed that the inertia and external forces associated with the deleted modes are relocated to the boundary nodes. Therefore, the third row from Eq. (6.15) is simplified to

$$\mathbf{z}_n^d \cong \left(-\bar{\mathbf{K}}_n^{d\,-1}\,\boldsymbol{\Psi}_n^{d\,\mathrm{T}}\,\mathbf{K}_{ib}\right)\boldsymbol{\delta}_b = \boldsymbol{\Theta}\,\boldsymbol{\delta}_b \tag{6.26}$$

where

---

[*] Cook explains that "inertia forces on slaves are negligible in comparison with elastic forces transmitted to slaves by the motion of masters."

$$\boldsymbol{\Theta} = -\bar{\mathbf{K}}_n^{d\,-1}\boldsymbol{\Psi}_n^{d\,\mathrm{T}}\mathbf{K}_{ib} \tag{6.27}$$

Substituting Eq. (6.26) into Eq. (6.10) yields

$$\begin{Bmatrix}\boldsymbol{\delta}_b\\ \boldsymbol{\delta}_i\end{Bmatrix} = \begin{bmatrix}\mathbf{I} & \mathbf{0} & \mathbf{0}\\ \mathbf{0} & \boldsymbol{\Psi}_n^k & \boldsymbol{\Psi}_n^d\end{bmatrix}\begin{Bmatrix}\boldsymbol{\delta}_b\\ \mathbf{z}_n^k\\ \boldsymbol{\Theta}\boldsymbol{\delta}_b\end{Bmatrix} = \begin{bmatrix}\mathbf{I} & \mathbf{0} & \mathbf{0}\\ \mathbf{0} & \boldsymbol{\Psi}_n^k & \boldsymbol{\Psi}_m\end{bmatrix}\begin{Bmatrix}\boldsymbol{\delta}_b\\ \mathbf{z}_n^k\\ \boldsymbol{\delta}_b\end{Bmatrix} = \boldsymbol{\Psi}_{\mathrm{MC}}\begin{Bmatrix}\boldsymbol{\delta}_b\\ \mathbf{z}_n^k\end{Bmatrix} \tag{6.28}$$

in which

$$\boldsymbol{\Psi}_m = \boldsymbol{\Psi}_n^d\boldsymbol{\Theta} = -\boldsymbol{\Psi}_n^d\bar{\mathbf{K}}_n^{d\,-1}\boldsymbol{\Psi}_n^{d\,\mathrm{T}}\mathbf{K}_{ib} \tag{6.29}$$

$$\boldsymbol{\Psi}_{\mathrm{MC}} = \begin{bmatrix}\mathbf{I} & \mathbf{0}\\ \boldsymbol{\Psi}_m & \boldsymbol{\Psi}_n^k\end{bmatrix} \tag{6.30}$$

Equation (6.30) defines the transformation matrix of reduction for this method.

6.5.2 Minimum potential energy

Equation (6.26) can also be derived from the potential energy function. Similar to a statement by Irons [53, 54]*, we may assume that the potential energy with respect to the deleted modes is a minimum (i.e., no generalized forces for $\mathbf{z}_n^d$). The potential (strain) energy of the body can be expressed as

$$PE = \frac{1}{2}\boldsymbol{\delta}^{\mathrm{T}}\mathbf{K}\boldsymbol{\delta} = \frac{1}{2}\begin{Bmatrix}\boldsymbol{\delta}_b\\ \mathbf{z}_n^k\\ \mathbf{z}_n^d\end{Bmatrix}^{\mathrm{T}}\begin{bmatrix}\mathbf{K}_{bb} & \mathbf{K}_{bi}\boldsymbol{\Psi}_n^k & \mathbf{K}_{bi}\boldsymbol{\Psi}_n^d\\ \boldsymbol{\Psi}_n^{k\,\mathrm{T}}\mathbf{K}_{ib} & \bar{\mathbf{K}}_n^k & \mathbf{0}\\ \boldsymbol{\Psi}_n^{d\,\mathrm{T}}\mathbf{K}_{ib} & \mathbf{0} & \bar{\mathbf{K}}_n^d\end{bmatrix}\begin{Bmatrix}\boldsymbol{\delta}_b\\ \mathbf{z}_n^k\\ \mathbf{z}_n^d\end{Bmatrix} \tag{6.31}$$

---

* According to Meirovitch's explanation on mass condensation [41], "Irons assumes that the potential energy has a minimum with respect to slave displacements, which is the same as saying that there are no applied forces associated with the slave displacements. By implication, inertia forces are included in the applied forces."

for which Eq. (6.10) has been used. Setting the partial derivatives of *PE* with respect to $\mathbf{z}_n^d$ to zero yields

$$\frac{\partial PE}{\partial \mathbf{z}_n^d} = \begin{Bmatrix} \grave{\boldsymbol{\delta}}_b \\ \mathbf{z}_n^d \end{Bmatrix}^{\mathrm{T}} \begin{bmatrix} \grave{\mathbf{K}}_{bi} \grave{\boldsymbol{\Psi}}_n^d \\ \grave{\bar{\mathbf{K}}}_n^d \end{bmatrix} = \grave{\boldsymbol{\delta}}_b^{\mathrm{T}} \grave{\mathbf{K}}_{bi} \grave{\boldsymbol{\Psi}}_n^d + \mathbf{z}_n^{d\,\mathrm{T}} \grave{\bar{\mathbf{K}}}_n^d = \mathbf{0}^{\mathrm{T}} \tag{6.32}$$

Equation (6.32) stands for the same relation obtained in Eq. (6.26).

6.5.3 Mode shapes

To demonstrate how the mode shapes in Eq. (6.30) may appear, we continue with the reduced beam model (c) from Section 6.2.2. Nodes 1 and 5 are the boundary nodes. Nodes 2, 3, and 4 are the interior nodes. There are six normal modes, which are the same as those of Figure 6-7. Among the six normal modes, say, only the first and second bending modes are kept. They are repeated in the right column of Figure 6-9. There are four "boundary" modes, which are plotted in the left column of Figure 6-9. The second and fourth boundary modes look wavy. This is due to the third bending mode of Figure 6-7. Together with other deleted modes, it finds the way into $\grave{\boldsymbol{\Psi}}_m$ via Eq. (6.29). Like the constraint modes in Figure 6-8, the boundary modes would pick up the static solutions when the normal modes die down.

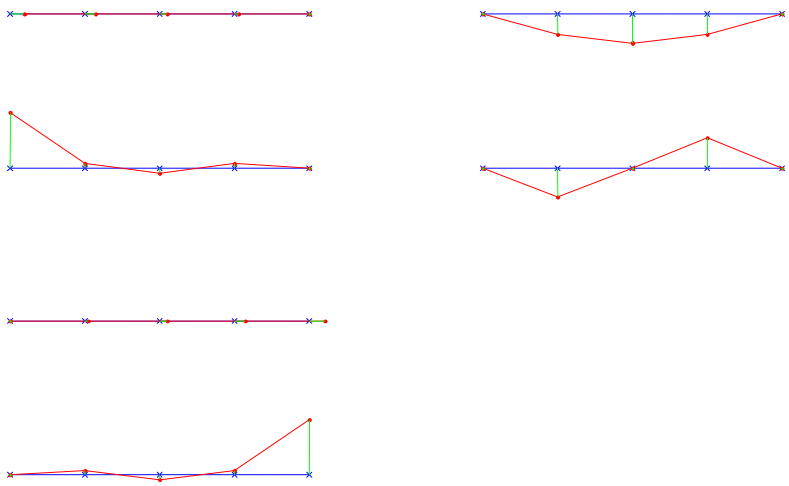

Figure 6-9: boundary and normal modes

6.5.4 Equivalence to Craig and Bampton reduction

The transformation matrix of reduction for Craig-Bampton's method from Section 6.4 is

$$\grave{\boldsymbol{\Psi}}_{\mathrm{CB}} = \begin{bmatrix} \mathbf{I} & \mathbf{0} \\ \grave{\boldsymbol{\Psi}}_s & \grave{\boldsymbol{\Psi}}_n^k \end{bmatrix} \tag{6.33}$$

which looks different from Eq. (6.30) for Nikravesh's method. Yet all test simulations show that Nikravesh's and Craig-Bampton's methods yield practically the same results ($\grave{\boldsymbol{\delta}}$). This leads us to wonder if Eqs. (6.30) and (6.33) indeed span the same column space. To answer the question, we seek if it is always feasible to manipulate the columns of Eq. (6.30) into those of Eq. (6.33) by the following conversion:

$$\grave{\boldsymbol{\Psi}}_m + \grave{\boldsymbol{\Psi}}_n^k \mathbf{X} \rightarrow \grave{\boldsymbol{\Psi}}_s \tag{6.34}$$

where $\mathbf{X}$ is a matrix to be found.* The existence of such $\mathbf{X}$ is proven as follows:

$$\begin{aligned}
\grave{\boldsymbol{\Psi}}_s &= -\grave{\mathbf{K}}_{ii}^{-1}\grave{\mathbf{K}}_{ib} = -\left(\grave{\boldsymbol{\Psi}}_n^{-\mathrm{T}}\grave{\bar{\mathbf{K}}}_n\grave{\boldsymbol{\Psi}}_n^{-1}\right)^{-1}\grave{\mathbf{K}}_{ib} \\
&= -\grave{\boldsymbol{\Psi}}_n\grave{\bar{\mathbf{K}}}_n^{-1}\grave{\boldsymbol{\Psi}}_n^{\mathrm{T}}\grave{\mathbf{K}}_{ib} = -\begin{bmatrix}\grave{\boldsymbol{\Psi}}_n^k & \grave{\boldsymbol{\Psi}}_n^d\end{bmatrix}\begin{bmatrix}\grave{\bar{\mathbf{K}}}_n^k & \mathbf{0} \\ \mathbf{0} & \grave{\bar{\mathbf{K}}}_n^d\end{bmatrix}^{-1}\begin{bmatrix}\grave{\boldsymbol{\Psi}}_n^{k\,\mathrm{T}} \\ \grave{\boldsymbol{\Psi}}_n^{d\,\mathrm{T}}\end{bmatrix}\grave{\mathbf{K}}_{ib} \\
&= -\begin{bmatrix}\grave{\boldsymbol{\Psi}}_n^k & \grave{\boldsymbol{\Psi}}_n^d\end{bmatrix}\begin{bmatrix}\grave{\bar{\mathbf{K}}}_n^{k\,-1}\grave{\boldsymbol{\Psi}}_n^{k\,\mathrm{T}}\grave{\mathbf{K}}_{ib} \\ \grave{\bar{\mathbf{K}}}_n^{d\,-1}\grave{\boldsymbol{\Psi}}_n^{d\,\mathrm{T}}\grave{\mathbf{K}}_{ib}\end{bmatrix} = \begin{bmatrix}\grave{\boldsymbol{\Psi}}_n^k & \grave{\boldsymbol{\Psi}}_n^d\end{bmatrix}\begin{bmatrix}\mathbf{X} \\ \boldsymbol{\Theta}\end{bmatrix} \\
&= \grave{\boldsymbol{\Psi}}_n^k\mathbf{X} + \grave{\boldsymbol{\Psi}}_n^d\boldsymbol{\Theta} = \grave{\boldsymbol{\Psi}}_n^k\mathbf{X} + \grave{\boldsymbol{\Psi}}_m
\end{aligned}$$

in which $\mathbf{X} = -\grave{\bar{\mathbf{K}}}_n^{k\,-1}\grave{\boldsymbol{\Psi}}_n^{k\,\mathrm{T}}\grave{\mathbf{K}}_{ib}$ is found. The proof shows that there exists such $\mathbf{X}$ that Nikravesh's method can be manipulated into Craig and Bampton's. Because the two transformation matrices of reduction do span the same column space, theoretically no discrepancy is expected in their simulation results. Yet, $\grave{\boldsymbol{\Psi}}_{\mathrm{MC}}$ is more conceptually correct as $\grave{\boldsymbol{\Psi}}_s$ shall emerge only when there is no $\grave{\boldsymbol{\Psi}}_n^k$ left.† Nonetheless, it is more convenient to prepare $\grave{\boldsymbol{\Psi}}_{\mathrm{CB}}$ because $\grave{\boldsymbol{\Psi}}_s$ is constant (whereas $\grave{\boldsymbol{\Psi}}_m$ in $\grave{\boldsymbol{\Psi}}_{\mathrm{MC}}$ is affected by $\grave{\boldsymbol{\Psi}}_n^d$). Besides, it is expensive to solve a large, complete eigen-problem first in order to obtain $\grave{\boldsymbol{\Psi}}_n$, which includes $\grave{\boldsymbol{\Psi}}_n^d$. On the contrary, $\grave{\boldsymbol{\Psi}}_n^k$ alone can be obtained by solving the eigen-problem partially or be measured experimentally.

---

* Numerous tests confirm that least-squared solutions of $\mathbf{X}$ solved from Eq. (6.34) with different $\grave{\boldsymbol{\Psi}}_m$ all satisfy Eq. (6.34) perfectly. This highly suggests that the conversion in Eq. (6.34) may be entirely possible.

† If all normal modes are deleted, $\grave{\boldsymbol{\Psi}}_m$ turns into $\grave{\boldsymbol{\Psi}}_s$. The condensation becomes Guyan reduction.

6.6 Eitelberg's Method

For linear time invariant systems, Eitelberg proposed a reduction method that offers zero steady state errors and minimizes dynamic errors [28, 29]. To apply this method to structures, the structural equations of motion are rearranged in state space form. Tests conclude that Eitelberg's method is equivalent to Guyan reduction for structures.

6.6.1 Problem statement and the algorithm

Given a linear time invariant system in state space form

$$\dot{\mathbf{x}} = \boldsymbol{A}\mathbf{x} + \boldsymbol{B}\mathbf{u} \tag{6.35}$$

$$\mathbf{y} = \boldsymbol{C}\mathbf{x} \tag{6.36}$$

where state vector $\mathbf{x} \in \mathbb{R}^n$, Eitelberg's method finds a reduced system

$$\dot{\boldsymbol{\xi}} = \boldsymbol{A}_r\boldsymbol{\xi} + \boldsymbol{B}_r\mathbf{u} \tag{6.37}$$

$$\boldsymbol{\eta} = \boldsymbol{C}_r\boldsymbol{\xi} \tag{6.38}$$

where state vector $\boldsymbol{\xi} \in \mathbb{R}^\nu$ ($\nu < n$) such that the following conditions are satisfied:

(1) The steady state errors between the original and reduced systems are zero.

(2) The dynamic errors between the original and reduced systems are minimized.

The output of the reduced system approximates the output of the original system; i.e., $\boldsymbol{\eta} \approx \mathbf{y}$. The relation between $\boldsymbol{C}$ and $\boldsymbol{C}_r$ is $\boldsymbol{C} = \boldsymbol{C}_r\boldsymbol{R}$ where $\boldsymbol{R}$ is a matrix that selects which state variables to keep; i.e., $\mathbf{x}_r = \boldsymbol{R}\mathbf{x}$ and $\mathbf{x}_r \approx \boldsymbol{\xi}$. Details about the derivation of this method are described in [28, 29]. Here, only the algorithm is briefed. If $\boldsymbol{A}$ is singular,

replace $\boldsymbol{A}$ with $\boldsymbol{A}$-$\boldsymbol{B}$*$\boldsymbol{L}$*$\boldsymbol{C}$ where $\boldsymbol{L}$ is a matrix for output feedback.* From the Lyapunov (Ljapunov) matrix equation, $\boldsymbol{AS}+\boldsymbol{SA}'=-(\boldsymbol{A}^{-1}\boldsymbol{B})(\boldsymbol{A}^{-1}\boldsymbol{B})'$, matrix $\boldsymbol{S}$ is first solved.† Matrix $\boldsymbol{A}_r$ is next computed by $\boldsymbol{A}_r=\boldsymbol{RASR}'(\boldsymbol{RSR}')^{-1}$ which fulfills condition (2). Matrix $\boldsymbol{B}_r$ is then computed by $\boldsymbol{B}_r=\boldsymbol{A}_r\boldsymbol{RA}^{-1}\boldsymbol{B}$ which is the necessary and sufficient condition for condition (1). Matrix $\boldsymbol{C}_r$ is simply computed by $\boldsymbol{C}_r$=$\boldsymbol{C}$/$\boldsymbol{R}$ (generalized inverse). In APPENDIX C, the MATLAB subroutine eitelberg() takes in $\boldsymbol{A}$, $\boldsymbol{B}$, $\boldsymbol{C}$, $\boldsymbol{R}$ and returns $\boldsymbol{A}_r$, $\boldsymbol{B}_r$, and $\boldsymbol{C}_r$.

6.6.2 Application to structural model reduction

The structural equations of motion without damping are

$$\mathbf{M}\ddot{\boldsymbol{\delta}}=-\mathbf{K}\boldsymbol{\delta}+\mathbf{f} \tag{6.39}$$

To put Eq. (6.39) in state space form, we let $\mathbf{x}_1=\boldsymbol{\delta}$ and $\mathbf{x}_2=\dot{\boldsymbol{\delta}}$. And,

$$\dot{\mathbf{x}}_1=\dot{\boldsymbol{\delta}}=\mathbf{x}_2 \tag{6.40}$$

$$\dot{\mathbf{x}}_2=\ddot{\boldsymbol{\delta}}=\mathbf{M}^{-1}\left(-\mathbf{K}\boldsymbol{\delta}+\mathbf{f}\right)=-\mathbf{M}^{-1}\mathbf{K}\mathbf{x}_1+\mathbf{M}^{-1}\mathbf{f} \tag{6.41}$$

or

$$\begin{Bmatrix}\dot{\mathbf{x}}_1\\ \dot{\mathbf{x}}_2\end{Bmatrix}=\begin{bmatrix}\mathbf{0} & \mathbf{I}\\ -\mathbf{M}^{-1}\mathbf{K} & \mathbf{0}\end{bmatrix}\begin{Bmatrix}\mathbf{x}_1\\ \mathbf{x}_2\end{Bmatrix}+\begin{bmatrix}\mathbf{0}\\ \mathbf{M}^{-1}\end{bmatrix}\mathbf{f} \tag{6.42}$$

---

* At this point, all poles of $\boldsymbol{A}$ are assumed stable. If not, one is advised to consult the sources.

† Note that operator ' means “complex conjugate transpose.”

Suppose that nodes are split into two sets—*b* for boundary DOFs and *i* for interior DOFs. Assume that there are no forces on set *i*; i.e., $\grave{\mathbf{f}}_i = \mathbf{0}$. Equation (6.42) is thus simplified to

$$\begin{Bmatrix} \dot{\mathbf{x}}_1 \\ \dot{\mathbf{x}}_2 \end{Bmatrix} = \begin{bmatrix} \mathbf{0} & \mathbf{I} \\ -\grave{\mathbf{M}}^{-1}\grave{\mathbf{K}} & \mathbf{0} \end{bmatrix} \begin{Bmatrix} \mathbf{x}_1 \\ \mathbf{x}_2 \end{Bmatrix} + \begin{bmatrix} \mathbf{0} \\ \left(\grave{\mathbf{M}}^{-1}\right)_{:b} \end{bmatrix} \grave{\mathbf{f}}_b \tag{6.43}$$

or

$$\begin{Bmatrix} \grave{\boldsymbol{\delta}} \\ \grave{\ddot{\boldsymbol{\delta}}} \end{Bmatrix} = \underbrace{\begin{bmatrix} \mathbf{0} & \mathbf{I} \\ -\grave{\mathbf{M}}^{-1}\grave{\mathbf{K}} & \mathbf{0} \end{bmatrix}}_{\boldsymbol{A}} \begin{Bmatrix} \grave{\boldsymbol{\delta}} \\ \grave{\dot{\boldsymbol{\delta}}} \end{Bmatrix} + \underbrace{\begin{bmatrix} \mathbf{0} \\ \left(\grave{\mathbf{M}}^{-1}\right)_{:b} \end{bmatrix}}_{\boldsymbol{B}} \grave{\mathbf{f}}_b \tag{6.44}$$

where $\left(\grave{\mathbf{M}}^{-1}\right)_{:b}$ contains only the *b* columns of $\grave{\mathbf{M}}^{-1}$. The $\boldsymbol{A}$ and $\boldsymbol{B}$ matrices are constructed as indicated in Eq. (6.44). Presume that $\grave{\boldsymbol{\delta}}_b$ and $\grave{\dot{\boldsymbol{\delta}}}_b$ are the state variables to keep. They are selected from the full state vector by matrix $\boldsymbol{R}$ as

$$\begin{Bmatrix} \grave{\boldsymbol{\delta}}_b \\ \grave{\dot{\boldsymbol{\delta}}}_b \end{Bmatrix} \Leftarrow \mathbf{x}_r = \boldsymbol{R}\mathbf{x} \Rightarrow \underbrace{\begin{bmatrix} \mathbf{I} & \mathbf{0} & \mathbf{0} & \mathbf{0} \\ \mathbf{0} & \mathbf{0} & \mathbf{I} & \mathbf{0} \end{bmatrix}}_{\boldsymbol{R}} \begin{Bmatrix} \grave{\boldsymbol{\delta}}_b \\ \grave{\boldsymbol{\delta}}_i \\ \grave{\dot{\boldsymbol{\delta}}}_b \\ \grave{\dot{\boldsymbol{\delta}}}_i \end{Bmatrix} \tag{6.45}$$

Matrix $\boldsymbol{C}$ is simply set to be $\boldsymbol{R}$. If $\boldsymbol{A}$ is singular, $\boldsymbol{A}$ should be replaced with $\boldsymbol{A}$-$\boldsymbol{B}$*$\boldsymbol{L}$*$\boldsymbol{C}$ where $\boldsymbol{L}$ is at our choice. Then, a function call is made to eitelberg(): $[\boldsymbol{A}_r, \boldsymbol{B}_r, \boldsymbol{C}_r] = \text{eitelberg}(\boldsymbol{A}, \boldsymbol{B}, \boldsymbol{C}, \boldsymbol{R})$. Afterwards, to undo the artificial change introduced by

$\boldsymbol{L}$—because it is not our intention here to design a controller—$\boldsymbol{A}_r$ is restored by $\boldsymbol{A}_r+\boldsymbol{B}_r*\boldsymbol{L}*\boldsymbol{C}_r$.[#]

6.6.3 Eigen-properties of the reduced model

The reduced mass and stiffness matrices do not immediately show themselves in the obtained matrices $\boldsymbol{A}_r$, $\boldsymbol{B}_r$, and $\boldsymbol{C}_r$. To find out where they are hiding, we begin with Eq. (6.44) by moving $\grave{}\mathbf{M}$ back to the left-hand-side:

$$\begin{Bmatrix} \grave{}\dot{\boldsymbol{\delta}} \\ \grave{}\mathbf{M}\grave{}\ddot{\boldsymbol{\delta}} \end{Bmatrix} = \begin{bmatrix} \mathbf{0} & \mathbf{I} \\ -\grave{}\mathbf{K} & \mathbf{0} \end{bmatrix} \begin{Bmatrix} \grave{}\boldsymbol{\delta} \\ \grave{}\dot{\boldsymbol{\delta}} \end{Bmatrix} + \begin{bmatrix} \mathbf{0} \\ \mathbf{I}_{:b} \end{bmatrix} \grave{}\mathbf{f}_b \tag{6.46}$$

Imagine that there exists a transformation matrix of reduction, $\grave{}\boldsymbol{\Psi}$, such that $\grave{}\boldsymbol{\delta} = \grave{}\boldsymbol{\Psi}\grave{}\boldsymbol{\delta}_b$, $\grave{}\dot{\boldsymbol{\delta}} = \grave{}\boldsymbol{\Psi}\grave{}\dot{\boldsymbol{\delta}}_b$, and $\grave{}\ddot{\boldsymbol{\delta}} = \grave{}\boldsymbol{\Psi}\grave{}\ddot{\boldsymbol{\delta}}_b$. Equation (6.46) is hence transformed into

$$\begin{Bmatrix} \grave{}\dot{\boldsymbol{\delta}}_b \\ \grave{}\boldsymbol{\Psi}^{\mathrm{T}}\grave{}\mathbf{M}\grave{}\boldsymbol{\Psi}\grave{}\ddot{\boldsymbol{\delta}}_b \end{Bmatrix} = \begin{bmatrix} \mathbf{0} & \mathbf{I} \\ -\grave{}\boldsymbol{\Psi}^{\mathrm{T}}\grave{}\mathbf{K}\grave{}\boldsymbol{\Psi} & \mathbf{0} \end{bmatrix} \begin{Bmatrix} \grave{}\boldsymbol{\delta}_b \\ \grave{}\dot{\boldsymbol{\delta}}_b \end{Bmatrix} + \begin{bmatrix} \mathbf{0} \\ \grave{}\boldsymbol{\Psi}^{\mathrm{T}}\mathbf{I}_{:b} \end{bmatrix} \grave{}\mathbf{f}_b \tag{6.47}$$

or

$$\begin{Bmatrix} \grave{}\dot{\boldsymbol{\delta}}_b \\ \underline{\mathbf{M}}\grave{}\ddot{\boldsymbol{\delta}}_b \end{Bmatrix} = \begin{bmatrix} \mathbf{0} & \mathbf{I} \\ -\grave{}\underline{\mathbf{K}} & \mathbf{0} \end{bmatrix} \begin{Bmatrix} \grave{}\boldsymbol{\delta}_b \\ \grave{}\dot{\boldsymbol{\delta}}_b \end{Bmatrix} + \begin{bmatrix} \mathbf{0} \\ \grave{}\boldsymbol{\Psi}^{\mathrm{T}}\mathbf{I}_{:b} \end{bmatrix} \grave{}\mathbf{f}_b \tag{6.48}$$

in which $\grave{}\underline{\mathbf{M}} = \grave{}\boldsymbol{\Psi}^{\mathrm{T}}\grave{}\mathbf{M}\grave{}\boldsymbol{\Psi}$ is the reduced mass matrix and $\grave{}\underline{\mathbf{K}} = \grave{}\boldsymbol{\Psi}^{\mathrm{T}}\grave{}\mathbf{K}\grave{}\boldsymbol{\Psi}$ is the reduced stiffness matrix. Moving $\grave{}\underline{\mathbf{M}}$ to the right-hand-side yields

---

[#] This is a trick suggested by Dr. François E. Cellier, fcellier@inf.ethz.ch. One shall check if the old $\boldsymbol{A}$ and the new $\boldsymbol{A}_r$ bear the same coherence. For instance, they should have the same number of zero singular values.

$$\begin{Bmatrix} \grave{\boldsymbol{\delta}}_b \\ \grave{\ddot{\boldsymbol{\delta}}}_b \end{Bmatrix} = \underbrace{\begin{bmatrix} \mathbf{0} & \mathbf{I} \\ -\grave{\underline{\mathbf{M}}}^{-1}\grave{\underline{\mathbf{K}}} & \mathbf{0} \end{bmatrix}}_{\boldsymbol{A}_r} \begin{Bmatrix} \grave{\boldsymbol{\delta}}_b \\ \grave{\dot{\boldsymbol{\delta}}}_b \end{Bmatrix} + \underbrace{\begin{bmatrix} \mathbf{0} \\ \grave{\underline{\mathbf{M}}}^{-1}\grave{\boldsymbol{\Psi}}^{\mathrm{T}}\mathbf{I}_{:b} \end{bmatrix}}_{\boldsymbol{B}_r} \grave{\mathbf{f}}_b \tag{6.49}$$

Equation (6.49) reveals what we would expect of $\boldsymbol{A}_r$ and $\boldsymbol{B}_r$. The trouble is that $\grave{\underline{\mathbf{M}}}$, $\grave{\underline{\mathbf{K}}}$, and $\grave{\boldsymbol{\Psi}}$ are not individually identifiable in them. Nonetheless, the eigen-properties of a regular eigen-problem as eig($\grave{\underline{\mathbf{M}}}^{-1}\grave{\underline{\mathbf{K}}}$) are not different from the eigen-properties of a generalized eigen-problem as eig($\grave{\underline{\mathbf{K}}}$,$\grave{\underline{\mathbf{M}}}$) if $\grave{\underline{\mathbf{M}}}$ and $\grave{\underline{\mathbf{K}}}$ were available.

6.6.4 Test on a beam model

In this section, we test Eitelberg's method on the beam model in APPENDIX A. To reduce the beam model to a smaller size, we choose nodes 1, 3, and 5 as the boundary nodes (set *b*) and nodes 2 and 4 as the interior nodes (set *i*). This is the case with the reduced beam model (a) in Figure 6-2. Matrices ***A***, ***B***, ***C***, and ***R*** are prepared accordingly. To get around the singularity of ***A***, we replace ***A*** with ***A***–***B*****L***C*** where ***L*** is chosen for convenience as $\boldsymbol{L} = [\mathbf{I}_{6x6}, \mathbf{I}_{6x6}]$ in which $\mathbf{I}_{6x6}$ is a 6 by 6 identity matrix. After the function call to $[\boldsymbol{A}_r,\boldsymbol{B}_r,\boldsymbol{C}_r]$ = eitelberg($\boldsymbol{A},\boldsymbol{B},\boldsymbol{C},\boldsymbol{R}$), we restore ***A****r* by ***A****r*+$\boldsymbol{B}_r$**L***$\boldsymbol{C}_r$. From the restored ***A****r*, we then extract $\grave{\underline{\mathbf{M}}}^{-1}\grave{\underline{\mathbf{K}}}$, which is

2.5e+005	0	-3e+005	0	50000	0
0	416.07	0	-832.14	0	416.07
-1.5e+005	0	3e+005	0	-1.5e+005	0
0	-284.68	0	569.36	0	-284.68
50000	0	-3e+005	0	2.5e+005	0
0	416.07	0	-832.14	0	416.07

Examining the eigen-properties of $\grave{\underline{\mathbf{M}}}^{-1}\grave{\underline{\mathbf{K}}}$ unveils that this reduced model has the same (non-zero) eigen-values (and matched eigen-vectors) as those in Figure 6-3(a) by Guyan reduction: 5.95823, 71.1763, and 123.281 Hz. The results indicate that for structures Eitelberg's method is basically Guyan reduction.* For our application purposes, there is no need to continue with Eitelberg's method since Guyan reduction is much easier to conduct.

* Tests are also performed on more complex models such as the slab model in APPENDIX B for which nodes 16, 18, 28, and 30 are the boundary nodes.

7 NUMERICAL TESTS

Several reduction methods have been reviewed in the previous chapter. Different reduction methods are distinguished by their transformation matrices. Each column of a transformation matrix represents a (generalized) mode shape. The columns or mode shapes span a particular subspace, called column space, for the associated reduction method. The success of a reduction method relies on how well the column space matches up with the conditions under which the deformable body is (or is not) restrained by joints or forces. To compare the reduction methods, we look at two aspects: deformed profiles and time simulations.

7.1 Deformed Profiles

In this section, the reduction methods of interest are modal truncation (MT), Craig and Bampton (CB) reduction, and mode condensation (MC). Their transformation matrices are tabulated in Table 7-1. The two-dimensional beam from APPENDIX A is again used as an example for illustration purpose because of its simplicity. Nodes 1 and 5 are chosen as the boundary nodes; there are four “boundary modes.” Only two normal modes are kept; they are the first and second bending modes. The mode shapes associated with the different reduction methods can be found through the figure numbers provided in the last column of Table 7-1.

Table 7-1: reduction methods and transformation matrices

Section	reduction method	Eq.	transformation matrix	mode shapes
6.3	modal truncation	(6.17)	$\boldsymbol{\Psi}_{\mathrm{MT}} = \begin{bmatrix} \mathbf{I} & \mathbf{0} \\ \mathbf{0} & \boldsymbol{\Psi}_n^k \end{bmatrix}$	Figure 6-6, Figure 6-7
6.4	Craig and Bampton reduction	(6.19)	$\boldsymbol{\Psi}_{\mathrm{CB}} = \begin{bmatrix} \mathbf{I} & \mathbf{0} \\ \boldsymbol{\Psi}_s & \boldsymbol{\Psi}_n^k \end{bmatrix}$	Figure 6-8
6.5	mode condensation	(6.30)	$\boldsymbol{\Psi}_{\mathrm{MC}} = \begin{bmatrix} \mathbf{I} & \mathbf{0} \\ \boldsymbol{\Psi}_m & \boldsymbol{\Psi}_n^k \end{bmatrix}$	Figure 6-9

In a transformation matrix, the rows correspond to nodal coordinates and the columns correspond to modal coordinates. The modal coordinates form a smaller set of coordinates than the nodal coordinates. Given a set of modal coordinates, the deformation in nodal coordinates can be easily computed. Section 7.1.1 will observe the deformed profiles due to the different reduction methods when a special set of modal coordinates is used. But when a set of nodal coordinates is given, generally no modal coordinates can exactly make up the desired nodal coordinates. Section 7.1.2 will illustrate how the different reduction methods can fit at best to the same set of nodal coordinates.

7.1.1 Profile 1

The deformation of nodes can be considered as a result of mode superposition. As we throw away more modes of higher frequencies, errors will eventually become more evident. Some reduction methods loose accuracy sooner than others, especially when the boundary modes can not endorse the boundary conditions. To see the effect of

inadequate boundary modes, a numerical experiment is devised. Assume that the beam takes on the following deformation:

$$\boldsymbol{\delta} = \begin{Bmatrix} \delta_{\xi}^{1} \\ \delta_{\eta}^{1} \\ \delta_{\xi}^{2} \\ \delta_{\eta}^{2} \\ \delta_{\xi}^{3} \\ \delta_{\eta}^{3} \\ \delta_{\xi}^{4} \\ \delta_{\eta}^{4} \\ \delta_{\xi}^{5} \\ \delta_{\eta}^{5} \end{Bmatrix} = \begin{Bmatrix} 0 \\ 0 \\ 0.0500 \\ 0.2600 \\ 0.1000 \\ 0.2200 \\ 0.1100 \\ 0.0400 \\ 0.2500 \\ 0 \end{Bmatrix} \tag{7.1}$$

Notice that node 1 is totally fixed since δ_{ξ}^{1} and δ_{η}^{1} are both zeroes. And, node 5 is just fixed in the vertical direction since only δ_{η}^{5} is zero. That is, the beam is being simply supported. The nodal deflections of δ_{ξ}^{1}, δ_{η}^{1}, and δ_{η}^{5} are referred to as $\boldsymbol{\delta}_o$. The other nodal deflections are referred to as $\boldsymbol{\delta}_u$. Arbitrary but reasonable deflections are assigned to $\boldsymbol{\delta}_u$. We may transform $\boldsymbol{\delta}_u$ to modal space by $\boldsymbol{\delta}_u = \boldsymbol{\Psi}_u \mathbf{z}_u$ where $\boldsymbol{\Psi}_u$ is the modal matrix from solving the generalized eigen-problem of $\mathbf{K}_{uu}$ and $\mathbf{M}_{uu}$. Let $\boldsymbol{\delta}_o$ stay in nodal space. The overall transformation is $\boldsymbol{\delta} = \boldsymbol{\Psi}\mathbf{z}$ or

$$\begin{Bmatrix} \boldsymbol{\delta}_o \\ \boldsymbol{\delta}_u \end{Bmatrix} = \begin{bmatrix} \mathbf{I} & \mathbf{0} \\ \mathbf{0} & \boldsymbol{\Psi}_u \end{bmatrix} \begin{Bmatrix} \boldsymbol{\delta}_o \\ \mathbf{z}_u \end{Bmatrix} \tag{7.2}$$

Matrix $\boldsymbol{\Psi}$ is

1	0	0	0	0	0	0	0	0	0
0	1	0	0	0	0	0	0	0	0
0	0	0	0	0	0	-0.605076	-1.46078	1.46078	-0.605076
0	0	0	-1.11803	-1.58114	-1.11803	0	0	0	0
0	0	0	0	0	0	-1.11803	-1.11803	-1.11803	1.11803
0	0	0	-1.58114	0	1.58114	0	0	0	0
0	0	0	0	0	0	-1.46078	0.605076	-0.605076	-1.46078
0	0	0	-1.11803	1.58114	-1.1103	0	0	0	0
0	0	0	0	0	0	-1.58114	1.58114	1.58114	1.58114
0	0	1	0	0	0	0	0	0	0

Note that the rows have been sorted back to the original order. Also, the four and fifth columns of $\boldsymbol{\Psi}$ are exactly the same vectors as the two kept normal mode shapes. The corresponding modal coordinates are $\mathbf{z} = \boldsymbol{\Psi}^{-1}\boldsymbol{\delta}$ or

$$\mathbf{z} = \begin{Bmatrix} z_1 \\ z_2 \\ z_3 \\ z_4 \\ z_5 \\ z_6 \\ z_7 \\ z_8 \\ z_9 \\ z_{10} \end{Bmatrix} = \begin{Bmatrix} 0 \\ 0 \\ 0 \\ -0.1367 \\ -0.0696 \\ 0.0025 \\ -0.1001 \\ 0.0159 \\ 0.0185 \\ 0.0237 \end{Bmatrix} \tag{7.3}$$

The modal coordinates associated with the two kept normal mode shapes are

$$\mathbf{z}_n^k = \begin{Bmatrix} z_4 \\ z_5 \end{Bmatrix} = \begin{Bmatrix} -0.1367 \\ -0.0696 \end{Bmatrix} \tag{7.4}$$

The nodal deflections at the boundary are

$$\boldsymbol{\delta}_b = \begin{Bmatrix} \delta_\xi^1 \\ \delta_\eta^1 \\ \delta_\xi^5 \\ \delta_\eta^5 \end{Bmatrix} = \begin{Bmatrix} 0 \\ 0 \\ 0.2500 \\ 0 \end{Bmatrix} \tag{7.5}$$

The generalized, truncated modal coordinates are hence

$$\mathbf{z}^* = \begin{Bmatrix} \boldsymbol{\delta}_b \\ \mathbf{z}_n^k \end{Bmatrix} \tag{7.6}$$

The nodal deflections by the different reduction methods are $\boldsymbol{\delta}_{\text{MT}}^* = \boldsymbol{\Psi}_{\text{MT}}\mathbf{z}^*$, $\boldsymbol{\delta}_{\text{CB}}^* = \boldsymbol{\Psi}_{\text{CB}}\mathbf{z}^*$, and $\boldsymbol{\delta}_{\text{MC}}^* = \boldsymbol{\Psi}_{\text{MC}}\mathbf{z}^*$:

$\boldsymbol{\delta}_{\text{MT}}^*$	$\boldsymbol{\delta}_{\text{CB}}^*$	$\boldsymbol{\delta}_{\text{MC}}^*$
0	0	0
0	0	0
0	0.0625	0.0625
0.262782	0.262782	0.262782
0	0.125	0.125
0.216066	0.216066	0.216066
0	0.1875	0.1875
0.0427817	0.0427817	0.0427817
0.25	0.25	0.25
0	0	0

It is observed that $\boldsymbol{\delta}_{\text{CB}}^*$ is identical to $\boldsymbol{\delta}_{\text{MC}}^*$.[@] The errors between the nodal deflections and $\boldsymbol{\delta}$ are

$\left\|\boldsymbol{\delta}_{\text{MT}}^* - \boldsymbol{\delta}\right\|$	$\left\|\boldsymbol{\delta}_{\text{CB}}^* - \boldsymbol{\delta}\right\|$	$\left\|\boldsymbol{\delta}_{\text{MC}}^* - \boldsymbol{\delta}\right\|$
0.1569	0.0826	0.0826

[@] This might not be always so in all cases because generally $\boldsymbol{\Psi}_s$ and $\boldsymbol{\Psi}_m$ are different.

The error by modal truncation is larger than the others. All the deformed profiles are plotted in Figure 7-1. The line marked with "reference" is the deformed profile due to $\boldsymbol{\delta}$. Since there is no difference between the nodal deflections by Craig-Bampton reduction and mode condensation, their deformed profiles are seen as one, and they are not far away from the reference profile. For modal truncation, however, the deformed profile is further away from the reference profile. It is because the boundary modes by modal truncation can not contribute any horizontal displacements to the interior nodes (2, 3, and 4). This suggests that modal truncation is not suitable in cases where boundary nodes are not fixed.

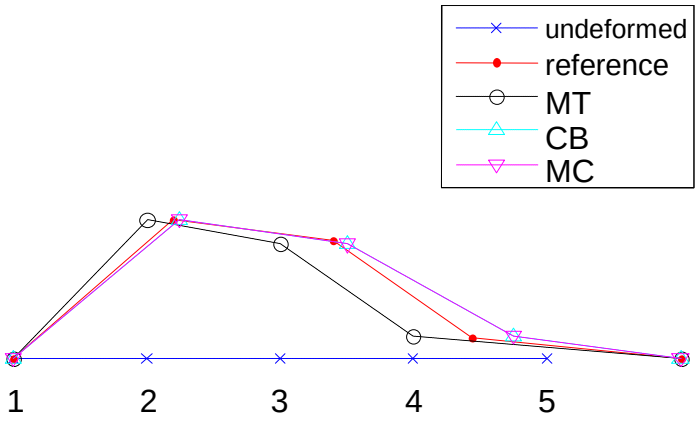

Figure 7-1: deformed profiles, given the same z*

7.1.2 Profile 2

Given arbitrary nodal deflections, $\boldsymbol{\delta}$, there might exist no such modal deflections, $\mathbf{z}$, that $\boldsymbol{\Psi}\mathbf{z}$ is equal to $\boldsymbol{\delta}$.[@] The transformation matrix of reduction, $\boldsymbol{\Psi}$, is generally not a square

[@] That $\boldsymbol{\Psi}\mathbf{z}^* = \boldsymbol{\delta}$ is possible only if $\boldsymbol{\delta}$ resides in the column space of $\boldsymbol{\Psi}$.

matrix. At most, one can least-square-fit $\boldsymbol{\delta}$ with $\boldsymbol{\delta}^*$: first, $\mathbf{z}^* = \left(\boldsymbol{\Psi}^{\mathrm{T}}\boldsymbol{\Psi}\right)^{-1}\boldsymbol{\Psi}^{\mathrm{T}}\boldsymbol{\delta}$; then, $\boldsymbol{\delta}^* = \boldsymbol{\Psi}\mathbf{z}^*$. Suppose that the same $\boldsymbol{\delta}$ from Eq. (7.1) is reused here. For the different reduction methods, $\boldsymbol{\Psi}_{\mathrm{MT}}$, $\boldsymbol{\Psi}_{\mathrm{CB}}$, and $\boldsymbol{\Psi}_{\mathrm{MC}}$ may substitute for $\boldsymbol{\Psi}$. The best-fit modal deflections can be found as

	$\mathbf{z}^*_{\mathrm{MT}}$	$\mathbf{z}^*_{\mathrm{CB}}$	$\mathbf{z}^*_{\mathrm{MC}}$
$\boldsymbol{\delta}_b$	0	-0.01	-0.01
	0	-0.000781244	-0.000781244
	0.25	0.214	0.214
	0	-0.000781244	-0.000781244
$\mathbf{z}_n^k$	-0.136652	-0.137249	-0.136652
	-0.0695701	-0.0695701	-0.0695701

The best-fit nodal deflections are thus $\boldsymbol{\delta}^*_{\mathrm{MT}} = \boldsymbol{\Psi}_{\mathrm{MT}}\mathbf{z}^*_{\mathrm{MT}}$, $\boldsymbol{\delta}^*_{\mathrm{CB}} = \boldsymbol{\Psi}_{\mathrm{CB}}\mathbf{z}^*_{\mathrm{CB}}$, $\boldsymbol{\delta}^*_{\mathrm{MC}} = \boldsymbol{\Psi}_{\mathrm{MC}}\mathbf{z}^*_{\mathrm{MC}}$:

$\boldsymbol{\delta}^*_{\mathrm{MT}}$	$\boldsymbol{\delta}^*_{\mathrm{CB}}$	$\boldsymbol{\delta}^*_{\mathrm{MC}}$
0	-0.01	-0.01
0	-0.000781244	-0.000781244
0	0.046	0.046
0.262782	0.262667	0.262667
0	0.102	0.102
0.216066	0.216228	0.216228
0	0.158	0.158
0.0427817	0.0426673	0.0426673
0.25	0.214	0.214
0	-0.000781244	-0.000781244

As expected, $\boldsymbol{\delta}^*_{\mathrm{CB}}$ must be identical to $\boldsymbol{\delta}^*_{\mathrm{MC}}$ because $\boldsymbol{\Psi}_{\mathrm{CB}}$ and $\boldsymbol{\Psi}_{\mathrm{MC}}$ span the same column space. The errors between the nodal deflections and $\boldsymbol{\delta}$ are

$\left\|\boldsymbol{\delta}^*_{\mathrm{MT}} - \boldsymbol{\delta}\right\|$	$\left\|\boldsymbol{\delta}^*_{\mathrm{CB}} - \boldsymbol{\delta}\right\|$	$\left\|\boldsymbol{\delta}^*_{\mathrm{MC}} - \boldsymbol{\delta}\right\|$
0.1569	0.0612	0.0612

The error by modal truncation is larger than the others. All the deformed profiles are plotted in Figure 7-2. The line marked with "reference" is the deformed profile due to δ. Since there is no difference between the nodal deflections by Craig-Bampton reduction and mode condensation, their deformed profiles are seen as one, and they are not far away from the reference profile. For modal truncation, however, the deformed profile is further away from the reference profile. The results show more direct and stronger indication (than do the last subsection's) that if a deformable body is restrained by moving joints and/or strong forces, Craig-Bampton reduction and mode condensation are likely to perform better since modal truncation lacks proper boundary modes.

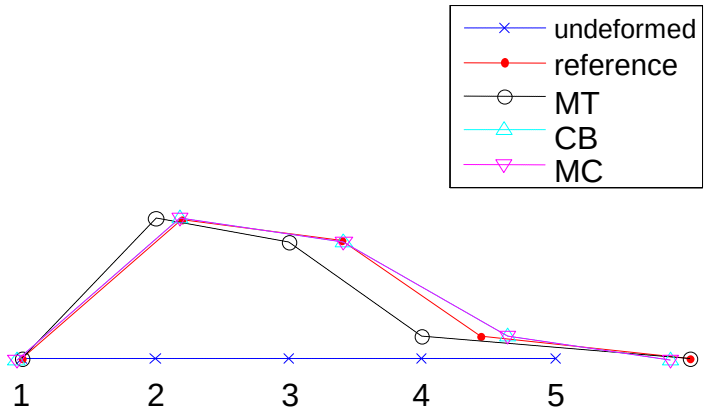

Figure 7-2: deformed profiles, given the same δ to fit

7.2 Time Simulations

In this section, we compare the time simulations with modal truncation (MT), Craig and Bampton (CB) reduction, mode condensation (MC), and Guyan reduction (GR) against the time simulation of a full system (NR). Three representative scenarios are considered in which they differ in boundary conditions.

7.2.1 The example system

Shown in Figure 7-3 is a slab whose dimensions are 4 meters long (along the ξ direction), 2 meters wide (along the η direction), and 1 meter high (along the ζ direction). It consists of thirty nodes. Each node has three translational DOFs. In total there are ninety DOFs. Other details about this slab are described in APPENDIX B.

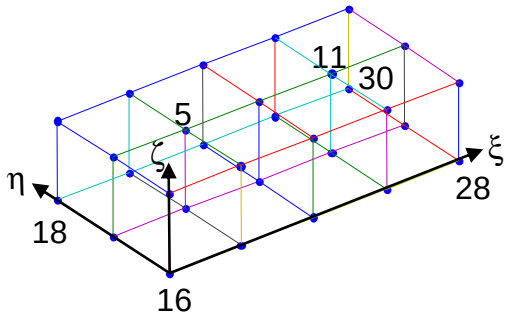

Figure 7-3: a slab model with nodal-fixed axes

The transformation matrices of the different methods regardless of the axis type are presented in the second column of Table 7-2. For the full system, the transformation matrix is simply a 90 by 90 identity matrix. For modal truncation, Craig and Bampton reduction, and mode condensation, the size of their matrices is 90 by 18 because four nodes—16, 18, 28, and 30—are chosen as the boundary nodes and six normal modes are kept. For Guyan reduction, two additional nodes—5 and 11—are added to its list of boundary nodes in order to make the number of static modes equal to the number of modes in the other methods.

A nodal-fixed frame is installed among nodes 16, 28, and 18. The origin is located at node 16; $\grave{\delta}_{\xi}^{16} = \grave{\delta}_{\eta}^{16} = \grave{\delta}_{\zeta}^{16} = 0$. The ξ axis goes through node 28; $\grave{\delta}_{\eta}^{28} = \grave{\delta}_{\zeta}^{28} = 0$.

Node 18 stays on the $\xi\eta$ plane; $\grave{}\delta_{\zeta}^{18} = 0$. For the nodal-fixed axes to take effect, six columns that correspond to the six zero deflections are removed from the transformation matrices.* The resultant matrices are placed in the third column of Table 7-2. Now the matrices' size is 90 by 12 except that of $\grave{}\underline{\Psi}_{\mathrm{NR}}$ which is 90 by 84.

Table 7-2: transformation matrices without and with nodal-fixed axis conditions

method	transformation matrix	$\grave{}\Psi$, nodal-fixed
no reduction	$\mathbf{I}$	$\grave{}\underline{\Psi}_{\mathrm{NR}}$
modal truncation	$\grave{}\Psi_{\mathrm{MT}} = \begin{bmatrix} \mathbf{I} & \mathbf{0} \\ \mathbf{0} & \grave{}\Psi_n^k \end{bmatrix}$	$\grave{}\underline{\Psi}_{\mathrm{MT}}$
Craig and Bampton reduction	$\grave{}\Psi_{\mathrm{CB}} = \begin{bmatrix} \mathbf{I} & \mathbf{0} \\ \grave{}\Psi_s & \grave{}\Psi_n^k \end{bmatrix}$	$\grave{}\underline{\Psi}_{\mathrm{CB}}$
mode condensation	$\grave{}\Psi_{\mathrm{MC}} = \begin{bmatrix} \mathbf{I} & \mathbf{0} \\ \grave{}\Psi_m & \grave{}\Psi_n^k \end{bmatrix}$	$\grave{}\underline{\Psi}_{\mathrm{MC}}$
Guyan reduction	$\grave{}\Psi_{\mathrm{GR}} = \begin{bmatrix} \mathbf{I} \\ \grave{}\Psi_S \end{bmatrix}$	$\grave{}\underline{\Psi}_{\mathrm{GR}}$

We assume that a subset of the boundary coordinates, here referred to as set *x*, has known motion as functions of time

$$\ddot{\mathbf{d}}_x(t) = \bar{\mathbf{I}}_{x:}\begin{bmatrix}\hat{\mathbf{I}} & -\tilde{\mathbf{b}} & \Psi\end{bmatrix}\begin{Bmatrix}\ddot{\mathbf{r}}\\ \dot{\boldsymbol{\omega}}\\ \ddot{\mathbf{z}}\end{Bmatrix} + \mathbf{w}_x = \begin{bmatrix}\hat{\mathbf{I}}_{x:} & -\tilde{\mathbf{b}}_{x:} & \Psi_{x:}\end{bmatrix}\begin{Bmatrix}\ddot{\mathbf{r}}\\ \dot{\boldsymbol{\omega}}\\ \ddot{\mathbf{z}}\end{Bmatrix} + \mathbf{w}_x \qquad (7.7)$$

Then, the constraint equations can be rearranged as

* Six rows of zeros should emerge after the six columns are removed.

$$\left[\hat{\mathbf{I}}_{x:} \quad -\tilde{\mathbf{b}}_{x:} \quad \boldsymbol{\Psi}_{x:}\right]\begin{Bmatrix}\ddot{\mathbf{r}}\\ \dot{\boldsymbol{\omega}}\\ \ddot{\mathbf{z}}\end{Bmatrix} = -\mathbf{w}_x + \ddot{\mathbf{d}}_x(t) \tag{7.8}$$

in which $\boldsymbol{\Psi} \triangleq \bar{\mathbf{A}}\grave{}\boldsymbol{\Psi}$ (see Section 5.4) and subscripts *x:* access the *x* rows and all the columns of the matrices. The constrained equations of motion (cf. Section 5.4.1) are therefore

$$\left[\begin{array}{ccc|c} \hat{\mathbf{I}}^{\mathrm{T}}\mathbf{M}\hat{\mathbf{I}} & -\hat{\mathbf{I}}^{\mathrm{T}}\mathbf{M}\tilde{\mathbf{b}} & \hat{\mathbf{I}}^{\mathrm{T}}\mathbf{M}\boldsymbol{\Psi} & \hat{\mathbf{I}}_{x:}^{\mathrm{T}} \\ -\tilde{\mathbf{b}}^{\mathrm{T}}\mathbf{M}\hat{\mathbf{I}} & \tilde{\mathbf{b}}^{\mathrm{T}}\mathbf{M}\tilde{\mathbf{b}} & -\tilde{\mathbf{b}}^{\mathrm{T}}\mathbf{M}\boldsymbol{\Psi} & -\tilde{\mathbf{b}}_{x:}^{\mathrm{T}} \\ \boldsymbol{\Psi}^{\mathrm{T}}\mathbf{M}\hat{\mathbf{I}} & -\boldsymbol{\Psi}^{\mathrm{T}}\mathbf{M}\tilde{\mathbf{b}} & \boldsymbol{\Psi}^{\mathrm{T}}\mathbf{M}\boldsymbol{\Psi} & \boldsymbol{\Psi}_{x:}^{\mathrm{T}} \\ \hline \hat{\mathbf{I}}_{x:} & -\tilde{\mathbf{b}}_{x:} & \boldsymbol{\Psi}_{x:} & \mathbf{0} \end{array}\right]\begin{Bmatrix}\ddot{\mathbf{r}}\\ \dot{\boldsymbol{\omega}}\\ \ddot{\mathbf{z}}\\ \hline \boldsymbol{\lambda}\end{Bmatrix} = \begin{Bmatrix} \hat{\mathbf{I}}^{\mathrm{T}}\mathbf{f} \\ -\tilde{\mathbf{b}}^{\mathrm{T}}\mathbf{f} \\ \boldsymbol{\Psi}^{\mathrm{T}}\mathbf{f} \\ \hline -\mathbf{w}_x + \ddot{\mathbf{d}}_x(t) \end{Bmatrix} \tag{7.9}$$

where $\mathbf{f} = \mathbf{M}\hat{\mathbf{g}} - \mathbf{M}\mathbf{w} - \mathbf{K}\boldsymbol{\delta}$.*

In the next three subsections, different nodes are fixed or driven using $\ddot{\mathbf{d}}_x(t)$. For each scenario, the results by those reduction methods are compared.

7.2.2 Simulation 1

Six coordinates of the slab in Figure 7-4 are held:

- Node 16 is totally fixed; $\ddot{d}_x^{16}(t) = \ddot{d}_y^{16}(t) = \ddot{d}_z^{16}(t) = 0$.
- Node 18 is only restricted in the x direction; $\ddot{d}_x^{18}(t) = 0$.
- Nodes 28 and 30 can not move in the z direction. $\ddot{d}_z^{28}(t) = \ddot{d}_z^{30}(t) = 0$

---

* Gravity, 9.80665 m/s^2, is present in the -z direction.

As a result, there is no rigid-body motion. Initially, the slab is undeformed and at rest (no velocities). Only the gravity acts upon the slab. The local nodal deflections of node 8 are plotted in Figure 7-5 ($\grave{\delta}^8_\xi$), Figure 7-6 ($\grave{\delta}^8_\eta$), and Figure 7-7 ($\grave{\delta}^8_\zeta$). The results by Craig and Bampton reduction and mode condensation are the same. They stay very close to the full solutions (no reduction). The results by Guyan reduction overall outline the full solutions but lead most of the time. The reason is that Guyan reduction has raised (free-free) eigen-frequencies. The results by modal truncation are much unsatisfactory. The magnitudes are quite insufficient because modal truncation has not compensated the boundary effects.

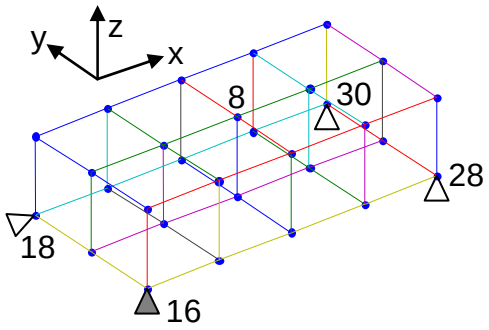

Figure 7-4: a slab exhibiting no rigid-body motion

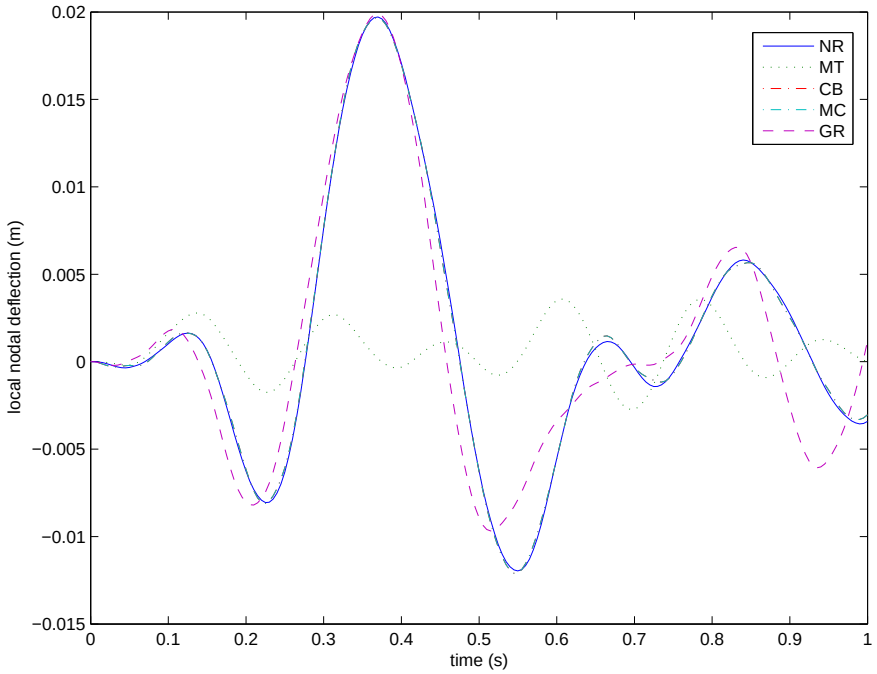

Figure 7-5: deflections at node 8 in the ξ direction

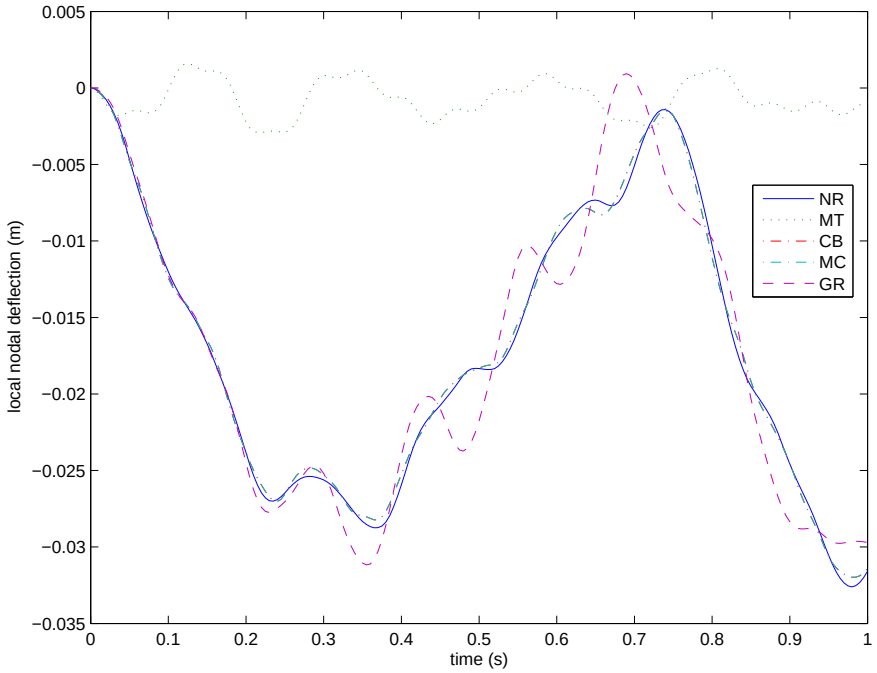

Figure 7-6: deflections at node 8 in the η direction

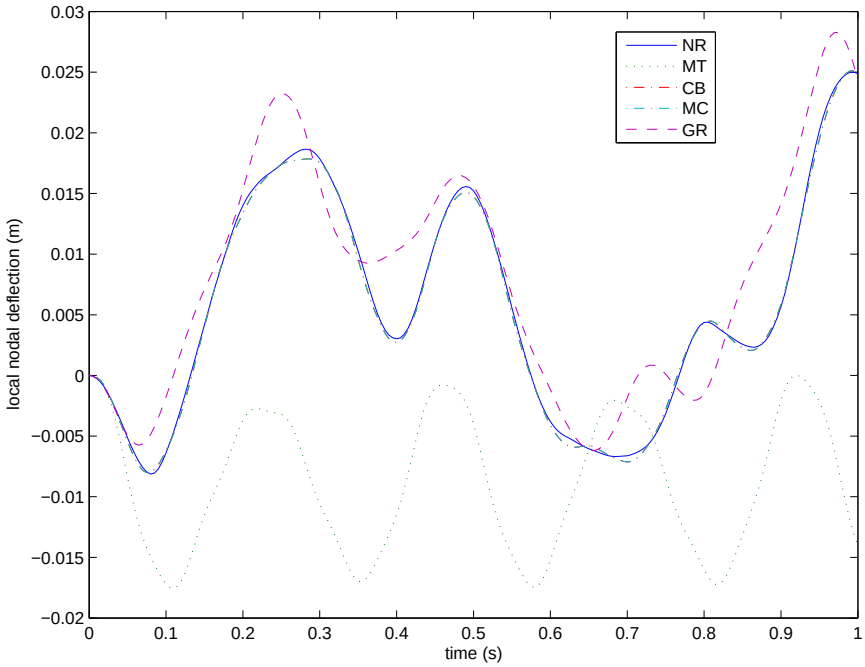

Figure 7-7: deflections at node 8 in the ζ direction

7.2.3 Simulation 2

The slab in Figure 7-8 is fixed at nodes 16 and 18; $\ddot{\mathbf{d}}^{16} = \mathbf{0}$ and $\ddot{\mathbf{d}}^{18} = \mathbf{0}$. At the same time, node 30 orbits around the line that connects nodes 16 and 18.* The absolute accelerations of node 30 are

$$\ddot{\mathbf{d}}^{30}(t) = \begin{Bmatrix} -a\left(\cos(\Omega t) + \frac{1}{4}\cos(2\Omega t)\right) \\ 0 \\ -a\left(\sin(\Omega t) + \frac{1}{8}\sin(2\Omega t)\right) \end{Bmatrix} \tag{7.10}$$

* The connection between the slab and nodes 16 and 18 works like a revolute joint.

in which $a = R\Omega^2$ (m/s^2), R = 4 (m), $\Omega = \frac{2\pi}{T}$ (rad/s), and T = 1 (s).* Note that the motion of node 30 is confined to the z-x plane. Initially the slab is undeformed and given an angular velocity of $-\Omega$ about the y axis. The local nodal deflections of node 8 are plotted in Figure 7-9 ($\grave{\delta}^8_\xi$), Figure 7-10 ($\grave{\delta}^8_\eta$), and Figure 7-11 ($\grave{\delta}^8_\zeta$). The results by Craig and Bampton reduction and mode condensation are the same. They stay reasonably close to the full solutions (no reduction). The results by Guyan reduction try to trace the full solutions but still lead most of the time. The results by modal truncation are evidently the poorest.

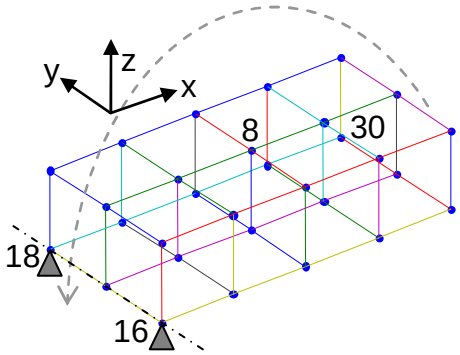

Figure 7-8: a slab exhibiting limited rigid-body motion

* The second harmonic adds some jitters.

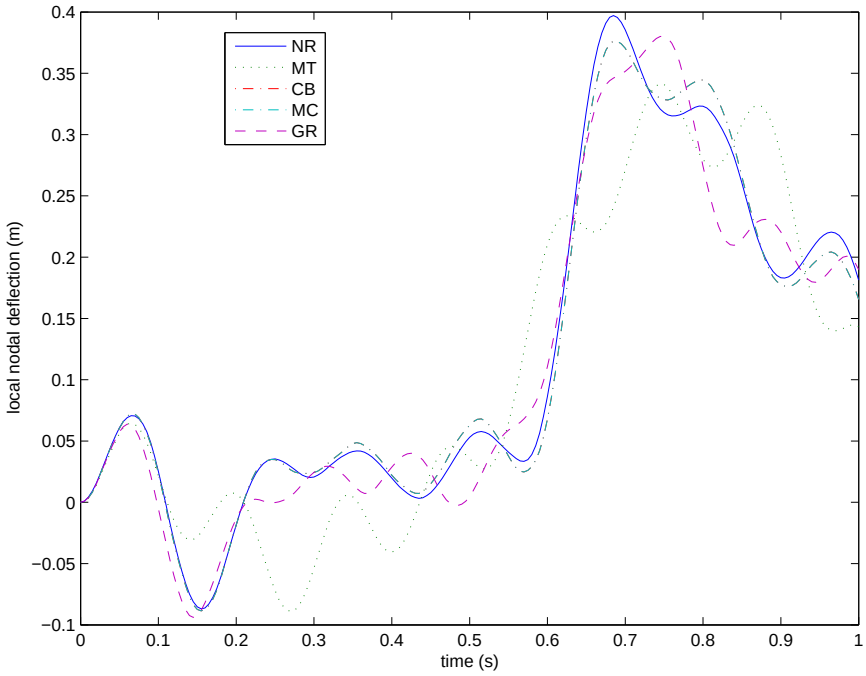

Figure 7-9: deflections at node 8 in the ξ direction

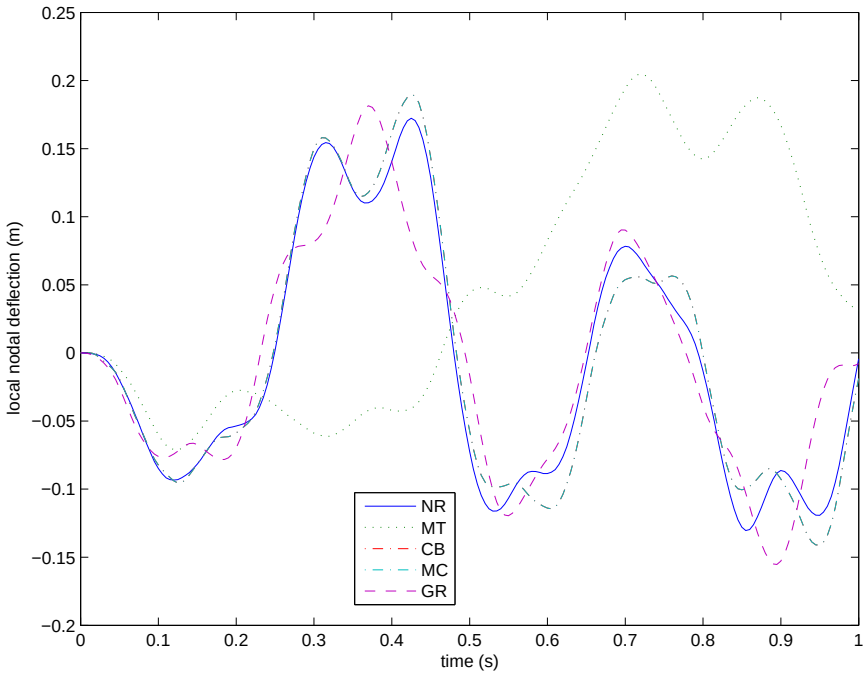

Figure 7-10: deflections at node 8 in the η direction

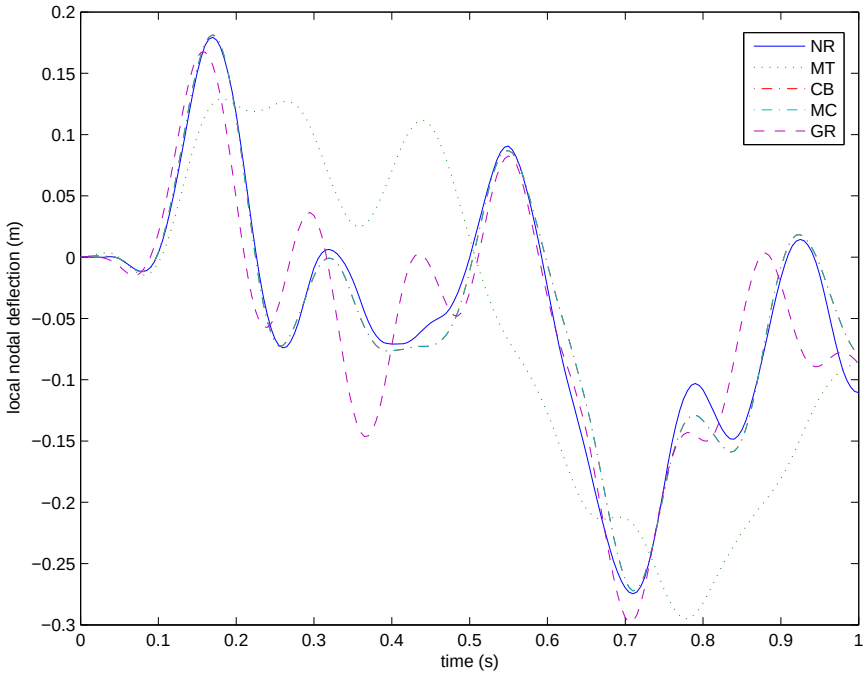

Figure 7-11: deflections at node 8 in the ζ direction

7.2.4 Simulation 3

For the slab in Figure 7-12(a) to have general rigid-body motion (emulation), nodes 16, 18, 28, and 30 are driven by known time functions as

$$\ddot{\mathbf{d}}_x(t) = \begin{Bmatrix} \ddot{\mathbf{d}}^{16} \\ \ddot{\mathbf{d}}^{18} \\ \ddot{\mathbf{d}}^{28} \\ \ddot{\mathbf{d}}^{30} \end{Bmatrix} \tag{7.11}$$

The time functions were actually prepared in lookup tables from a previous simulation as shown in Figure 7-12(b). Two rigid links were attached to the slab: a short one by two meters long at node 18 and a long one by three meters long at node 30. Initially, the links were parallel to the x axis. The other ends of the links were always fixed in space. Undeformed, the slab inclined at an angle of 45 degrees towards the –y direction. It was

then released from rest (no velocities). Two constant forces were applied: {-40, 160, -20} Newton (N) at node 16 and {60, -240, -30} Newton (N) at node 28.* Records of $\ddot{\mathbf{d}}_x$ were reported at an interval of 5 milliseconds (ms). To solve the system in Figure 7-12(a), values of $\ddot{\mathbf{d}}_x(t)$ are linear-interpolated from the lookup tables and injected into Eq. (7.9).† The local nodal deflections of node 8 are plotted in Figure 7-13 ($\grave{\delta}_\xi^8$), Figure 7-14 ($\grave{\delta}_\eta^8$), and Figure 7-15 ($\grave{\delta}_\zeta^8$). The results by Craig and Bampton reduction and mode condensation are the same. They stay close to the full solutions (no reduction). This time, however, Guyan reduction doe not perform much better than modal truncation. The explanation is that Guyan reduction does not do well when higher frequencies are incited. Conversely, the situation is in favor of modal truncation to some extend because the normal modes take the hit. Still, modal truncation and Guyan reduction can not be as good as Craig and Bampton reduction or mode condensation.

---

* The numbers in a pair of braces, {fx, fy, fz}, are applied forces in the x, y, and z directions.

† The reason for not simulating the system in Figure 7-12(b) directly is that the responses are quite chaotic during rebound after the slab hits the bottom. This is unfair and thus makes no sense for comparison.

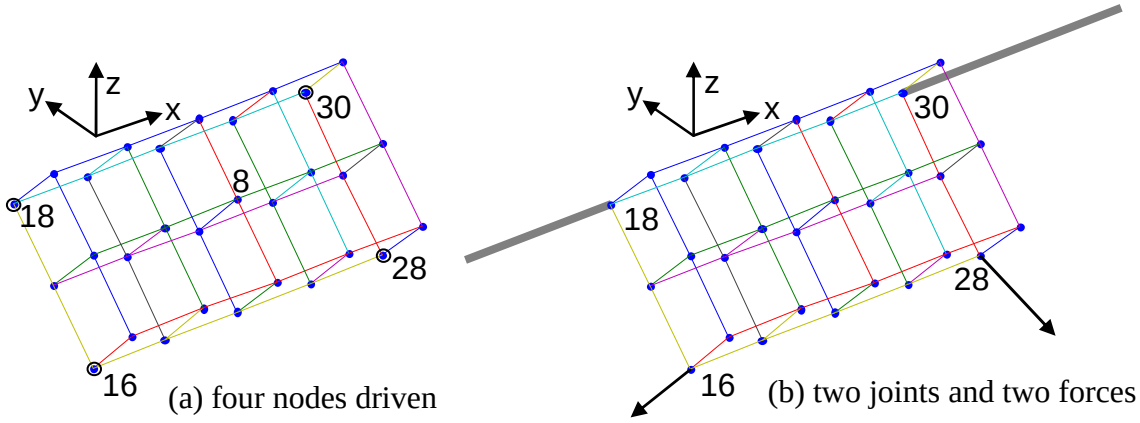

Figure 7-12: a slab exhibiting general rigid-body motion

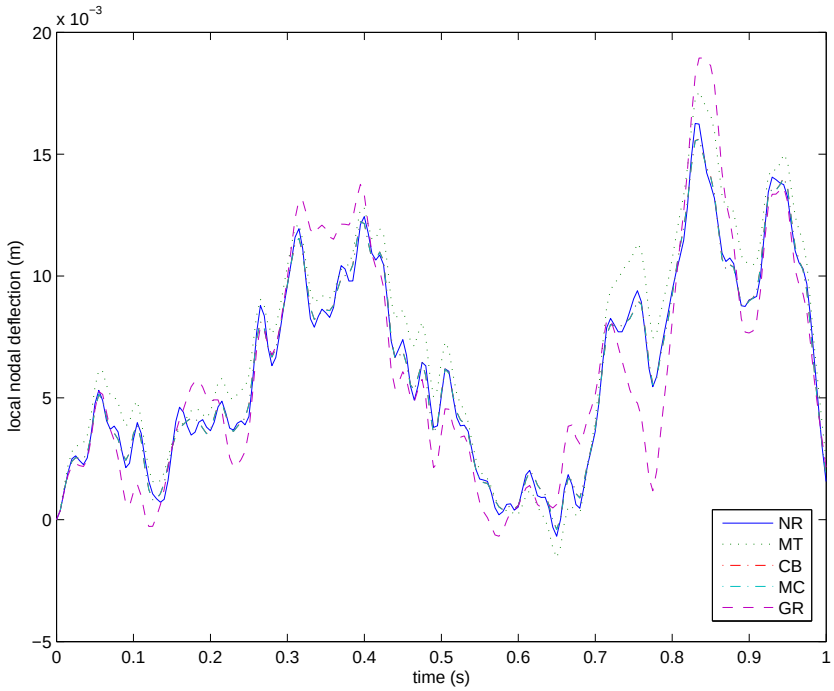

Figure 7-13: deflections at node 8 in the ξ direction

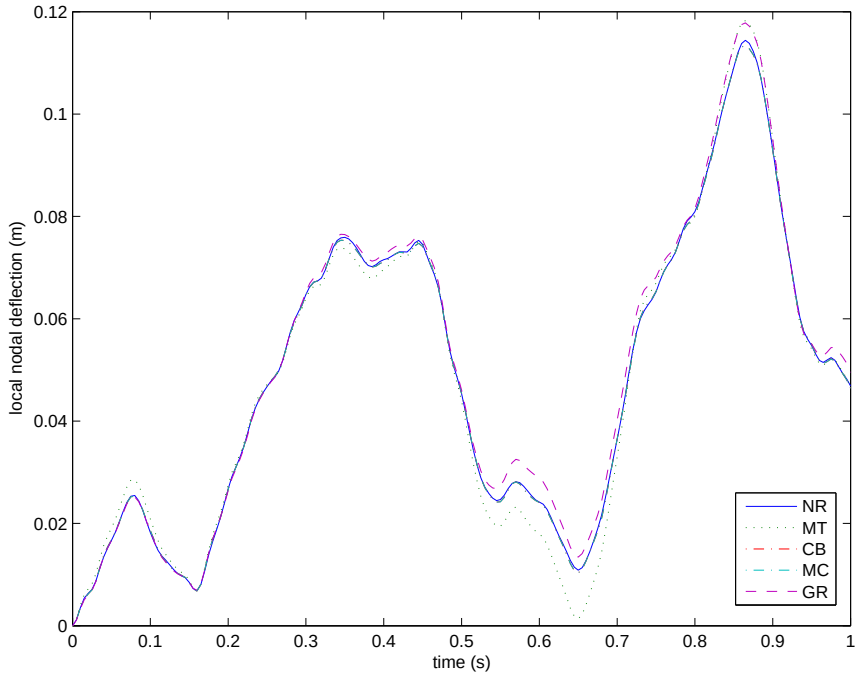

Figure 7-14: deflections at node 8 in the η direction

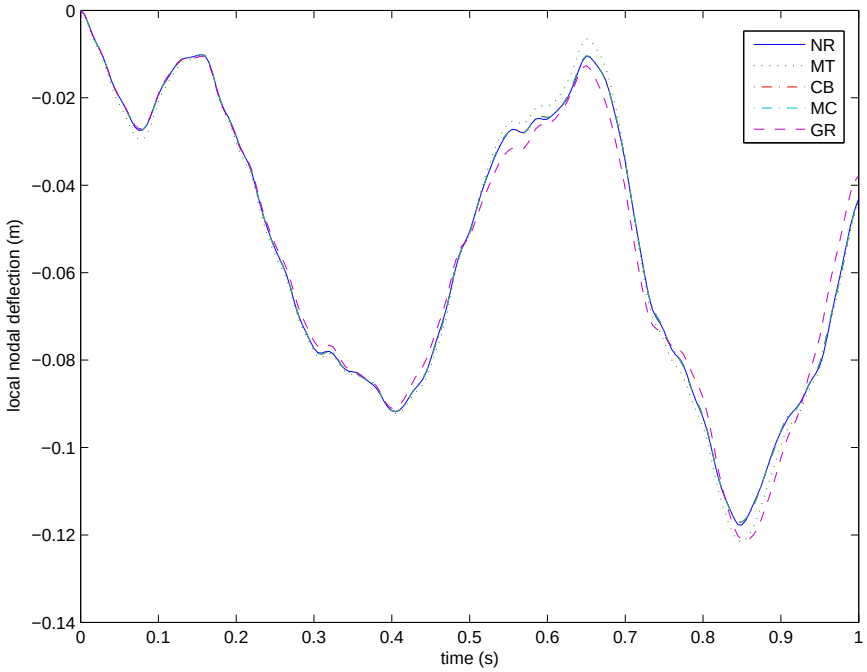

Figure 7-15: deflections at node 8 in the ζ direction

7.2.5 Summary

We have carried out the time simulations of three scenarios with different reduction methods. In Simulation 1, the slab has a minimum of six DOFs constrained, exhibiting no rigid-body motion. In Simulation 2, the slab is allowed to revolute around a fixed axis, exhibiting limited rigid-body motion. In Simulation 3, the slab exhibits general rigid-body motion. Those scenarios represent typical applications where a deformable body is under various boundary conditions. The results show that Guyan reduction tends to lead because of raised eigen-frequencies. Therefore, it is only suitable for low frequency excitation. In fact, Guyan reduction preserves exact solutions for static problems (see Section 6.2). Modal truncation often yields insufficient deformation because it lacks the ability to well receive forces and displacements at the moving boundary. Yet sometimes modal truncation appears to work just fine if the normal modes alone can deal with the situation. Craig and Bampton reduction and mode condensation always agree to each other since they share the same column space (see Section 6.5.4). Their results are also consistently close to the full solutions. The reason why these two methods perform so well is that they have combined normal modes with some correction modes, making them appropriate for a broader range of applications.

8 MODEL REDUCTION WITH MEAN AXES

Although the deployment of a nodal-fixed frame is easy to understand, such a frame does not always return symmetrical responses when expected as we pointed out in Section 5.3.3. A mean axes frame, on the contrary, does not have this problem. For that reason, mean axes frames are favored over nodal-fixed frames for general purpose employment. But, there is a misconception in the community of multibody dynamics that if mean axes are adopted as the moving reference frame for a deformable body, only free-free modes should be used (or not at all) for model reduction. This is probably due to the misunderstanding that mean axes are only compatible with free-free modes since the axes are not fixed to any nodes. It was not clear how a restrained deformable body can be condensed properly if mean axes are the choice. In this chapter, we show that mean axes can be indeed used under this circumstance. An implementation that allows various reduction methods to use mean axes is described. Procedures are also provided to evaluate a reduced model. A simple beam is used as an example to demonstrate that a reduction method such as mode condensation can still works well with mean axes.

8.1 Misconception

Reduction methods such as mode truncation, Craig and Bampton reduction, and mode condensation have been reviewed in Chapter 6. To incorporate a nodal-fixed frame, their transformation matrices require only minor changes. The columns (or mode shapes) that

correspond to the DOFs occupied by the nodal-fixed axes are simply removed.* The remaining mode shapes are still what the nodal-fixed frame sees. As an example, consider two typical mode shapes which are illustrated in Figure 8-1 as they are seen by a nodal-fixed frame. However, the same displacements are seen differently by a mean axes frame as illustrated in Figure 8-2 because the origin is located at the mass center. Mode shapes prepared for nodal-fixed axes seem to be incompatible with mean axes. Therefore, they should not be used with mean axes if model reduction is desired.† This is the misconception we want to clarify.

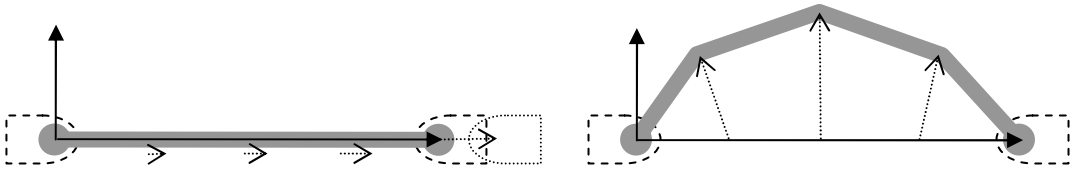

(a) constraint mode (b) normal mode

Figure 8-1: mode shapes with nodal-fixed axes

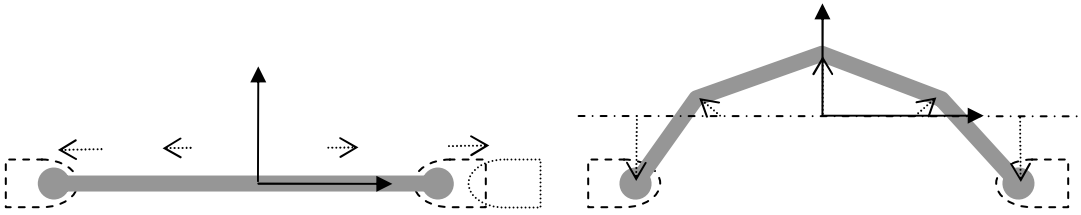

(a) constraint mode (b) normal mode

Figure 8-2: mode shapes with mean axes

---

* With the columns removed, Craig and Bampton reduction effectively becomes Hurty reduction.

† Rather, free-free mode shapes are often used with mean axes for model reduction despite that the results may be inaccurate if the deformable body is restrained.

8.2 Kinematics with Mean Axes

A deformable body that has undergone rigid-body motion and small deformation (exaggerated) is shown in Figure 8-3. The deformable body is depicted in the undeformed and deformed profiles. The absolute nodal displacements from the undeformed profile are $\Delta\mathbf{d}$'s as illustrated in Figure 8-3(a).* The displacements are seen differently as illustrated in Figure 8-3(b) when a mean axes frame is adopted. Vector $\Delta\mathbf{r}$ denotes how much the mean axes frame travels from the undeformed profile, $\Delta\boldsymbol{\theta}$ describes the small rotation of the mean axes frame from the undeformed profile, and $\Delta\boldsymbol{\delta}$'s measure the nodal deflections relative to the mean axes frame.

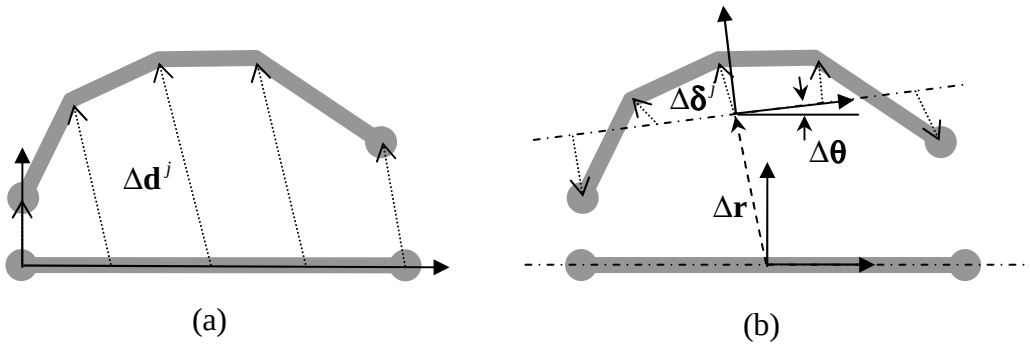

Figure 8-3: absolute nodal displacements vs. displacements with mean axes

The absolute nodal displacements can be approximated from Eq. (3.15) by

$$\Delta\mathbf{d} = \hat{\mathbf{I}}\Delta\mathbf{r} - \tilde{\mathbf{s}}\Delta\boldsymbol{\theta} + \Delta\boldsymbol{\delta} \tag{8.1}$$

The linearized mean axis conditions derived from Eqs. (4.10) and (4.11) are

---

* There is a nodal-fixed frame attached to the undeformed profile from which the absolute nodal displacements are measured.

$$\hat{\mathbf{I}}^{\mathrm{T}}\mathbf{M}\Delta\boldsymbol{\delta}=\mathbf{0} \tag{8.2}$$

$$\tilde{\mathbf{s}}^{\mathrm{T}}\mathbf{M}\Delta\boldsymbol{\delta}=\mathbf{0} \tag{8.3}$$

Appending Eqs. (8.2) and (8.3) to Eq. (8.1) leads to

$$\begin{bmatrix}\hat{\mathbf{I}} & -\tilde{\mathbf{s}} & \bar{\mathbf{I}}\\ \mathbf{0} & \mathbf{0} & \hat{\mathbf{I}}^{\mathrm{T}}\mathbf{M}\\ \mathbf{0} & \mathbf{0} & \tilde{\mathbf{s}}^{\mathrm{T}}\mathbf{M}\end{bmatrix}\begin{Bmatrix}\Delta\mathbf{r}\\ \Delta\boldsymbol{\theta}\\ \Delta\boldsymbol{\delta}\end{Bmatrix}=\begin{Bmatrix}\Delta\mathbf{d}\\ \mathbf{0}\\ \mathbf{0}\end{Bmatrix} \tag{8.4}$$

Assume that matrix $\boldsymbol{\Psi}$ contains mode shapes seen as absolute nodal displacements from the undeformed profile. If $\Delta\mathbf{d}$ in Eq. (8.4) represents each mode shape of $\boldsymbol{\Psi}$ one at a time, the corresponding mode shape seen as $\Delta\mathbf{r}$, $\Delta\boldsymbol{\theta}$, and $\Delta\boldsymbol{\delta}$'s can be solved by

$$\begin{bmatrix}\hat{\mathbf{I}} & -\tilde{\mathbf{s}} & \bar{\mathbf{I}}\\ \mathbf{0} & \mathbf{0} & \hat{\mathbf{I}}^{\mathrm{T}}\mathbf{M}\\ \mathbf{0} & \mathbf{0} & \tilde{\mathbf{s}}^{\mathrm{T}}\mathbf{M}\end{bmatrix}\begin{Bmatrix}\Delta\mathbf{r}\\ \Delta\boldsymbol{\theta}\\ \Delta\boldsymbol{\delta}\end{Bmatrix}_{l}=\begin{Bmatrix}\boldsymbol{\psi}_{l}\\ \mathbf{0}\\ \mathbf{0}\end{Bmatrix} \tag{8.5}$$

where $\boldsymbol{\psi}_{l}$ is the l-th column of $\boldsymbol{\Psi}$ and $\{\Delta\mathbf{r};\Delta\boldsymbol{\theta};\Delta\boldsymbol{\delta}\}_{l}$ is the "solution" or displacements with the mean axes frame. If matrix $\boldsymbol{\Psi}$ as a whole substitutes for $\Delta\mathbf{d}$ in Eq. (8.4)—i.e., there are multiple right-hand-sides—multiple solutions are solved at once. Hence, the following matrix equation is true:

$$\begin{bmatrix}\hat{\mathbf{I}} & -\tilde{\mathbf{s}} & \bar{\mathbf{I}}\\ \mathbf{0} & \mathbf{0} & \hat{\mathbf{I}}^{\mathrm{T}}\mathbf{M}\\ \mathbf{0} & \mathbf{0} & \tilde{\mathbf{s}}^{\mathrm{T}}\mathbf{M}\end{bmatrix}\begin{bmatrix}\Delta\mathbf{r}^{\#}\\ \Delta\boldsymbol{\theta}^{\#}\\ \Delta\boldsymbol{\delta}^{\#}\end{bmatrix}=\begin{bmatrix}\boldsymbol{\Psi}\\ \mathbf{0}\\ \mathbf{0}\end{bmatrix} \tag{8.6}$$

We designate the three "rows" in the solutions of Eq. (8.6) as $[\Delta\mathbf{r}^{\#}]$ $[\Delta\boldsymbol{\theta}^{\#}]$, and $[\Delta\boldsymbol{\delta}^{\#}]$.* From the first row of Eq. (8.6), we observe that

$$\hat{\mathbf{I}}\left[\Delta\mathbf{r}^{\#}\right]-\tilde{\mathbf{s}}\left[\Delta\boldsymbol{\theta}^{\#}\right]+\left[\Delta\boldsymbol{\delta}^{\#}\right]=\boldsymbol{\Psi} \tag{8.7}$$

That is, matrix $\boldsymbol{\Psi}$ can always be decomposed into three parts: translational rigid-body motion, rotational rigid-body motion, and body deformation.

The absolute nodal displacements $\Delta\mathbf{d}$ may also be expressed as

$$\Delta\mathbf{d}=\boldsymbol{\Psi}\mathbf{y} \tag{8.8}$$

where $\mathbf{y}$ is a vector of modal coordinates. Substituting Eq. (8.7) into Eq. (8.8) yields

$$\Delta\mathbf{d}=\hat{\mathbf{I}}\left[\Delta\mathbf{r}^{\#}\right]\mathbf{y}-\tilde{\mathbf{s}}\left[\Delta\boldsymbol{\theta}^{\#}\right]\mathbf{y}+\left[\Delta\boldsymbol{\delta}^{\#}\right]\mathbf{y} \tag{8.9}$$

When Eq. (8.9) is compared to Eq. (8.1), we observe that $\Delta\mathbf{r}=\left[\Delta\mathbf{r}^{\#}\right]\mathbf{y}$, $\Delta\boldsymbol{\theta}=\left[\Delta\boldsymbol{\theta}^{\#}\right]\mathbf{y}$, and $\Delta\boldsymbol{\delta}=\left[\Delta\boldsymbol{\delta}^{\#}\right]\mathbf{y}$. Vector $\Delta\boldsymbol{\delta}$ may be replaced by $\boldsymbol{\Psi}\Delta\mathbf{z}$ where $\mathbf{z}$ is another set of modal coordinates. Therefore, Eq. (8.9) is rewritten as

$$\Delta\mathbf{d}=\hat{\mathbf{I}}\Delta\mathbf{r}-\tilde{\mathbf{s}}\Delta\boldsymbol{\theta}+\boldsymbol{\Psi}\Delta\mathbf{z} \tag{8.10}$$

Equation (8.10) claims that the difference between $\Delta\mathbf{d}$ and $\hat{\mathbf{I}}\Delta\mathbf{r}-\tilde{\mathbf{s}}\Delta\boldsymbol{\theta}$, which is equal to $\Delta\boldsymbol{\delta}$, can be filled by $\boldsymbol{\Psi}\Delta\mathbf{z}$. This is sustained by the fact that given $\mathbf{y}$, $\Delta\mathbf{z}$ can always be solved from

---

* A pair of brackets "[]" assembles vectors into a matrix. For example, matrix $\begin{bmatrix}\Delta\mathbf{r}\\ \Delta\boldsymbol{\theta}\\ \Delta\boldsymbol{\delta}\end{bmatrix}$ or $[\Delta\mathbf{r};\Delta\boldsymbol{\theta};\Delta\boldsymbol{\delta}]$ collects mode shapes in columns.

$$\boldsymbol{\Psi}\mathbf{y} - \left(\hat{\mathbf{I}}\Delta\mathbf{r} - \tilde{\mathbf{s}}\Delta\boldsymbol{\theta}\right) = \boldsymbol{\Psi}\Delta\mathbf{z} \tag{8.11}$$

as $\Delta\mathbf{z} = \mathbf{y} - \boldsymbol{\Psi}^{-1}\left(\hat{\mathbf{I}}\Delta\mathbf{r} - \tilde{\mathbf{s}}\Delta\boldsymbol{\theta}\right)$ provided that $\boldsymbol{\Psi}^{-1}$ exists. In other words, both $\mathbf{y}$ and $\Delta\mathbf{z}$ are capable of composing the same $\Delta\mathbf{d}$. The former ($\mathbf{y}$) achieves so by Eq. (8.8), and the latter ($\Delta\mathbf{z}$) by Eq. (8.10). However, here we are not interested in using $\mathbf{y}$ because it is not with a mean axes frame whereas $\Delta\mathbf{z}$ is. If $\mathbf{y}$ is not available, $\Delta\mathbf{r}$ and $\Delta\boldsymbol{\theta}$ must be considered as free variables.

8.2.1 Adaptation of modal coordinates

Equation (8.10) possesses two copies of rigid-body motion: one shows as $\hat{\mathbf{I}}\Delta\mathbf{r} - \tilde{\mathbf{s}}\Delta\boldsymbol{\theta}$ and the other hides in $\boldsymbol{\Psi}\Delta\mathbf{z}$. For $\hat{\mathbf{I}}\Delta\mathbf{r} - \tilde{\mathbf{s}}\Delta\boldsymbol{\theta}$ to keep up with the reference frame, $\Delta\mathbf{z}$ must adjust in some way. Let $\Delta\mathbf{z}$ be replaced by $\mathbf{x}$+$\mathbf{y}$ where $\mathbf{x}$ is the adapting vector that we wish to uncover. Equation (8.10) becomes

$$\Delta\mathbf{d} = \hat{\mathbf{I}}\Delta\mathbf{r} - \tilde{\mathbf{s}}\Delta\boldsymbol{\theta} + \boldsymbol{\Psi}\mathbf{x} + \boldsymbol{\Psi}\mathbf{y} \tag{8.12}$$

Because $\Delta\mathbf{d} = \boldsymbol{\Psi}\mathbf{y}$, according to Eq. (8.8), $\boldsymbol{\Psi}\mathbf{x}$ is expected to offset $\hat{\mathbf{I}}\Delta\mathbf{r} - \tilde{\mathbf{s}}\Delta\boldsymbol{\theta}$; i.e.,

$$\boldsymbol{\Psi}\mathbf{x} = -\left(\hat{\mathbf{I}}\Delta\mathbf{r} - \tilde{\mathbf{s}}\Delta\boldsymbol{\theta}\right) \tag{8.13}$$

Such unique $\mathbf{x}$ exists if there are six complete rigid-body mode shapes (three translational and three rotational) in $\boldsymbol{\Psi}$.* To expose the rigid-body modes, first we solve the following (generalized) eigen-problem:

$$[\mathbf{V}, \boldsymbol{\Lambda}] = \text{eig}(\boldsymbol{\Psi}^{\mathrm{T}}\mathbf{K}\boldsymbol{\Psi}, \boldsymbol{\Psi}^{\mathrm{T}}\mathbf{M}\boldsymbol{\Psi}) \tag{8.14}$$

---

* Matrix $\boldsymbol{\Psi}$ is not a square for the sake of model reduction; $\boldsymbol{\Psi}^{-1}$ does not exist.

The modal matrix, $\mathbf{V}$, has two parts, $[\mathbf{V}_0,\mathbf{V}_1]$, where $\mathbf{V}_0$ corresponds to six zero eigen-values and $\mathbf{V}_1$ corresponds to the non-zero eigen-values. Next, $\mathbf{x}$ is transformed into another space by

$$\mathbf{x} = \begin{bmatrix}\mathbf{V}_0 & \mathbf{V}_1\end{bmatrix}\begin{Bmatrix}\mathbf{x}_0 \\ \mathbf{x}_1\end{Bmatrix} \tag{8.15}$$

Thus,

$$\boldsymbol{\Psi}\mathbf{x} = \boldsymbol{\Psi}\begin{bmatrix}\mathbf{V}_0 & \mathbf{V}_1\end{bmatrix}\begin{Bmatrix}\mathbf{x}_0 \\ \mathbf{x}_1\end{Bmatrix} = \begin{bmatrix}\boldsymbol{\Psi}\mathbf{V}_0 & \boldsymbol{\Psi}\mathbf{V}_1\end{bmatrix}\begin{Bmatrix}\mathbf{x}_0 \\ \mathbf{x}_1\end{Bmatrix} = \begin{bmatrix}\boldsymbol{\Psi}_0 & \boldsymbol{\Psi}_1\end{bmatrix}\begin{Bmatrix}\mathbf{x}_0 \\ \mathbf{x}_1\end{Bmatrix} = \boldsymbol{\Psi}_0\mathbf{x}_0 + \boldsymbol{\Psi}_1\mathbf{x}_1 \tag{8.16}$$

in which $\boldsymbol{\Psi}_0 = \boldsymbol{\Psi}\mathbf{V}_0$ and $\boldsymbol{\Psi}_1 = \boldsymbol{\Psi}\mathbf{V}_1$.* Substituting Eq. (8.16) into Eq. (8.13) yields

$$\boldsymbol{\Psi}_0\mathbf{x}_0 + \boldsymbol{\Psi}_1\mathbf{x}_1 = -\left(\hat{\mathbf{I}}\Delta\mathbf{r} - \tilde{\mathbf{s}}\Delta\boldsymbol{\theta}\right) \tag{8.17}$$

Since the right hand side of Eq. (8.17) is asking for rigid-body modes, $\mathbf{x}_1$ is forced to be zeros in order to remove any effect from $\boldsymbol{\Psi}_1$ which carries the deformation modes. Hence, $\boldsymbol{\Psi}_0\mathbf{x}_0$ is solely responsible for canceling $\hat{\mathbf{I}}\Delta\mathbf{r} - \tilde{\mathbf{s}}\Delta\boldsymbol{\theta}$; i.e.,

$$\boldsymbol{\Psi}_0\mathbf{x}_0 = -\begin{bmatrix}\hat{\mathbf{I}} & -\tilde{\mathbf{s}}\end{bmatrix}\begin{Bmatrix}\Delta\mathbf{r} \\ \Delta\boldsymbol{\theta}\end{Bmatrix} = -\mathbf{P}\begin{Bmatrix}\Delta\mathbf{r} \\ \Delta\boldsymbol{\theta}\end{Bmatrix} \tag{8.18}$$

where $\mathbf{P} = \begin{bmatrix}\hat{\mathbf{I}} & -\tilde{\mathbf{s}}\end{bmatrix}$. As $\boldsymbol{\Psi}_0$ (which carries the rigid-body mode shapes) and $\mathbf{P}$ span the same column space, it shall be always possible to have $\boldsymbol{\Psi}_0 = \mathbf{PR}$ where $\mathbf{R}$ is a 6 by 6 invertible matrix.* Equation (8.18) becomes

---

* A totally different approach [44, 45] rejects $\boldsymbol{\Psi}_0\mathbf{x}_0$. Thus, $\Delta\mathbf{d} = \hat{\mathbf{I}}\Delta\mathbf{r} - \tilde{\mathbf{s}}\Delta\boldsymbol{\theta} + \boldsymbol{\Psi}_1\mathbf{x}_1$. Axis conditions are hereby implied although they are not exactly of mean axes.

$$\mathbf{PRx}_0 = -\mathbf{P}\begin{Bmatrix}\Delta\mathbf{r}\\ \Delta\boldsymbol{\theta}\end{Bmatrix} \quad \text{or} \quad \mathbf{P}\left(\mathbf{Rx}_0 + \begin{Bmatrix}\Delta\mathbf{r}\\ \Delta\boldsymbol{\theta}\end{Bmatrix}\right) = \mathbf{0} \tag{8.19}$$

Since $\mathbf{P}$ is a matrix with linearly independent columns, $\mathbf{Rx}_0 + \begin{Bmatrix}\Delta\mathbf{r}\\ \Delta\boldsymbol{\theta}\end{Bmatrix} = \mathbf{0}$ is the only chance for Eq. (8.19) to be true. Therefore,

$$\mathbf{x}_0 = -\mathbf{R}^{-1}\begin{Bmatrix}\Delta\mathbf{r}\\ \Delta\boldsymbol{\theta}\end{Bmatrix} \tag{8.20}^{\dagger}$$

Consequently,

$$\mathbf{x} = \mathbf{V}_0\mathbf{x}_0 + \cancel{\mathbf{V}_1\mathbf{x}_1} = -\mathbf{V}_0\mathbf{R}^{-1}\begin{Bmatrix}\Delta\mathbf{r}\\ \Delta\boldsymbol{\theta}\end{Bmatrix} \tag{8.21}$$

As long as $\boldsymbol{\Psi}$ has full (column) rank and contains complete rigid-body mode shapes, $\boldsymbol{\Psi}\mathbf{x}$ is able to neutralize $\hat{\mathbf{I}}\Delta\mathbf{r} - \tilde{\mathbf{s}}\Delta\boldsymbol{\theta}$. At the same time, $\hat{\mathbf{I}}\Delta\mathbf{r} - \tilde{\mathbf{s}}\Delta\boldsymbol{\theta} + \boldsymbol{\Psi}\Delta\mathbf{z}$ still amounts to $\Delta\mathbf{d}$. Using Eq. (8.10) is not different from using Eq. (8.8).

8.2.2 Non-linear frame motion

Equation (8.10) only offers linearized rigid-body motion around the undeformed configuration as indicated by the presence of **s**. To prepare for fully non-linear frame

---

* Matrix $\mathbf{R} = \left(\mathbf{P}^{\mathrm{T}}\mathbf{P}\right)^{-1}\mathbf{P}^{\mathrm{T}}\boldsymbol{\Psi}_0$ is the exact solution of $\mathbf{PR} = \boldsymbol{\Psi}_0$ if $\mathbf{P}$ and $\boldsymbol{\Psi}_0$ span the same column space.

† We could have solved the same $\mathbf{x}_0$ at Eq. (8.18):

$$\boldsymbol{\Psi}_0\mathbf{x}_0 = -\mathbf{P}\begin{Bmatrix}\Delta\mathbf{r}\\ \Delta\boldsymbol{\theta}\end{Bmatrix} \;\Rightarrow\; \boldsymbol{\Psi}_0{}^{\mathrm{T}}\boldsymbol{\Psi}_0\mathbf{x}_0 = -\boldsymbol{\Psi}_0{}^{\mathrm{T}}\mathbf{P}\begin{Bmatrix}\Delta\mathbf{r}\\ \Delta\boldsymbol{\theta}\end{Bmatrix} \;\Rightarrow\; \mathbf{x}_0 = -\left(\boldsymbol{\Psi}_0{}^{\mathrm{T}}\boldsymbol{\Psi}_0\right)^{-1}\boldsymbol{\Psi}_0{}^{\mathrm{T}}\mathbf{P}\begin{Bmatrix}\Delta\mathbf{r}\\ \Delta\boldsymbol{\theta}\end{Bmatrix}$$

motion, we substitute **b** for **s** in Eq. (8.10). Vector **b** contains the deformed locations of nodes. Equation (8.10) is then slightly modified as

$$\Delta\mathbf{d} = \hat{\mathbf{I}}\Delta\mathbf{r} - \tilde{\mathbf{b}}\Delta\boldsymbol{\theta} + \boldsymbol{\Psi}\Delta\mathbf{z} \tag{8.22}$$

Dividing (8.22) by Δt and taking Δt to the limit of zero yields

$$\dot{\mathbf{d}} = \hat{\mathbf{I}}\dot{\mathbf{r}} - \tilde{\mathbf{b}}\boldsymbol{\omega} + \boldsymbol{\Psi}\dot{\mathbf{z}} = \begin{bmatrix} \hat{\mathbf{I}} & -\tilde{\mathbf{b}} & \boldsymbol{\Psi} \end{bmatrix} \begin{Bmatrix} \dot{\mathbf{r}} \\ \boldsymbol{\omega} \\ \dot{\mathbf{z}} \end{Bmatrix} \tag{8.23}$$

The time derivative of Eq. (8.23) is

$$\ddot{\mathbf{d}} = \hat{\mathbf{I}}\ddot{\mathbf{r}} - \tilde{\mathbf{b}}\dot{\boldsymbol{\omega}} + \boldsymbol{\Psi}\ddot{\mathbf{z}} + \mathbf{w} = \begin{bmatrix} \hat{\mathbf{I}} & -\tilde{\mathbf{b}} & \boldsymbol{\Psi} \end{bmatrix} \begin{Bmatrix} \ddot{\mathbf{r}} \\ \dot{\boldsymbol{\omega}} \\ \ddot{\mathbf{z}} \end{Bmatrix} + \mathbf{w} \tag{8.24}$$

where $\mathbf{w} = \bar{\tilde{\boldsymbol{\omega}}}\bar{\tilde{\boldsymbol{\omega}}}\mathbf{b} + 2\bar{\tilde{\boldsymbol{\omega}}}\dot{\boldsymbol{\delta}}$.*

8.2.3 Mean axis conditions in modal coordinates

Accepting that $\Delta\mathbf{r}$, $\Delta\boldsymbol{\theta}$, $\Delta\mathbf{z}$ are all free variables in Eq. (8.10) makes the total number of independent variables exceed the original number of DOFs by six. Mean axis conditions are therefore necessary. Pre-multiplying Eq. (8.10) by **M** yields

$$\mathbf{M}\Delta\mathbf{d} = \mathbf{M}\hat{\mathbf{I}}\Delta\mathbf{r} - \mathbf{M}\tilde{\mathbf{s}}\Delta\boldsymbol{\theta} + \mathbf{M}\boldsymbol{\Psi}\Delta\mathbf{z} \tag{8.25}$$

Equation (8.25) is then pre-multiplied by $\hat{\mathbf{I}}^{\mathrm{T}}$:

$$\underbrace{\hat{\mathbf{I}}^{\mathrm{T}}\mathbf{M}\Delta\mathbf{d}}_{m\Delta\mathbf{r}} = \underbrace{\hat{\mathbf{I}}^{\mathrm{T}}\mathbf{M}\hat{\mathbf{I}}}_{m\mathbf{I}}\Delta\mathbf{r} - \underbrace{\hat{\mathbf{I}}^{\mathrm{T}}\mathbf{M}\tilde{\mathbf{s}}}_{\mathbf{0}}\Delta\boldsymbol{\theta} + \hat{\mathbf{I}}^{\mathrm{T}}\mathbf{M}\boldsymbol{\Psi}\Delta\mathbf{z} \quad \Rightarrow \quad \hat{\mathbf{I}}^{\mathrm{T}}\mathbf{M}\boldsymbol{\Psi}\Delta\mathbf{z} = \mathbf{0} \tag{8.26}$$

---

* Note that $\boldsymbol{\delta} = \boldsymbol{\Psi}\mathbf{z}$, $\dot{\boldsymbol{\delta}} \triangleq \boldsymbol{\Psi}\dot{\mathbf{z}}$, and $\ddot{\boldsymbol{\delta}} \triangleq \boldsymbol{\Psi}\ddot{\mathbf{z}}$; see Section 5.4.

Since the mean axes are positioned at the mass center, $\hat{\mathbf{I}}^{\mathrm{T}}\mathbf{M}\tilde{\mathbf{s}} = \mathbf{0}$ and $\hat{\mathbf{I}}^{\mathrm{T}}\mathbf{M}\Delta\mathbf{d} = m\Delta\mathbf{r}$. Also, $\hat{\mathbf{I}}^{\mathrm{T}}\mathbf{M}\hat{\mathbf{I}}\Delta\mathbf{r} = m\Delta\mathbf{r}$. As a result, Eq. (8.26) simply represents the translational mean axis conditions. Similarly, pre-multiplying Eq. (8.25) by $\tilde{\mathbf{s}}^{\mathrm{T}}$ results in the rotational mean axis conditions (in sense of virtual displacements):

$$\underbrace{\tilde{\mathbf{s}}^{\mathrm{T}}\mathbf{M}\Delta\mathbf{d}}_{-\mathbf{J}\Delta\boldsymbol{\theta}} = \underbrace{\tilde{\mathbf{s}}^{\mathrm{T}}\mathbf{M}\hat{\mathbf{I}}}_{\mathbf{0}}\Delta\mathbf{r} - \underbrace{\tilde{\mathbf{s}}^{\mathrm{T}}\mathbf{M}\tilde{\mathbf{s}}}_{\mathbf{J}}\Delta\boldsymbol{\theta} + \tilde{\mathbf{s}}^{\mathrm{T}}\mathbf{M}\boldsymbol{\Psi}\Delta\mathbf{z} \quad \Rightarrow \quad \tilde{\mathbf{s}}^{\mathrm{T}}\mathbf{M}\boldsymbol{\Psi}\Delta\mathbf{z} = \mathbf{0} \tag{8.27}$$

Equations (8.26) and (8.27) should look familiar when compared to Eqs (8.2) and (8.3) which are the linearized mean axis conditions in nodal coordinates. The true mean axis conditions at the velocity level are $\hat{\mathbf{I}}^{\mathrm{T}}\mathbf{M}\boldsymbol{\Psi}\dot{\mathbf{z}} = \mathbf{0}$ and $\tilde{\mathbf{b}}^{\mathrm{T}}\mathbf{M}\boldsymbol{\Psi}\dot{\mathbf{z}} = \mathbf{0}$. Their further time derivatives are $\hat{\mathbf{I}}^{\mathrm{T}}\mathbf{M}\boldsymbol{\Psi}\ddot{\mathbf{z}} = \mathbf{0}$ and $\tilde{\mathbf{b}}^{\mathrm{T}}\mathbf{M}\boldsymbol{\Psi}\ddot{\mathbf{z}} = -\tilde{\tilde{\boldsymbol{\delta}}}^{\mathrm{T}}\mathbf{M}\dot{\boldsymbol{\delta}}$.

8.3 Equations of Motion

A deformable body is connected to its surrounding thru several nodes as shown in Figure 8-4. Body 1 is directly attached to the deformable body at one node. There is a spring/damper/actuator between body 2 and a second node. The deformable body is fixed to the ground at another node. A strong force is applied at a fourth node. These nodes are the *b*oundary nodes (set *b*). The remaining nodes (not marked) are the *i*nterior nodes (set *i*). A mean axes frame is assigned to the deformable body.

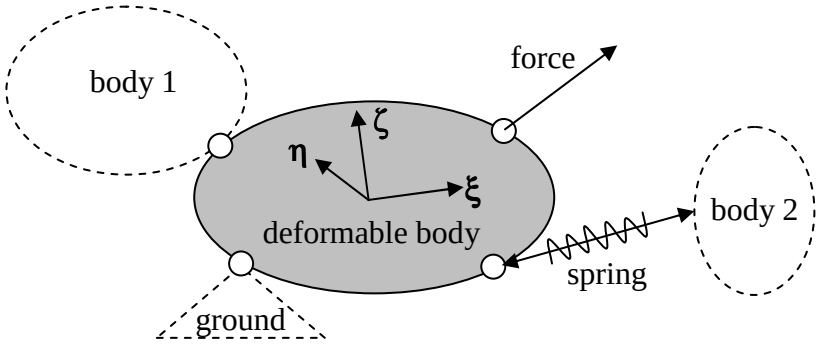

Figure 8-4: an embedded deformable body

For simplicity, the kinematics of the other bodies and the constraints of the kinematic joints are not discussed in detail. The equations of motion for the sole deformable body along with mean axis conditions are

$$\left[\begin{array}{ccc|cc} \hat{\mathbf{I}}^T\mathbf{M}\hat{\mathbf{I}} & -\hat{\mathbf{I}}^T\mathbf{M}\tilde{\mathbf{b}} & \hat{\mathbf{I}}^T\mathbf{M} & \mathbf{0} & \mathbf{0} \\ -\tilde{\mathbf{b}}^T\mathbf{M}\hat{\mathbf{I}} & \tilde{\mathbf{b}}^T\mathbf{M}\tilde{\mathbf{b}} & -\tilde{\mathbf{b}}^T\mathbf{M} & \mathbf{0} & \mathbf{0} \\ \mathbf{M}\hat{\mathbf{I}} & -\mathbf{M}\tilde{\mathbf{b}} & \mathbf{M} & \mathbf{M}\hat{\mathbf{I}} & \mathbf{M}\tilde{\mathbf{b}} \\ \hline \mathbf{0} & \mathbf{0} & \hat{\mathbf{I}}^T\mathbf{M} & \mathbf{0} & \mathbf{0} \\ \mathbf{0} & \mathbf{0} & \tilde{\mathbf{b}}^T\mathbf{M} & \mathbf{0} & \mathbf{0} \end{array}\right] \left\{\begin{array}{c} \ddot{\mathbf{r}} \\ \dot{\boldsymbol{\omega}} \\ \ddot{\boldsymbol{\delta}} \\ \hline \boldsymbol{\lambda}_1 \\ \boldsymbol{\lambda}_2 \end{array}\right\} = \left\{\begin{array}{c} \hat{\mathbf{I}}^T\mathbf{f} \\ -\tilde{\mathbf{b}}^T\mathbf{f} \\ \mathbf{f} \\ \hline \mathbf{0} \\ -\tilde{\dot{\boldsymbol{\delta}}}^T\mathbf{M}\dot{\boldsymbol{\delta}} \end{array}\right\} \tag{8.28}$$

Equation (8.28) is repeated from Eq. (4.22). With $\ddot{\boldsymbol{\delta}} \triangleq \boldsymbol{\Psi}\ddot{\mathbf{z}}$, where $\boldsymbol{\Psi} \triangleq \bar{\mathbf{A}}\grave{\boldsymbol{\Psi}}$, Eq. (8.28) is transformed to

$$\left[\begin{array}{ccc|cc} \hat{\mathbf{I}}^T\mathbf{M}\hat{\mathbf{I}} & -\hat{\mathbf{I}}^T\mathbf{M}\tilde{\mathbf{b}} & \hat{\mathbf{I}}^T\mathbf{M}\boldsymbol{\Psi} & \mathbf{0} & \mathbf{0} \\ -\tilde{\mathbf{b}}^T\mathbf{M}\hat{\mathbf{I}} & \tilde{\mathbf{b}}^T\mathbf{M}\tilde{\mathbf{b}} & -\tilde{\mathbf{b}}^T\mathbf{M}\boldsymbol{\Psi} & \mathbf{0} & \mathbf{0} \\ \boldsymbol{\Psi}^T\mathbf{M}\hat{\mathbf{I}} & -\boldsymbol{\Psi}^T\mathbf{M}\tilde{\mathbf{b}} & \boldsymbol{\Psi}^T\mathbf{M}\boldsymbol{\Psi} & \boldsymbol{\Psi}^T\mathbf{M}\hat{\mathbf{I}} & \boldsymbol{\Psi}^T\mathbf{M}\tilde{\mathbf{b}} \\ \hline \mathbf{0} & \mathbf{0} & \hat{\mathbf{I}}^T\mathbf{M}\boldsymbol{\Psi} & \mathbf{0} & \mathbf{0} \\ \mathbf{0} & \mathbf{0} & \tilde{\mathbf{b}}^T\mathbf{M}\boldsymbol{\Psi} & \mathbf{0} & \mathbf{0} \end{array}\right] \left\{\begin{array}{c} \ddot{\mathbf{r}} \\ \dot{\boldsymbol{\omega}} \\ \ddot{\mathbf{z}} \\ \hline \boldsymbol{\lambda}_1 \\ \boldsymbol{\lambda}_2 \end{array}\right\} = \left\{\begin{array}{c} \hat{\mathbf{I}}^T\mathbf{f} \\ -\tilde{\mathbf{b}}^T\mathbf{f} \\ \boldsymbol{\Psi}^T\mathbf{f} \\ \hline \mathbf{0} \\ -\tilde{\dot{\boldsymbol{\delta}}}^T\mathbf{M}\dot{\boldsymbol{\delta}} \end{array}\right\} \tag{8.29}$$

For different reduction methods, we simply substitute their transformation matrix for $\grave{\boldsymbol{\Psi}}$ even though the mode shapes are not prepared with mean axes in mind. Provided

that `$\boldsymbol{\Psi}$ has full (column) rank and contains complete rigid-body mode shapes (see Section 8.2.1), the mean axis conditions will keep the reference frame on the mass center (see Section 8.2.3). The implementation makes model reduction with mean axes as easy as with nodal-fixed axes.*

8.4 Evaluation

To evaluate a reduction method without actually performing a time simulation, we conduct two associated analyses. The first one is a static analysis which produces constraint modes. The second one is an eigen-analysis which produces (fixed-constraint) normal modes.

To obtain the constraint modes, the following static problem is solved for which each boundary coordinate of $\mathbf{d}_b$ is displaced by one unit, one at a time:

$$\left[\begin{array}{ccc|ccc} \mathbf{0} & \mathbf{0} & \mathbf{0} & \mathbf{0} & \mathbf{0} & \hat{\mathbf{I}}_{b:}^{\mathrm{T}} \\ \mathbf{0} & \mathbf{0} & \mathbf{0} & \mathbf{0} & \mathbf{0} & -\tilde{\mathbf{s}}_{b:}^{\mathrm{T}} \\ \mathbf{0} & \mathbf{0} & \boldsymbol{\Psi}^{\mathrm{T}}\mathbf{K}\boldsymbol{\Psi} & \boldsymbol{\Psi}^{\mathrm{T}}\mathbf{M}\hat{\mathbf{I}} & \boldsymbol{\Psi}^{\mathrm{T}}\mathbf{M}\tilde{\mathbf{s}} & \boldsymbol{\Psi}_{b:}^{\mathrm{T}} \\ \hline \mathbf{0} & \mathbf{0} & \hat{\mathbf{I}}^{\mathrm{T}}\mathbf{M}\boldsymbol{\Psi} & \mathbf{0} & \mathbf{0} & \mathbf{0} \\ \mathbf{0} & \mathbf{0} & \tilde{\mathbf{s}}^{\mathrm{T}}\mathbf{M}\boldsymbol{\Psi} & \mathbf{0} & \mathbf{0} & \mathbf{0} \\ \hat{\mathbf{I}}_{b:} & -\tilde{\mathbf{s}}_{b:} & \boldsymbol{\Psi}_{b:} & \mathbf{0} & \mathbf{0} & \mathbf{0} \end{array}\right] \left\{\begin{array}{c} \Delta\mathbf{r} \\ \Delta\boldsymbol{\theta} \\ \Delta\mathbf{z} \\ \hline \boldsymbol{\lambda}_1 \\ \boldsymbol{\lambda}_2 \\ \boldsymbol{\lambda}_3 \end{array}\right\}_l^c = \left\{\begin{array}{c} \mathbf{0} \\ \mathbf{0} \\ \mathbf{0} \\ \hline \mathbf{0} \\ \mathbf{0} \\ \mathbf{i}_l \end{array}\right\} \tag{8.30}$$

* It is very likely that this implementation may also work with principal axes (see Section 4.3). We only need to replace the mean axis conditions by the principal axis conditions.

where l = 1, …, lc; lc is the total number of constraint modes, which is the same as the total number of boundary coordinates.* The last row of Eq. (8.30) is the constraint equations

$$\left[\hat{\mathbf{I}}_{b:} \quad -\tilde{\mathbf{s}}_{b:} \quad \boldsymbol{\Psi}_{b:}\right]\begin{Bmatrix}\Delta\mathbf{r}\\ \Delta\boldsymbol{\theta}\\ \Delta\mathbf{z}\end{Bmatrix}_l^c = \mathbf{i}_l \tag{8.31}$$

under which the constraint modes are obtained.† The l-th constraint mode seen as absolute nodal displacements is computed by

$$\{\Delta\mathbf{d}\}_l^c = \left[\hat{\mathbf{I}} \quad -\tilde{\mathbf{s}} \quad \boldsymbol{\Psi}\right]\begin{Bmatrix}\Delta\mathbf{r}\\ \Delta\boldsymbol{\theta}\\ \Delta\mathbf{z}\end{Bmatrix}_l^c \tag{8.32}$$

To obtain the normal modes, the following eigen-problem is solved for which all the boundary coordinates of $\mathbf{d}_b$ are fixed:

$$\left(\left[\begin{array}{ccc|ccc} \mathbf{0}&\mathbf{0}&\mathbf{0}&\mathbf{0}&\mathbf{0}&\mathbf{0}\\ \mathbf{0}&\mathbf{0}&\mathbf{0}&\mathbf{0}&\mathbf{0}&\mathbf{0}\\ \mathbf{0}&\mathbf{0}&\boldsymbol{\Psi}^{\mathrm{T}}\mathbf{K}\boldsymbol{\Psi}&\mathbf{0}&\mathbf{0}&\mathbf{0}\\ \hline \mathbf{0}&\mathbf{0}&\mathbf{0}&\mathbf{0}&\mathbf{0}&\mathbf{0}\\ \mathbf{0}&\mathbf{0}&\mathbf{0}&\mathbf{0}&\mathbf{0}&\mathbf{0}\\ \mathbf{0}&\mathbf{0}&\mathbf{0}&\mathbf{0}&\mathbf{0}&\mathbf{0} \end{array}\right] - \omega_l^2\left[\begin{array}{ccc|ccc} \hat{\mathbf{I}}^{\mathrm{T}}\mathbf{M}\hat{\mathbf{I}}&-\hat{\mathbf{I}}^{\mathrm{T}}\mathbf{M}\tilde{\mathbf{s}}&\hat{\mathbf{I}}^{\mathrm{T}}\mathbf{M}\boldsymbol{\Psi}&\mathbf{0}&\mathbf{0}&\hat{\mathbf{I}}_{b:}^{\mathrm{T}}\\ -\tilde{\mathbf{s}}^{\mathrm{T}}\mathbf{M}\hat{\mathbf{I}}&\tilde{\mathbf{s}}^{\mathrm{T}}\mathbf{M}\tilde{\mathbf{s}}&-\tilde{\mathbf{s}}^{\mathrm{T}}\mathbf{M}\boldsymbol{\Psi}&\mathbf{0}&\mathbf{0}&-\tilde{\mathbf{s}}_{b:}^{\mathrm{T}}\\ \boldsymbol{\Psi}^{\mathrm{T}}\mathbf{M}\hat{\mathbf{I}}&-\boldsymbol{\Psi}^{\mathrm{T}}\mathbf{M}\tilde{\mathbf{s}}&\boldsymbol{\Psi}^{\mathrm{T}}\mathbf{M}\boldsymbol{\Psi}&\boldsymbol{\Psi}^{\mathrm{T}}\mathbf{M}\hat{\mathbf{I}}&\boldsymbol{\Psi}^{\mathrm{T}}\mathbf{M}\tilde{\mathbf{s}}&\boldsymbol{\Psi}_{b:}^{\mathrm{T}}\\ \hline \mathbf{0}&\mathbf{0}&\hat{\mathbf{I}}^{\mathrm{T}}\mathbf{M}\boldsymbol{\Psi}&\mathbf{0}&\mathbf{0}&\mathbf{0}\\ \mathbf{0}&\mathbf{0}&\tilde{\mathbf{s}}^{\mathrm{T}}\mathbf{M}\boldsymbol{\Psi}&\mathbf{0}&\mathbf{0}&\mathbf{0}\\ \hat{\mathbf{I}}_{b:}&-\tilde{\mathbf{s}}_{b:}&\boldsymbol{\Psi}_{b:}&\mathbf{0}&\mathbf{0}&\mathbf{0} \end{array}\right]\right)\begin{Bmatrix}\Delta\mathbf{r}\\ \Delta\boldsymbol{\theta}\\ \Delta\mathbf{z}\\ \hline \boldsymbol{\lambda}_1\\ \boldsymbol{\lambda}_2\\ \boldsymbol{\lambda}_3\end{Bmatrix}_l^n = \mathbf{0} \tag{8.33}$$

where l = 1, …, lnk; lnk is the total number of kept normal modes.* The last row of Eq. (8.33) is the constraint equations

---

* Subscripts of b: access the b rows and all the columns of the matrices.

† Vector $\mathbf{i}_l$ is a unit vector with 1 at the l-th position only.

$$\left[\hat{\mathbf{I}}_{b:} \quad -\tilde{\mathbf{s}}_{b:} \quad \boldsymbol{\Psi}_{b:}\right]\begin{Bmatrix}\Delta\mathbf{r}\\ \Delta\boldsymbol{\theta}\\ \Delta\mathbf{z}\end{Bmatrix}_l^n = \mathbf{0} \tag{8.34}$$

under which the normal modes are obtained. The *l*-th normal mode seen as absolute nodal displacements is computed by

$$\{\Delta\mathbf{d}\}_l^n = \left[\hat{\mathbf{I}} \quad -\tilde{\mathbf{s}} \quad \boldsymbol{\Psi}\right]\begin{Bmatrix}\Delta\mathbf{r}\\ \Delta\boldsymbol{\theta}\\ \Delta\mathbf{z}\end{Bmatrix}_l^n \tag{8.35}$$

For a full model, the mode shapes that are seen with mean axes and as absolute nodal displacements can be solved and computed by replacing all $\boldsymbol{\Psi}$ above by $\bar{\mathbf{I}}$ (identity matrix). Alternatively, the absolute nodal displacements can first be computed directly as (see Section 6.4)

$$\left[\begin{array}{c|c}\mathbf{I} & \mathbf{0}\\ \boldsymbol{\Psi}_s & \boldsymbol{\Psi}_n\end{array}\right] = [[\Delta\mathbf{d}]^c, [\Delta\mathbf{d}]^n] = [\Delta\mathbf{d}] \tag{8.36}$$

where

$$[\Delta\mathbf{d}]^c = \begin{bmatrix}\mathbf{I}\\ \boldsymbol{\Psi}_s\end{bmatrix} \tag{8.37}$$

has the constraint modes, and

$$[\Delta\mathbf{d}]^n = \begin{bmatrix}\mathbf{0}\\ \boldsymbol{\Psi}_n\end{bmatrix} \tag{8.38}$$

---

* We are only interested in the normal modes whose eigen-frequencies are not zeros; i.e., $\omega_l \neq 0$.

has the normal modes. If desired, the corresponding mode shapes of $[\Delta\mathbf{r};\Delta\boldsymbol{\theta};\Delta\boldsymbol{\delta}]^c$ and $[\Delta\mathbf{r};\Delta\boldsymbol{\theta};\Delta\boldsymbol{\delta}]^n$ can be solved from Eq. (8.6) at once with $[\Delta\mathbf{d}]$ substituting for $\boldsymbol{\Psi}$ there.

The results of the reduced model are then compared against the results of the full model. A good reduction method shall provide matched or close static solutions and (kept) eigen-frequencies.

8.5 Example

Based on the procedures provided in Section 8.4, this section inspects the use of mean axes with mode condensation on the beam model from APPENDIX A. The mean axes frame is located at the mass center as shown in Figure 8-5. The (undeformed) coordinates of the nodes are given in vector **s**:

$$\mathbf{s} = \begin{Bmatrix} s_\xi^1 \\ s_\eta^1 \\ s_\xi^2 \\ s_\eta^2 \\ s_\xi^3 \\ s_\eta^3 \\ s_\xi^4 \\ s_\eta^4 \\ s_\xi^5 \\ s_\eta^5 \end{Bmatrix} = \begin{Bmatrix} -0.5000 \\ 0 \\ -0.2500 \\ 0 \\ 0 \\ 0 \\ 0.2500 \\ 0 \\ 0.5000 \\ 0 \end{Bmatrix} \tag{8.39}$$

Since the beam is two-dimensional, some prior formulas need changes. For instance, all $-\tilde{\mathbf{s}}$ (three-dimensional) are to be replaced by $\breve{\mathbf{s}}$ where

$$\breve{\mathbf{s}} = \begin{Bmatrix} -s_\eta^1 \\ s_\xi^1 \\ \hline -s_\eta^2 \\ s_\xi^2 \\ \hline -s_\eta^3 \\ s_\xi^3 \\ \hline -s_\eta^4 \\ s_\xi^4 \\ \hline -s_\eta^5 \\ s_\xi^5 \end{Bmatrix} = \begin{Bmatrix} 0 \\ -0.5000 \\ 0 \\ -0.2500 \\ 0 \\ 0 \\ 0 \\ 0.2500 \\ 0 \\ 0.5000 \end{Bmatrix} \tag{8.40}$$

The absolute nodal displacements are now

$$\Delta\mathbf{d} \approx \hat{\mathbf{I}}\Delta\mathbf{r} + \breve{\mathbf{s}}\Delta\theta + \Delta\boldsymbol{\delta} = \begin{bmatrix} \hat{\mathbf{I}} & \breve{\mathbf{s}} & \bar{\mathbf{I}} \end{bmatrix} \begin{Bmatrix} \Delta\mathbf{r} \\ \Delta\theta \\ \Delta\boldsymbol{\delta} \end{Bmatrix} \tag{8.41}$$

in which $\mathbf{I}$ is a 2 by 2 identity matrix, $\Delta\mathbf{r}$ is a 2-vector, $\Delta\theta$ is a small angle*, and $\Delta\boldsymbol{\delta}$ is also a 10-vector. The linearized mean axis conditions of Eqs. (8.2) and (8.3) can be expressed for two-dimensional systems as

$$\hat{\mathbf{I}}^{\mathrm{T}}\mathbf{M}\Delta\boldsymbol{\delta} = \mathbf{0} \tag{8.42}$$

$$\breve{\mathbf{s}}^{\mathrm{T}}\mathbf{M}\Delta\boldsymbol{\delta} = \mathbf{0} \tag{8.43}$$

For the reduced model, nodes 1 and 5 are the boundary nodes; the rest are the interior nodes. Corresponding to the two boundary nodes, there are four "boundary" modes. Corresponding to the three interior nodes, there are six normal modes but only two of

---

* Variable $\Delta\theta$ describes the small rotation of the reference frame. It is actually the tangent value of the angle.

them are kept.* The transformation matrix of mode condensation, $\grave{\boldsymbol{\Psi}}_{MC}$, is constructed by Eq. (6.30). The mode shapes can be found in Figure 6-9. The total number of (generalized) modal coordinates, $\Delta\mathbf{z}$, is a 6-vector. In the coming subsections, we compare the constraint and normal modes of the reduced model against those of the full model.

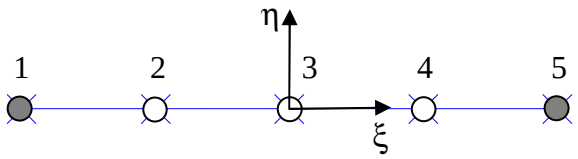

Figure 8-5: beam with mean axes

8.5.1 Constraint modes of the reduced model

For a 2-D reduced model, its constraint modes are obtained by solving the following static problem:

$$\left[\begin{array}{ccc|ccc} \mathbf{0} & \mathbf{0} & \mathbf{0} & \mathbf{0} & \mathbf{0} & \hat{\mathbf{I}}_{b:}^{\mathrm{T}} \\ \mathbf{0} & \mathbf{0} & \mathbf{0} & \mathbf{0} & \mathbf{0} & \breve{\mathbf{s}}_{b:}^{\mathrm{T}} \\ \mathbf{0} & \mathbf{0} & \boldsymbol{\Psi}^{\mathrm{T}}\mathbf{K}\boldsymbol{\Psi} & \boldsymbol{\Psi}^{\mathrm{T}}\mathbf{M}\hat{\mathbf{I}} & \boldsymbol{\Psi}^{\mathrm{T}}\mathbf{M}\breve{\mathbf{s}} & \boldsymbol{\Psi}_{b:}^{\mathrm{T}} \\ \hline \mathbf{0} & \mathbf{0} & \hat{\mathbf{I}}^{\mathrm{T}}\mathbf{M}\boldsymbol{\Psi} & \mathbf{0} & \mathbf{0} & \mathbf{0} \\ \mathbf{0} & \mathbf{0} & \breve{\mathbf{s}}^{\mathrm{T}}\mathbf{M}\boldsymbol{\Psi} & \mathbf{0} & \mathbf{0} & \mathbf{0} \\ \hat{\mathbf{I}}_{b:} & \breve{\mathbf{s}}_{b:} & \boldsymbol{\Psi}_{b:} & \mathbf{0} & \mathbf{0} & \mathbf{0} \end{array}\right] \left\{\begin{array}{c} \Delta\mathbf{r} \\ \Delta\theta \\ \Delta\mathbf{z} \\ \hline \boldsymbol{\lambda}_1 \\ \lambda_2 \\ \boldsymbol{\lambda}_3 \end{array}\right\}_l^c = \left\{\begin{array}{c} \mathbf{0} \\ \mathbf{0} \\ \mathbf{0} \\ \hline \mathbf{0} \\ \mathbf{0} \\ \mathbf{i}_l \end{array}\right\} \tag{8.44}$$

* The two kept normal modes are the first and second bending modes.

Equation (8.44) is modified from Eq. (8.30) for 2-D purposes.* For mode condensation, all $\boldsymbol{\Psi}$ are replaced by $\boldsymbol{\Psi}_{\text{MC}}$. The (partial) solutions of Eq. (8.44) for the beam are

$$\begin{bmatrix} \Delta\mathbf{r} \\ \Delta\theta \\ \Delta\mathbf{z} \end{bmatrix}^c_{\text{MC}} = \begin{bmatrix} [\Delta\mathbf{r}]^c_{\text{MC}} \\ [\Delta\theta]^c_{\text{MC}} \\ [\Delta\mathbf{z}]^c_{\text{MC}} \end{bmatrix} = \begin{bmatrix} 0.5 & 0 & 0.5 & 0 \\ 0 & 0.5 & 0 & 0.5 \\ 0 & -1 & 0 & 1 \\ 0.5 & 0 & -0.5 & 0 \\ 0 & 0 & 0 & 0 \\ -0.5 & 0 & 0.5 & 0 \\ 0 & 0 & 0 & 0 \\ 0 & 0 & 0 & 0 \\ 0 & 0 & 0 & 0 \end{bmatrix}$$

The constraint modes as absolute nodal displacements are computed by

$$[\Delta\mathbf{d}]^c_{\text{MC}} = \begin{bmatrix} \hat{\mathbf{I}} & \breve{\mathbf{s}} & \boldsymbol{\Psi}_{\text{MC}} \end{bmatrix} \begin{bmatrix} \Delta\mathbf{r} \\ \Delta\theta \\ \Delta\mathbf{z} \end{bmatrix}^c_{\text{MC}} = \begin{bmatrix} 1 & 0 & 0 & 0 \\ 0 & 1 & 0 & 0 \\ 0.75 & 0 & 0.25 & 0 \\ 0 & 0.75 & 0 & 0.25 \\ 0.5 & 0 & 0.5 & 0 \\ 0 & 0.5 & 0 & 0.5 \\ 0.25 & 0 & 0.75 & 0 \\ 0 & 0.25 & 0 & 0.75 \\ 0 & 0 & 1 & 0 \\ 0 & 0 & 0 & 1 \end{bmatrix}$$

The constraint modes of the full model, $[\Delta\mathbf{d}]^c$, can be computed directly by Eq. (8.37). The mode shapes of $[\Delta\mathbf{d}]^c$ are the same as those in Figure 6-5. Comparing $[\Delta\mathbf{d}]^c_{\text{MC}}$ against $[\Delta\mathbf{d}]^c$ shows that they are identical. That is, the static solutions are preserved.

---

* Vector $\mathbf{i}_l$ is a unit vector with 1 at the l-th position only.

8.5.2 Normal modes of the reduced model

For a 2-D reduced model, its normal modes are obtained by solving the following eigen-problem:

$$\left(\left[\begin{array}{ccc|ccc} \mathbf{0} & \mathbf{0} & \mathbf{0} & \mathbf{0} & \mathbf{0} & \mathbf{0} \\ \mathbf{0} & \mathbf{0} & \mathbf{0} & \mathbf{0} & \mathbf{0} & \mathbf{0} \\ \mathbf{0} & \mathbf{0} & \boldsymbol{\Psi}^{\mathrm{T}}\mathbf{K}\boldsymbol{\Psi} & \mathbf{0} & \mathbf{0} & \mathbf{0} \\ \hline \mathbf{0} & \mathbf{0} & \mathbf{0} & \mathbf{0} & \mathbf{0} & \mathbf{0} \\ \mathbf{0} & \mathbf{0} & \mathbf{0} & \mathbf{0} & \mathbf{0} & \mathbf{0} \\ \mathbf{0} & \mathbf{0} & \mathbf{0} & \mathbf{0} & \mathbf{0} & \mathbf{0} \end{array}\right] - \omega_l^2 \left[\begin{array}{ccc|ccc} \hat{\mathbf{I}}^{\mathrm{T}}\mathbf{M}\hat{\mathbf{I}} & \hat{\mathbf{I}}^{\mathrm{T}}\mathbf{M}\breve{\mathbf{s}} & \hat{\mathbf{I}}^{\mathrm{T}}\mathbf{M}\boldsymbol{\Psi} & \mathbf{0} & \mathbf{0} & \hat{\mathbf{I}}_{b:}{}^{\mathrm{T}} \\ \breve{\mathbf{s}}^{\mathrm{T}}\mathbf{M}\hat{\mathbf{I}} & \breve{\mathbf{s}}^{\mathrm{T}}\mathbf{M}\breve{\mathbf{s}} & \breve{\mathbf{s}}^{\mathrm{T}}\mathbf{M}\boldsymbol{\Psi} & \mathbf{0} & \mathbf{0} & \breve{\mathbf{s}}_{b:}{}^{\mathrm{T}} \\ \boldsymbol{\Psi}^{\mathrm{T}}\mathbf{M}\hat{\mathbf{I}} & \boldsymbol{\Psi}^{\mathrm{T}}\mathbf{M}\breve{\mathbf{s}} & \boldsymbol{\Psi}^{\mathrm{T}}\mathbf{M}\boldsymbol{\Psi} & \boldsymbol{\Psi}^{\mathrm{T}}\mathbf{M}\hat{\mathbf{I}} & \boldsymbol{\Psi}^{\mathrm{T}}\mathbf{M}\breve{\mathbf{s}} & \boldsymbol{\Psi}_{b:}{}^{\mathrm{T}} \\ \hline \mathbf{0} & \mathbf{0} & \hat{\mathbf{I}}^{\mathrm{T}}\mathbf{M}\boldsymbol{\Psi} & \mathbf{0} & \mathbf{0} & \mathbf{0} \\ \mathbf{0} & \mathbf{0} & \breve{\mathbf{s}}^{\mathrm{T}}\mathbf{M}\boldsymbol{\Psi} & \mathbf{0} & \mathbf{0} & \mathbf{0} \\ \hat{\mathbf{I}}_{b:} & \breve{\mathbf{s}}_{b:} & \boldsymbol{\Psi}_{b:} & \mathbf{0} & \mathbf{0} & \mathbf{0} \end{array}\right] \right) \left\{\begin{array}{c} \Delta\mathbf{r} \\ \Delta\theta \\ \Delta\mathbf{z} \\ \hline \boldsymbol{\lambda}_1 \\ \lambda_2 \\ \boldsymbol{\lambda}_3 \end{array}\right\}_l^n = \mathbf{0} \tag{8.45}$$

Equation (8.45) is modified from Eq. (8.33) for 2-D purposes. For mode condensation, all $\boldsymbol{\Psi}$ are replaced by $\boldsymbol{\Psi}_{\mathrm{MC}}$. The (partial) solutions of Eq. (8.45) for the beam are

$$\left[\begin{array}{c} \Delta\mathbf{r} \\ \Delta\theta \\ \Delta\mathbf{z} \end{array}\right]_{\mathrm{MC}}^n = \left[\begin{array}{c} [\Delta\mathbf{r}]_{\mathrm{MC}}^n \\ \hline [\Delta\theta]_{\mathrm{MC}}^n \\ \hline [\Delta\mathbf{z}]_{\mathrm{MC}}^n \end{array}\right] = \begin{array}{|c|c|} \hline 0 & 0 \\ 1 & 0 \\ \hline 0 & -1 \\ \hline 0 & 0 \\ -1 & -0.5 \\ 0 & 0 \\ -1 & 0.5 \\ -0.28445 & 0 \\ 0 & -0.31623 \\ \hline \end{array}$$

The normal modes as absolute nodal displacements are computed by

$$[\Delta\mathbf{d}]_{\mathrm{MC}}^n = \left[\hat{\mathbf{I}} \quad \breve{\mathbf{s}} \quad \boldsymbol{\Psi}_{\mathrm{MC}}\right] \left[\begin{array}{c} \Delta\mathbf{r} \\ \Delta\theta \\ \Delta\mathbf{z} \end{array}\right]_{\mathrm{MC}}^n = \begin{array}{|c|c|} \hline 0 & 0 \\ 0 & 0 \\ 0 & 0 \\ 1.1716 & 0.75 \\ 0 & 0 \\ 1.6569 & 0 \\ 0 & 0 \\ 1.1716 & -0.75 \\ 0 & 0 \\ 0 & 0 \\ \hline \end{array}$$

The normal modes of the full model, $[\Delta\mathbf{d}]^n$, can be computed directly by Eq. (8.38). The mode shapes of $[\Delta\mathbf{d}]^n$ are basically identical to those in Figure 6-7. Comparing $[\Delta\mathbf{d}]^n_{\text{MC}}$ against $[\Delta\mathbf{d}]^n$ shows that $[\Delta\mathbf{d}]^n_{\text{MC}}$ spans the same column space as the first two columns of $[\Delta\mathbf{d}]^n$. And, the two eigen-frequencies—also solved from Eq. (8.45)—are 3.10366 and 12.3283 (Hz); they match the two lowest frequencies in Figure 6-7. That is, the eigen-properties of the kept normal modes are preserved.

8.6 Observation

The results from the previous section show that the reduced model preserves both the static solutions and the (kept) eigen-properties, even though the mode shapes in the transformation matrix of mode condensation ($\mathbf{\Psi}_{\text{MC}}$) are simply prepared in the conventional way (nodal-fixed like). This is also true for Craig and Bampton reduction although the test data are not presented. For other reduction methods that are not mentioned, the same evaluation procedures still apply. However, if a reduction method is known not to perform well with one type of axes such as nodal-fixed axes, it will not do better with mean axes or any other axes.

9 CONCLUSION AND FUTURE WORK

Among the reduction methods we have discussed in this dissertation, modal truncation is often used for the cases where at least six degrees of freedom are removed. The results are acceptable if the kept (normal or) eigen-modes have been carefully selected. Guyan reduction, another commonly used method, preserves exact solutions for static problems. However, large errors may occur if it is applied to dynamic problems because of raised eigen-frequencies. Therefore, its applications shall be limited to low frequency excitation. Craig and Bampton reduction, originated from substructuring, combines constraint modes and normal modes to improve the quality of model reduction. It performs well over a broader range of dynamic excitation.

Component mode synthesis is a family of methods (such as Craig and Bampton reduction) that intuitively combine different types of modes. But, these methods do not provide physical explanations. Conversely, Nikravesh derived his method, mode condensation, from the equations of motion by assuming that the inertia associated with the deleted modes is relocated to the boundary nodes and, furthermore, there are no forces associated with the deleted modes. This is the same to say, as we have found, that the potential energy with respect to the deleted modes is a minimum. We have also proven that mode condensation is equivalent to Craig and Bampton reduction. That is, mode condensation explains why Craig and Bampton reduction works. And, since the two methods span the same column space, they always give the same results.

Unlike in structural analysis, a deformable body may exhibit partial or total rigid-body motion in a multibody system; i.e., not all boundary nodes of the deformable body are fixed to the ground. For modal truncation, because forces and displacements at the moving boundary are not taken into account, more often it yields insufficient, unsatisfactory deformation. Thus, this method is not recommended for use in multibody dynamic settings. Guyan reduction may be applied in these cases but should be used with care due to the raised eigen-frequencies. Craig and Bampton and mode condensation still perform well because their column spaces can response to forces and displacements at the boundary nodes, and at the same time they allow normal vibration for the interior nodes.

Although a nodal-fixed frame is commonly used for a moving deformable body due to its ease of use, the associated dynamic responses may not be as accurate as they should be. The cause is that some nodes are treated differently than the others because of how the nodal-fixed frame is installed. On the contrary, a mean axes frame does not have this problem, hence giving more accurate results. For that reason, mean axes frames are favored over nodal-fixed frames for general purpose employment. But, mean axes were thought to be only compatible with free-free modes since the axes are not fixed to any nodes. It was not clear how a restrained deformable body can be condensed properly if mean axes are the choice. We have shown that the conventional (nodal-fixed) mode shapes can be used with mean axes as long as the transformation matrix has full (column) rank and contains complete rigid-body mode shapes. The implementation makes model reduction with mean axes as easy as with nodal-fixed axes. The quality of a reduction method is not affected, regardless of the axis type.

One possible future application of model reduction is in tire and vehicle dynamic analyses. Though the finite element method has been used in the tire design process, it can be very inefficient to apply detailed finite element models for tire testing and vehicle simulation. We reason that model reduction by component mode synthesis should help maintain static accuracy and improve dynamic efficiency. Michelin Tire Company (Nov., 2002) has explored Craig and Bampton reduction in tire modeling but the scope is limited to ride studies [55]. Our prospective investigations may focus more on rolling and cornering, which are in the category of handling performance. The challenges could be in the following areas: impact and disengagement detection, friction model, complex terrains, and robust time integration.

APPENDIX A BEAM MODEL

A two-dimensional beam is shown in Figure A-1. The beam is 1 meter long, its width (b) is 0.1 m, and its height (h) is 0.05 m. The cross section area ($b*h$) is 0.005 m^2. The area moment of inertia ($b*h$^3/12) is 1.0417e-006 m^4. Five nodes are evenly spaced along its length. The coordinates are given in Table A-1.

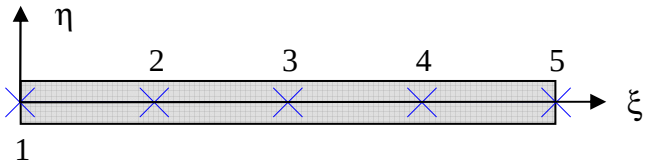

Figure A-1: a 2-D beam with five nodes and four elements

Table A-1: node locations of the beam

node	coordinate	value
1	s_ξ^1	0
	s_η^1	0
2	s_ξ^2	0.2500
	s_η^2	0
3	s_ξ^3	0.5000
	s_η^3	0
4	s_ξ^4	0.7500
	s_η^4	0
5	s_ξ^5	1.0000
	s_η^5	0

The point masses concentrated at the nodes are 0.1, 0.2, 0.2, 0.2, and 0.1 kg. The mass matrix, **M**, is simply a diagonal matrix as diag([0.1 0.1, 0.2 0.2, 0.2 0.2, 0.2 0.2, 0.1 0.1]).

There are four beam elements of Euler-Bernoulli beam type. The modulus of elasticity (*E*) is 30e5 Pa. Originally, a stiffness matrix is generated by using FElt [56]. Each node carries three DOFs—two translational and one rotational. The stiffness matrix is then condensed by Guyan reduction to remove all rotational DOFs. The resultant stiffness matrix, **K**, in N/m is

60000	0	-60000	0	0	0	0	0	0	0
0	321.439	0	-728.595	0	514.302	0	-128.576	0	21.4293
-60000	0	120000	0	-60000	0	0	0	0	0
0	-728.595	0	1971.49	0	-1885.77	0	771.453	0	-128.576
0	0	-60000	0	120000	0	-60000	0	0	0
0	514.302	0	-1885.77	0	2742.94	0	-1885.77	0	514.302
0	0	0	0	-60000	0	120000	0	-60000	0
0	-128.576	0	771.453	0	-1885.77	0	1971.49	0	-728.595
0	0	0	0	0	0	-60000	0	60000	0
0	21.4293	0	-128.576	0	514.302	0	-728.595	0	321.439

APPENDIX B SLAB MODEL

A slab is shown in Figure B-1. Its dimensions are 4 (length) x 2 (width) x l (height) meters. The slab is meshed into eight brick elements and thirty nodes. Each node has three degrees of freedom. In total, there are ninety degrees of freedom. The origin of the reference frame is positioned at node 16. The ξ axis goes through node 28; the η axis goes through node 18; the ζ axis goes through node 1. The node locations are given in Table B-1 where *j* is the node number. Point masses are also given in Table B-1; the total mass is $\sum m_j = 62.4$ kg. The modulus of elasticity is 0.2E+06 Pa; Poisson's ratio is 0.33. The stiffness matrix (90 x 90) is too large to show here.

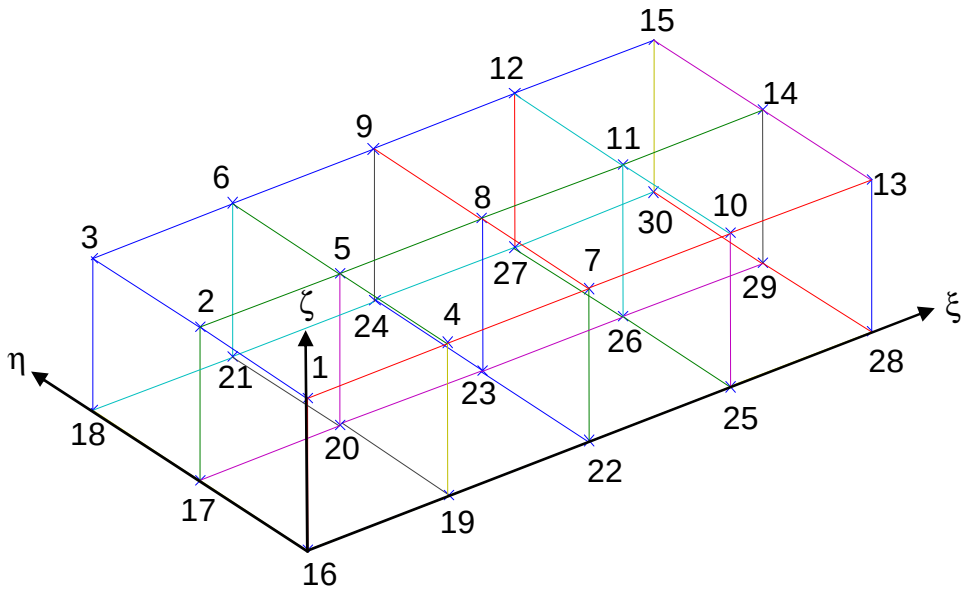

Figure B-1: a 3-D slab with eight elements and thirty nodes

Table B-1: node locations and point masses of the slab

j	s_ξ^j	s_η^j	s_ζ^j	m_j	j	s_ξ^j	s_η^j	s_ζ^j	m_j
1	0	0	1	0.975	16	0	0	0	0.975
2	0	1	1	1.95	17	0	1	0	1.95
3	0	2	1	0.975	18	0	2	0	0.975
4	1	0	1	1.95	19	1	0	0	1.95
5	1	1	1	3.9	20	1	1	0	3.9
6	1	2	1	1.95	21	1	2	0	1.95
7	2	0	1	1.95	22	2	0	0	1.95
8	2	1	1	3.9	23	2	1	0	3.9
9	2	2	1	1.95	24	2	2	0	1.95
10	3	0	1	1.95	25	3	0	0	1.95
11	3	1	1	3.9	26	3	1	0	3.9
12	3	2	1	1.95	27	3	2	0	1.95
13	4	0	1	0.975	28	4	0	0	0.975
14	4	1	1	1.95	29	4	1	0	1.95
15	4	2	1	0.975	30	4	2	0	0.975

APPENDIX C EITELBERG'S METHOD IN MATLAB FUNCTION

```
function [Ar,Br,Cr] = eitelberg(A,B,C,R)

%
%  This function performs a model reduction on a continuous system
%  using the algorithm of Eitelberg.
%
%  Reference:  Eduard Eitelberg: Ph.D. Dissertation, University of Karlsruhe,
%              1979
%       also:  Eduard Eitelberg: Modellreduktion durch Minimierung des
%              Gleichungsfehlers, Regelungstechnik, 10, 1978.
%
%   coded by:  Dr. Cellier,
%              department of Electrical and Computer Engineering,
%              University of Arizona, Tucson, Arizona, USA
%


%  Input Parameter:
%  ----------------
%  A, B, C     := The system {A, B, C}
%  R           := The output reduction matrix  (xr = R*x)
%
%  Output parameter:
%  -----------------
%  Ar, Br, Cr  := reduced order system

%  Check whether there are unstable modes.

lmax = max(real(eig(A)));
if lmax >= 0,
  error('This EITELBERG only works for stable systems!')
end

%  Perform the model reduction.

Cr = C/R;
P = A\B;
[U,S,V] = svd(P);
Ah = U'*A*U;
S2 = S*S';
Sh = lyap(Ah,S2);
S = U*Sh*U';
Ar = R*A*S*R'/(R*S*R');
Br = Ar*R*P;
```

REFERENCES

1. J. L. Meriam, L. G. Kraig; 2002. *Engineering Mechanics: Dynamics* (5th ed.), John Wiley & Sons.
2. Robert L. Norton; 2004. *Design of Machinery* (3rd ed.), The McGraw-Hill Companies.
3. Jerry H. Ginsberg; 1995. *Advanced Engineering Dynamics*, Cambridge University Press, New York.
4. R. L. Huston; 1991, March. "Multibody Dynamics"; *Appl Mech Rev*, VOL. 44, NO. 3, pp. 109-117.
5. R. L. Huston; 1996, Oct. "Multibody Dynamics Since 1990"; *Appl Mech Rev*, VOL. 49, NO. 10, part 2, pp. S35-S40.
6. Parviz E. Nikravesh; 1988. *Computer-Aided Analysis of Mechanical Systems*, Englewood Cliffs, New Jersey.
7. Edward J. Haug; 1989. Computer Aided Kinematics and Dynamics of Mechanical Systems, Volume I: Basic Methods, Allyn and Bacon, Needham Heights, Massachusetts.
8. Ronald L. Huston; 1990. *Multibody Dynamics*, Butterworths, Boston.
9. Javier Garcia de Jalon, Eduardo Bayo; 1993. *Kinematic and Dynamic Simulation of Multibody Systems*; Springer-Verlag.
10. Werner O. Schiehlen (editor); 1990. *Multibody Systems Handbook*, Springer-Verlag, New York.
11. U.S. Small Business Administration, TIBBETTS AWARDs 1999. http://www.sba.gov/sbir/tibbetts/mechanical.html
12. Center for Computer-Aided Design, The University of Iowa. http://www.ccad.uiowa.edu/technologies/dads/main.html
13. G. G. Lowen, C. Chassapis; 1986. "The Elastic Behavior of Linkages: An Update"; *Mechanism and Machine Theory*, VOL. 21, NO. 1, pp. 33-42.

14. B. S. Thompson, C. K. Sung; 1986. "A Survey of Finite Element Techniques for Mechanism Design"; *Mechanism and Machine Theory*, VOL. 21, NO. 4, pp. 351-359.

15. Daryl L. Logan; 1997. *A First Course in the Finite Element Method Using Algor*, PWS Publishing Group.

16. T. R. Kane, R. R. Ryan, A. K. Banerjee; 1987. "Dynamics of a Cantilever Beam Attached to a Moving Base"; *Journal of Guidance, Control, and Dynamics*, VOL. 10, NO. 2, pp. 139-151.

17. E. M. Baker, A. A. Shabana; 1987. "TIMOSHENKO BEAMS AND FLEXIBLE MULTIBODY SYSTEM DYNAMICS"; *Journal of Sound and Vibration*, 116(1), pp. 89-107.

18. D. J. Zhang, R. L. Huston; 1996. "On Dynamic Stiffening of Flexible Bodies Having High Angular Velocity"; *MECH. STRUCT. & MACH.*, 24(3), pp. 313-329.

19. Ahmed A. Shabana; 1998. *Dynamics of Multibody Systems* (2nd ed.), Cambridge University Press.

20. Parviz E. Nikravesh; 1994. *Rigid-Flexible Multibody Dynamics* (unpublished notes), Department of Aerospace and Mechanical Engineering, The University of Arizona, Tucson, AZ 85721, USA.

21. J. R. Canavin, P. W. Likins; 1977, Dec. "Floating Reference Frames for Flexible Spacecraft"; *J. SPACECRAFT*, VOL. 14, NO. 12, pp. 724-732.

22. B.F. De Veubeke; 1976. "The Dynamics of Flexible Bodies"; *INTERNATIONAL JOURNAL OF ENGINEERING SCIENCE*, VOL. 14, pp. 895-913.

23. O. P. Agrawal, A. A. Shabana; 1986. "Application of Deformable-body Mean Axis to Flexible Multibody System Dynamics"; *Computer Methods in Applied Mechanics and Engineering*, VOL. 56, pp. 217-245.

24. Parviz E. Nikravesh, Yi-shih Lin; 2003. "Body Reference Frames in Deformable Multibody Systems"; *International Journal for Multiscale Computational Engineering*, VOL. 1, NO. 2 & 3, pp. 201-217.

25. Parviz E. Nikravesh, Yi-shih Lin; 2005. "Use of Principal Axes as the Floating Reference Frame for a Moving Deformable Body"; *Multibody System Dynamics*, VOL. 13, NO. 2, pp. 211-231.

26. James M. Gere; 2000. *Mechanics of Materials* (5th ed.), published by Brooks/Cole, a division of Thomson Learning.

27. Robert J. Guyan; 1965. "Reduction of Stiffness and Mass Matrices"; *AIAA Journal*, VOL. 3, NO. 2, p. 380.

28. Edward Eitelberg; 1979. *Model Reduction of Linear, Time-Invariant Systems by Minimizing the Equation Error* (translated from German), PhD dissertation, University of Karlsruhe, Germany.

29. F. E. Cellier; 2001, spring. *Numerical Linear Algebra in Control*, class notes for ECE 544, Tucson, Arizona, USA.

30. C. A. Miller; 1980. "Dynamic Reduction of Structural Models"; *Journal of the Structural Division ASCE*, pp. 2097-2108.

31. C. A. Miller; 1975. "Errors Resulting from Dynamic Reduction"; *Proceedings of the First National Conference on Computers in Civil Engineering*, pp. 58-71.

32. Carlos Alberto Malpartida; 1983, May. *Dynamic Condensation of Structural Eigenproblems* (Master's thesis), Department of Civil Engineering, University of Louisville, Louisville, KY, USA.

33. Mario Paz; 1984. "Dynamic Condensation"; *AIAA Journal*, VOL. 22, NO. 5, pp. 724-727.

34. Parviz E. Nikravesh, Manuel S. Pereira; 1997, June. *Dynamic Condensation of Mass and Stiffness Matrices*, Technical Report No. CAEL-97-1, Department of Aerospace and Mechanical Engineering, The University of Arizona, Tucson, AZ 85721, USA.

35. Wan S. Yoo, Edward J. Haug; 1986. "Dynamics of Articulated Structures. Part I. Theory"; *J. STRUCT. MECH.*, 14(1), 105-126.

36. Wan S. Yoo, Edward J. Haug; 1986. "Dynamics of Articulated Structures. Part I. Theory"; *J. STRUCT. MECH.*, 14(2), 177-189.

37. Richard H. MacNeal; 1971. "A Hybrid Method of Component Mode Synthesis"; *Computers & Structures*, VOL. 1, NO.4, pp. 581-601.

38. S. Rubin; 1975. "Improved component-mode representation for structural dynamics analysis"; *AIAA Journal*, VOL. 12, pp. 995-1006.

39. D. N. Herting; 1985. "A General Purpose, Multi-stage, Component Modal Synthesis Method"; *Finite Elements in Analysis and Design*, VOL. 1, pp. 153-164.

40. MSC.Software Corporation, 2 MacArthur Place, Santa Ana, CA 92707. http://www.mscsoftware.com

41. Leonard Meirovitch; 1980. *Computational Methods in Structural Dynamics*, Sijthoff & Noordhoff.

42. Walter C. Hurty; 1965. "Dynamic Analysis of Structural Systems Using Component Modes"; *AIAA Journal*, VOL. 2, NO. 4, pp. 678-685.

43. Roy R. Craig Jr., Mervyn C. C. Bampton; 1968. "Coupling of Substructures for Dynamic Analyses"; *AIAA Journal*, VOL. 6, NO. 7, pp. 1313-1319.

44. Olof Friberg; 1991. "A Method for Selecting Deformation Modes in Flexible Multibody Dynamics"; *International Journal for Numerical Methods in Engineering*, VOL. 32, pp. 1637-1655.

45. Gisli Ottarsson; 1998, March, 31. "MODAL FLEXIBILITY METHOD IN ADAMS/FLEX"; *ADAMS/Flex documentation*, Mechanical Dynamics Inc.

46. Wen-Hwa Shyu, Zheng-Dong Ma, Gregory M. Hulbert; 1997. "A new component mode synthesis method: Quasi-static mode compensation"; *Finite Elements in Analysis and Design*, VOL. 24, NO. 4, pp. 271-281.

47. Wen-Hwa Shyu, Jianmin Gu, Gregory M. Hulbert, Zheng-Dong Ma; 2000. "On the use of multiple quasi-static mode compensation sets for component mode synthesis of complex structures"; *Finite Elements in Analysis and Design*, VOL. 35, NO. 2, pp. 119-140.

48. G. M. L. Gladwell; 1964. "Branch Mode Analysis of Vibrating Systems"; *J. of Sound and Vibration*, VOL. 1, NO. 1, pp. 41-59.

49. W. A. Benfield, R. F. Hruda; 1971. "Vibration Analysis of Structures by Component Mode Substitution"; *AIAA Journal*, VOL. 9, NO. 7, pp. 1255-1261.

50. Parviz E. Nikravesh; 2003. "Model Reduction Techniques in Flexible Multibody Dynamics"; W. Schiehlen and M. Valasek (eds.), *Virtual Nonlinear Multibody Systems*, pp. 83-102, Kluwer Academic Publishers.

51. Richard Schwertassek, Oskar Wallrapp, Ahmed A. Shabana; 1999. "Flexible Multibody Simulation and Choice of Shape Functions"; *Nonlinear Dynamics*, VOL. 20, pp. 361-380.

52. Robert D. Cook; 1994. *Finite Element Modeling for Stress Analysis*, John and Wiley & Sons, Inc.

53. Bruce Irons; 1963, August. "Eigenvalue Economisers in Vibration Problems"; *Journal of the Royal Aeronautical Society*, VOL. 67, pp. 526-528.

54. Bruce Irons; 1965, May. "Structural Eivenvalue Problems: Elimination of Unwanted Variables"; *AIAA Journal*, VOL. 3, NO. 5, pp. 961-962.

55. Marc DUVERNIER, Patrice FRAYSSE, Viviane BOMBLAIN, Eric DORMEGNIE; 2002, Nov. "Tyre Modelling for NVH Engineering in ADAMS"; *The 1st MSC.ADAMS European User Conference*, London.

56. FElt is an open source software system for finite element analysis. For its home page, please visit http://felt.sourceforge.net/.